

THE EFFECTS OF RANDOM SEEKER NOISE AND TARGET MANEUVER
ON GUIDANCE PERFORMANCE

A THESIS SUBMITTED TO
THE GRADUATE SCHOOL OF NATURAL AND APPLIED SCIENCES
OF
MIDDLE EAST TECHNICAL UNIVERSITY

BY

ONUR ÖZGÜR

IN PARTIAL FULFILLMENT OF THE REQUIREMENTS
FOR
THE DEGREE OF MASTER OF SCIENCE
IN
MECHANICAL ENGINEERING

SEPTEMBER 2014

Approval of the thesis:

**THE EFFECTS OF RANDOM SEEKER NOISE AND TARGET
MANEUVER ON GUIDANCE PERFORMANCE**

submitted by **ONUR ÖZGÜR** in partial fulfillment of the requirements for the degree of **Master of Science in Mechanical Engineering Department, Middle East Technical University** by,

Prof. Dr. Canan Özgen
Dean, Graduate School of **Natural and Applied Sciences** _____

Prof. Dr. Süha Oral
Head of Department, **Mechanical Engineering** _____

Prof. Dr. M. Kemal Özgören
Supervisor, **Mechanical Engineering Dept., METU** _____

Examining Committee Members:

Asst. Prof. Dr. Kivanç Azgin
Mechanical Engineering Dept., METU _____

Prof. Dr. M. Kemal Özgören
Mechanical Engineering Dept., METU _____

Prof. Dr. M. Kemal Leblebicioğlu
Electrical and Electronics Engineering Dept., METU _____

Prof. Dr. Ozan Tekinalp
Aerospace Engineering Dept., METU _____

M. Özgür Ateşoğlu, Ph.D.
ASELSAN Inc. _____

Date: 01/09/2014

I hereby declare that all information in this document has been obtained and presented in accordance with academic rules and ethical conduct. I also declare that, as required by these rules and conduct, I have fully cited and referenced all material and results that are not original to this work.

Name, Last name : Onur ÖZGÜR

Signature :

ABSTRACT

THE EFFECTS OF RANDOM SEEKER NOISE AND TARGET MANEUVER ON GUIDANCE PERFORMANCE

Özgür, Onur

M.S., Department of Mechanical Engineering

Supervisor: Prof. Dr. M. Kemal Özgören

September 2014, 190 pages

The aim of this thesis is to scrutinize the effects of challenging target maneuvers and distinctive random seeker noise on guidance performance. The guidance problem is formulated as a feedback control system and a homing loop is modeled via Matlab-Simulink software to simulate possible 3D engagement scenarios. In order to track maneuverable targets and derive the rates of LOS angles in azimuth and elevation planes, a couple of seeker models are presented. Moreover, *blind flight* phenomenon is investigated for gimbaled seeker models. Besides, prominent random seeker noise and error sources are mathematically modeled and introduced into the homing guidance loop. A target estimator is implemented to estimate the states of the maneuvering target, including target's acceleration components. Augmented Proportional Navigation Guidance Law is mechanized to compute the required lateral acceleration components in azimuth and elevation planes of the line of sight frame. Furthermore, a new technique is proposed to deal with the *blind flight* predicament, which may be regarded as a contribution to the missile guidance literature. Finally, the resulting end-game plots of the pursuer and the evader for challenging guidance scenarios are presented. Multiple *Monte Carlo* simulations are carried out randomly to judge the performance of the overall guidance system based on a statistical approach. By doing so, the effects of target maneuver types, different

engagement geometries, seeker models, random noise sources, target estimator models and guidance algorithms on overall guidance performance are compared. Overall guidance performances are assessed in terms of average miss distance values, hit ratios and average engagement times.

Keywords: Random Seeker Noise, Maneuverable Target Tracking, Target Estimator, Augmented Proportional Navigation Guidance Law, Monte Carlo Simulation

ÖZ

RASTGELE ARAYICI BAŞLIK GÜRÜLTÜLERİ VE HEDEF MANEVRALARININ GÜDÜM PERFORMANSI ÜZERİNE ETKİLERİ

Özgür, Onur

Yüksek Lisans, Makina Mühendisliği Bölümü

Tez Yöneticisi: Prof. Dr. M. Kemal Özgören

Eylül 2014, 190 sayfa

Bu tezin amacı zorlu hedef manevralarının ve farklı rastgele arayıcı başlık gürültülerinin güdüm performansı üzerine etkilerini araştırmaktır. Güdüm problemi bir geri beslemeli kontrol sistemi olarak formüle edilmiş ve üç boyutlu uzayda karşılaşılabilen hava mücadele senaryolarının benzetimini gerçekleştirmek üzere Matlab-Simulink yazılımı aracılığıyla bir güdüm döngüsü modellenmiştir. Manevra kabiliyetine sahip hedeflerin takibi ile yanca ve yükseliş düzlemlerinde görüş hattı açılarının değişimini türetmek amacıyla bir çift arayıcı başlık modeli sunulmuştur. Buna ek olarak, gimballı arayıcı başlık modelleri için *kör uçuş* durumu incelenmektedir. Bunun yanı sıra, onde gelen rastgele arayıcı başlık gürültü ve hata kaynakları matematiksel olarak modellenmiş ve güdüm döngüsünde rol almıştır. Manevra yapan hedefin ivme bileşenlerini de içeren durumlarını tahmin etmek amacıyla bir hedef kestirici uygulanmıştır. Görüş hattı koordinat sisteminin yanca ve yükseliş düzlemlerindeki gerekli yanal ivme bileşenlerinin hesaplanması için genişletilmiş oransal güdüm kanunu kullanılmıştır. Bununla birlikte, *kör uçuş* sorununu çözmek üzere füze güdüm literatüründe yer almayan yeni bir teknik önerilmiştir. Son olarak, zorlu güdüm senaryoları için takipçi ve hedef hareketleri gösterilmektedir. Güdüm sisteminin genel performansını istatistiksel temellere dayandırarak ölçmek amacıyla çoklu *Monte Carlo* simülasyonları rastgele bir

biçimde koşturulmaktadır. Böylece, hedef manevra tiplerinin, farklı mücadele geometrilerinin, arayıcı başlık modellerinin, rastgele gürültü faktörlerinin, hedef kestirim modellerinin ve güdüm algoritmalarının genel güdüm performansına etkileri karşılaştırılmaktadır. Genel güdüm performansları ortalama ıskalama mesafe değerleri, isabet oranları ve ortalama mücadele süreleri açısından değerlendirilmektedir.

Anahtar Kelimeler: Rastgele Arayıcı Başlık Gürültüleri, Manevra Kabiliyetli Hedef Takibi, Hedef Kestirici, Genişletilmiş Oransal Seyrüsefer Güdüm Kanunu, Monte Carlo Simülasyonu

*To my guardian angels
for their endless love...*

ACKNOWLEDGEMENTS

First of all, I would like to thank my mother and father who have proven the existence of angels on Earth to me with their endless love, encouragement, sacrifice, care and support at all stages of my life. I am grateful to them for teaching me so many things about life, not to give up, how to get through the storms of life and that being a good and straight person is incomparable to any other sorts of power in this world. They have been my endless source of passion and inspiration all my life.

I would like to express my sincere gratitude to my supervisor Prof. Dr. M. Kemal ÖZGÖREN for his key advices, trust, encouragement, valuable discussions on the thesis subject for long hours, sharing his precious experience and knowledge in the guidance and control area with me and his visionary mentorship. Certainly, it was my chance to be able to work with him and I wish him a healthy and peaceful retirement life with his never disappearing smile.

Special thanks go to my sweet sister, who ignited the love of mathematics in my heart years ago as a talented mathematician, for her loving support, heartening words and motivating me despite the long distance between us. I feel so lucky to have a sister like her who brings so much fun, laughter and joy into my life.

I would also like to thank my managers and colleagues at the Radar, Electronic Warfare and Intelligence Systems division of ASELSAN, Inc. for their patience, understanding, support and kind friendship over the three years.

Besides, I wish to thank Dr. Özgür ATEŞOĞLU for his constructive criticism and valuable feedback during the finalization stage of the thesis report.

Lastly, ASELSAN, Inc. is appreciated for supporting me in conducting my graduate studies and the monetary support provided by the Turkish Scientific and Technological Research Council (TÜBİTAK) is greatly acknowledged.

TABLE OF CONTENTS

ABSTRACT	V
ÖZ.....	VII
ACKNOWLEDGEMENTS.....	X
TABLE OF CONTENTS.....	XI
LIST OF TABLES	XV
LIST OF FIGURES	XVI
LIST OF SYMBOLS	XXII
LIST OF ABBREVIATIONS	XXX
CHAPTERS	
1 INTRODUCTION.....	1
1.1 A BRIEF LOOK AT HOMING GUIDANCE AND ITS HISTORICAL DEVELOPMENT	1
1.2 HOMING MISSILE GUIDANCE TYPES.....	5
1.2.1 Passive Guidance	6
1.2.2 Semi-Active Guidance	7
1.2.3 Active Guidance.....	7
1.3 THE AIM AND SCOPE OF THE STUDY	8
1.4 OUTLINE OF THE THESIS	9
2 OVERVIEW OF MISSILE GUIDANCE SYSTEM.....	11
2.1 MISSILE GUIDANCE SYSTEM REPRESENTATION AS A CLOSED-LOOP FEEDBACK SYSTEM.....	11
2.2 SUBCOMPONENTS OF THE OVERALL MISSILE GUIDANCE LOOP.....	12

3 TARGET MANEUVER MODELS	15
3.1 CONSTANT STEP MANEUVER - ZERO JERK MODEL	17
3.2 PIECEWISE CONTINUOUS STEP MANEUVER	17
3.3 RAMP MANEUVER – CONSTANT JERK MODEL.....	18
3.4 WEAVING MANEUVER – VARIABLE JERK MODEL	19
4 MISSILE-TARGET KINEMATICS, SEEKER MODELING AND NOISE MODELS.....	21
4.1 MISSILE-TARGET RELATIVE SPATIAL KINEMATICS.....	21
4.1.1 Inertial Reference Frame	21
4.1.2 Line of Sight Frame.....	23
4.1.3 The Use of Line of Sight Concept in Missile Guidance Applications	24
4.1.4 Determination of Relative Range, Range Rate and Azimuth-Elevation LOS Angles	26
4.1.5 Definition of Miss Distance Concept	31
4.1.6 Definition of ‘Blind Flight’ and ‘Mid-Course Guidance’ Conditions	32
4.2 SEEKER MODELING	33
4.2.1 Review of Seekers	33
4.2.1.1 Mission of the Seekers in Guidance	33
4.2.1.2 Definition of Field of View and Field of Regard Concepts	34
4.2.2 Types of Seekers	36
4.2.3 Gimbaled vs Strapdown Seekers	38
4.2.4 Gimbaled Seeker Model.....	41
4.2.4.1 LOS Rate Reconstruction Method	41
4.2.4.2 Tracking and Stabilization Loops	44
4.2.4.3 Saturation Limits of Pitch and Yaw Gimbal Angles.....	48
4.2.5 Strapdown Seeker Model	49
4.2.5.1 Noisy LOS Angle Filtering by Second Order Fading Memory Filters	49
4.2.5.2 LOS Rate Estimation via Second Order Fading Memory Filters	51

4.3 NOISE AND ERROR MODELS	53
4.3.1 Glint Noise	53
4.3.2 Receiver Angle Tracking Noise	58
4.3.2.1 Radar Cross Section Fluctuation.....	58
4.3.2.2 Eclipsing Effect.....	59
4.3.3 Sinusoidal Noise	62
4.3.4 Random Gaussian Noise	63
4.3.5 Radome-Boresight Errors.....	64
4.3.6 Bias Errors.....	65
4.3.7 Heading Errors	65
5 NOISE FILTER AND TARGET ESTIMATOR MODELS	67
5.1 LOS RATE NOISE FILTERING BY FIRST ORDER FADING MEMORY FILTERS	67
5.2 TARGET STATE ESTIMATION VIA THIRD ORDER FADING MEMORY FILTERS	69
5.2.1 Target Position Estimation.....	73
5.2.2 Target Velocity Estimation	75
5.2.3 Target Acceleration Estimation.....	76
6 GUIDANCE, AUTOPILOT AND MISSILE MANEUVER MODELS.....	79
6.1 A BRIEF INTRODUCTORY BACKGROUND ON PROPORTIONAL NAVIGATION.....	79
6.2 PROPORTIONAL NAVIGATION GUIDANCE LAW	80
6.3 EFFECTS OF EFFECTIVE NAVIGATION CONSTANT ON GUIDANCE PERFORMANCE	83
6.4 AUGMENTED PROPORTIONAL NAVIGATION GUIDANCE LAW	84
6.5 A NOVEL SUPPORTIVE GUIDANCE ALGORITHM TO BE APPLIED IN BLIND FLIGHT SCENARIOS.....	86
6.5.1 Attitude Control of Missile Airframe in Blind Flight	86
6.5.2 Geometric Illustration of the Developed Novel Algorithm	87
6.5.3 Explicit Explanation of the Method from Mathematical Point of View ..	90
6.5.4 Discussion on Benefits of the Novel Algorithm	93

6.6 AUTOPILOT MODEL	93
6.7 MISSILE MANEUVER MODEL.....	99
7 SIMULATION RESULTS.....	101
7.1 END-GAME PLOTS OF PURSUER AND EVADER FOR DISTINCT TARGET MANEUVER TYPES AND GUIDANCE SCENARIOS	101
7.2 MONTE CARLO SIMULATIONS AND MISS DISTANCE ANALYSIS.....	113
7.2.1 Comparison of Target Maneuver Models	115
7.2.2 Comparison of Engagement Scenarios.....	130
7.2.3 Comparison of Noise and Error Models.....	138
7.2.4 Comparison of Seeker Models	152
7.2.5 Comparison of Target Estimator Models	159
7.2.6 Comparison of Guidance Law Algorithms	164
8 CONCLUSION.....	181
8.1 EVALUATION OF MODELING AND SIMULATION STUDIES	181
8.2 SUMMARY OF OUTCOMES.....	182
8.3 RECOMMENDATIONS FOR FURTHER WORK.....	184
REFERENCES	185
APPENDICES	
A. COORDINATE TRANSFORMATIONS	187
A.1 Coordinate Transformation from Inertial Reference Frame to Line of Sight Frame	187
A.2 Coordinate Transformation from Line of Sight Frame to Inertial Reference Frame	189

LIST OF TABLES

TABLES

Table 7-1: Guidance Performance Index for Target Maneuver Comparisons	118
Table 7-2: Guidance Performance Index for Engagement Scenario Comparisons.	132
Table 7-3: Guidance Performance Index for Noise and Error Comparisons	141
Table 7-4: Guidance Performance Index for Seeker Model Comparisons	153
Table 7-5: Guidance Performance Index for Target Estimator Comparisons.....	160
Table 7-6: Guidance Performance Index for Guidance Algorithm Comparisons..	168

LIST OF FIGURES

FIGURES

Figure 1.1: Henschel Hs. 298 Missile	2
Figure 1.2: Ruhrstahl Kramer X4 Missile	2
Figure 1.3: Rheintochter R-1 Missile	3
Figure 1.4: Schmetterling Missile	3
Figure 1.5: Enzian Missile	4
Figure 1.6: Radio Control of Wasserfall Missile	4
Figure 1.7: Feuerlilie Missile on Launch Bed.....	5
Figure 1.8: Missile Types and Classification	6
Figure 1.9: Basic Types of Homing Missile Guidance	8
Figure 2.1: Missile Homing Loop Simulink Diagram	11
Figure 3.1: $5g$ Step Target Maneuver	17
Figure 3.2: Piecewise Continuous Step Maneuver.....	18
Figure 3.3: Ramp Target Maneuver	19
Figure 3.4: Weaving Target Maneuver	20
Figure 3.5: Derivation of Position from Acceleration.....	20
Figure 4.1: The Representation of Inertial Reference Frame in Air Engagement ...	22
Figure 4.2: Line of Sight Frame	24
Figure 4.3: The Effect of LOS Angle in Missile Guidance	26
Figure 4.4: Range vs Time Variation for a Successful Interception	27
Figure 4.5: Closing Velocity vs Time Variation for a Successful Interception	28
Figure 4.6: LOS Angle Psi vs Time Variation for a Successful Interception	29
Figure 4.7: LOS Angle Theta vs Time Variation for a Successful Interception.....	30
Figure 4.8: Spherical Coordinate Sytem Representation	31
Figure 4.9: Gimbaled Infrared Seeker of Short-Range Infrared IRIS-T Missile	34
Figure 4.10: Gimbal and Field of View Angles of a Two-Axis Gimbaled Seeker.	34
Figure 4.11: Field of View and Field of Regard Concepts	35

Figure 4.12: Seeker Types	37
Figure 4.13: Seeker Frequency Bands	38
Figure 4.14: Two-Axis (2-DoF) Gyro Frame	39
Figure 4.15: Roll-Pitch-Yaw Motion of a 3-DoF Gimbal Frame	39
Figure 4.16: Phased Array Antenna Electromagnetic Beam Steering	40
Figure 4.17: Angular Geometry of Missile Seeker	41
Figure 4.18: Block Diagram Model of a Gimbaled Seeker	43
Figure 4.19: Gimbaled Seeker Representation for Azimuth.....	44
Figure 4.20: Gimbaled Seeker Representation for Elevation	44
Figure 4.21: Azimuth Look Angle Variation with Flight Time.....	45
Figure 4.22: Azimuth Gimbal Angle Variation with Flight Time	46
Figure 4.23: Elevation Look Angle Variation with Flight Time	46
Figure 4.24: Elevation Gimbal Angle Variation with Flight Time.....	46
Figure 4.25: Noisy Azimuth LOS Rate Estimation	47
Figure 4.26: Noisy Elevation LOS Rate Estimation	47
Figure 4.27: Azimuth LOS Angle vs Flight Time	51
Figure 4.28: Elevation LOS Angle vs Flight Time	51
Figure 4.29: Second Order Fading Memory Filter Application for Azimuth.....	52
Figure 4.30: Azimuth LOS Rate vs Flight Time.....	52
Figure 4.31: Second Order Fading Memory Filter Application for Elevation	53
Figure 4.32: Elevation LOS Rate vs Flight Time	53
Figure 4.33: Gaussian Angular Noise Generation	55
Figure 4.34: Laplacian Angular Noise Generation	55
Figure 4.35: Gaussian + Laplacian Angular Noise Generation	56
Figure 4.36: Glint Noise.....	56
Figure 4.37: Range-Dependent Glint Noise Generation	57
Figure 4.38: Azimuth LOS Angle Corrupted by Range-Dependent Glint Noise	57
Figure 4.39: Elevation LOS Angle Corrupted by Range-Dependent Glint Noise...	58
Figure 4.40: Eclipsing Effect	59
Figure 4.41: Range-Dependent Receiver Noise Generation.....	61

Figure 4.42: Azimuth LOS Angle Corrupted by Range-Dependent Receiver Noise	61
Figure 4.43: Elevation LOS Angle Corrupted by Range-Dependent Receiver Noise	62
Figure 4.44: Azimuth LOS Rate Corrupted by Sinusoidal Noise	62
Figure 4.45: Elevation LOS Rate Corrupted by Sinusoidal Noise.....	63
Figure 4.46: Missile-Target Range Corrupted by Random Gaussian Noise	63
Figure 4.47: Compromise Radome Model.....	64
Figure 4.48: Radome-Boresight Error.....	65
Figure 5.1: First Order Fading Memory Filter Application for Azimuth LOS Rate Noise Filtering	68
Figure 5.2: Azimuth LOS Rate Filtered by First Order Fading Memory Filter.....	69
Figure 5.3: Elevation LOS Rate Filtered by First Order Fading Memory Filter	69
Figure 5.4: Third Order Fading Memory Filter Application for Target Estimation	71
Figure 5.5: Target Position Estimation along X_{ref} by 3 rd Order Fading Memory Filter.....	73
Figure 5.6: Target Position Estimation along Y_{ref} by 3 rd Order Fading Memory Filter.....	74
Figure 5.7: Target Position Estimation along Z_{ref} by 3 rd Order Fading Memory Filter.....	74
Figure 5.8: Target Velocity Estimation along X_{ref} by 3 rd Order Fading Memory Filter.....	75
Figure 5.9: Target Velocity Estimation along Y_{ref} by 3 rd Order Fading Memory Filter.....	75
Figure 5.10: Target Velocity Estimation along Z_{ref} by 3 rd Order Fading Memory Filter.....	76
Figure 5.11: Target Acceleration Estimation along X_{ref} by 3 rd Order Fading Memory Filter.....	77
Figure 5.12: Target Acceleration Estimation along Y_{ref} by 3 rd Order Fading Memory Filter.....	77

Figure 5.13: Target Acceleration Estimation along Z_{ref} by 3 rd Order Fading Memory Filter.....	78
Figure 6.1: Parallel Navigation	79
Figure 6.2: Proportional Navigation Guidance for a Planar Engagement	81
Figure 6.3: Proportional Navigation Guidance for a Spatial Engagement	82
Figure 6.4: Effect of N' on Missile Flight Path	83
Figure 6.5: Geometric Illustration of the Novel Method	88
Figure 6.6: Simulink Representation of the Novel Algorithm for Azimuth	92
Figure 6.7: Angle of Attack and Forces Acting on Missile	96
Figure 6.8: Angular Variations with Flight Time	98
Figure 6.9: Drag and Lift Force Variation with Flight Time	98
Figure 6.10: Missile Speed Variation with Flight Time	99
Figure 7.1: 5g Step Maneuvering Target.....	101
Figure 7.2: Hard Pull Return Target Maneuver	102
Figure 7.3: Target's Evasive Maneuver along all Directions	103
Figure 7.4: Piecewise Step Target Maneuver	103
Figure 7.5: Altitude Gaining Target.....	104
Figure 7.6: Target's Nose Dive Maneuver.....	105
Figure 7.7: 5g Weaving Maneuver of the Target in Horizontal Plane	105
Figure 7.8: 3.5g Weaving Maneuver of the Target in Vertical Plane	106
Figure 7.9: Guidance Scenario with 'Mid-Course Guidance' Condition	107
Figure 7.10: Missile Acceleration Components along Inertial Axes	107
Figure 7.11: Missile Latax Components along LOS Axes	108
Figure 7.12: Head-on Engagement	108
Figure 7.13: Air-to-Air Engagement.....	109
Figure 7.14: Delayed Target Maneuver	110
Figure 7.15: Target Making Combined Maneuver Types.....	110
Figure 7.16: Target Making Fast Circular Motion.....	111
Figure 7.17: Lateral Acceleration Demand of Missile in Azimuth	112
Figure 7.18: Target Switching in between Maneuver Types	113

Figure 7.19: Miss Distance Histogram for Case 1	119
Figure 7.20: Miss Distance Histogram for Case 2	120
Figure 7.21: Miss Distance Histogram for Case 3	121
Figure 7.22: Miss Distance Histogram for Case 4	122
Figure 7.23: Miss Distance Histogram for Case 5	123
Figure 7.24: Miss Distance Histogram for Case 6	124
Figure 7.25: Miss Distance Histogram for Case 7	125
Figure 7.26: Miss Distance Histogram for Case 8	126
Figure 7.27: Miss Distance Histogram for Case 9	127
Figure 7.28: Miss Distance Histogram for Case 10	133
Figure 7.29: Miss Distance Histogram for Case 11	134
Figure 7.30: Miss Distance Histogram for Case 12	135
Figure 7.31: Miss Distance Histogram for Case 13	136
Figure 7.32: Miss Distance Histogram for Case 14	142
Figure 7.33: Miss Distance Histogram for Case 15	143
Figure 7.34: Miss Distance Histogram for Case 16	144
Figure 7.35: Miss Distance Histogram for Case 17	145
Figure 7.36: Miss Distance Histogram for Case 18	146
Figure 7.37: Miss Distance Histogram for Case 19	147
Figure 7.38: Miss Distance Histogram for Case 20	148
Figure 7.39: Miss Distance Histogram for Case 21	149
Figure 7.40: Miss Distance Histogram for Case 22	150
Figure 7.41: Miss Distance Histogram for Case 23	154
Figure 7.42: Miss Distance Histogram for Case 24	155
Figure 7.43: Miss Distance Histogram for Case 25	156
Figure 7.44: Miss Distance Histogram for Case 26	157
Figure 7.45: Miss Distance Histogram for Case 27	161
Figure 7.46: Miss Distance Histogram for Case 28	162
Figure 7.47: Miss Distance Histogram for Case 29	169
Figure 7.48: Miss Distance Histogram for Case 30	170
Figure 7.49: Miss Distance Histogram for Case 31	171

Figure 7.50: Miss Distance Histogram for Case 32	172
Figure 7.51: Miss Distance Histogram for Case 33	173
Figure 7.52: Miss Distance Histogram for Case 34	174
Figure 7.53: Miss Distance Histogram for Case 35	175
Figure 7.54: Miss Distance Histogram for Case 36	176
Figure 7.55: Miss Distance Histogram for Case 37	177
Figure 7.56: Miss Distance Histogram for Case 38	178
Figure A.1: Coordinate Transformation from Inertial Reference Frame to Line of Sight Frame	187
Figure A.2: Coordinate Transformation from Line of Sight Frame to Inertial Reference Frame.....	189

LIST OF SYMBOLS

SYMBOLS

A, B, C	Nonzero constants
K	Nonzero slope constant
A_m	Maneuver amplitude
w_t	Weave frequency
t	Time
$t_m, t_{m1}, t_{m2}, t_{m3}$	Maneuver times
t_f	Final flight time
a_T	Target acceleration
v_T	Target velocity
v_{T_0}	Initial target velocity
R_T	Target position
R_{T_0}	Initial target position
R_M	Missile position
R_{MT}	Missile-to-target range
X_{ref}	X axis of the inertial reference frame
Y_{ref}	Y axis of the inertial reference frame
Z_{ref}	Z axis of the inertial reference frame
X_{ref_tr}	X axis of the translated inertial reference frame
Y_{ref_tr}	Y axis of the translated inertial reference frame
Z_{ref_tr}	Z axis of the translated inertial reference frame
X_{LOS}	X axis of the line of sight frame
Y_{LOS}	Y axis of the line of sight frame
Z_{LOS}	Z axis of the line of sight frame
ψ	Azimuth angle

θ	Elevation angle
$\dot{\psi}$	Time rate of azimuth angle
$\dot{\theta}$	Time rate of elevation angle
$\vec{r}_{M/IRF}$	Missile position vector as expressed in inertial reference frame
x_M	Missile position along X_{ref}
y_M	Missile position along Y_{ref}
z_M	Missile position along Z_{ref}
\vec{i}_{IRF}	Unit vector along X_{ref}
\vec{j}_{IRF}	Unit vector along Y_{ref}
\vec{k}_{IRF}	Unit vector along Z_{ref}
$\vec{r}_{T/IRF}$	Target position vector as expressed in inertial reference frame
x_T	Missile position along X_{ref}
y_T	Missile position along Y_{ref}
z_T	Missile position along Z_{ref}
$\vec{r}_{rel/IRF}$	Relative range vector as expressed in inertial reference frame
x_{MT}	Missile-target position along X_{ref}
y_{MT}	Missile-target position along Y_{ref}
z_{MT}	Missile-target position along Z_{ref}
\vec{r}_{rel}	Relative range vector
\vec{r}_T	Target position vector
\vec{r}_M	Missile position vector
\vec{r}_{MT}	Missile-target position vector
$\vec{r}_{rel/LOS}$	Relative range vector as expressed in LOS frame
\vec{i}_{LOS}	Unit vector along X_{LOS}
$\vec{v}_{rel/IRF}$	Relative velocity vector as expressed in inertial reference frame
$\vec{v}_{rel/LOS}$	Relative velocity vector as expressed in line of sight frame

R	Range
V_c	Closing velocity
V_M	Missile velocity
$\vec{\omega}_{LOS/IRF}$	Angular velocity of line of sight frame with respect to inertial reference frame
$\theta_{m_{pitch}}$	Missile body angle in pitch plane
$\dot{\theta}_{m_{pitch}}$	Missile body rate in pitch plane
$\theta_{g_{pitch}}$	Missile gimbal angle in pitch plane
ε_{pitch}	Angular measurement error in pitch plane
$\theta_{m_{yaw}}$	Missile body angle in yaw plane
$\dot{\theta}_{m_{yaw}}$	Missile body rate in yaw plane
$\theta_{g_{yaw}}$	Missile gimbal angle in yaw plane
ε_{yaw}	Angular measurement error in yaw plane
λ_w	Wavelength
c	Speed of light
f	Frequency of oscillations
\vec{L}_M	Angular momentum
\vec{I}	Moment of inertia
\vec{w}	Angular velocity
$\vec{\tau}_{ext}$	External torque
\vec{r}	Lever arm
\vec{F}	Applied force
λ	Sightline angle
θ_B	Body attitude angle
θ_D	Seeker dish angle
σ_G	Gimbal angle
σ_L	Look angle
ε	Tracking error

α	Angle of attack
α_{trim}	Angle of attack for trim flight condition
γ	Flight path angle
$\dot{\gamma}$	Flight path angle rate
$\dot{\alpha}$	Angle of attack rate
$\dot{\theta}_D$	Time rate of seeker dish angle
$\dot{\theta}_B$	Time rate of body attitude angle
$\dot{\sigma}_G$	Time rate of gimbal angle
$\dot{\lambda}$	Time rate of sightline angle
τ_s	Seeker track-loop time constant
$\dot{\theta}_{D_c}$	Time rate of commanded dish rate
ε_m	Measured tracking error
$\dot{\varepsilon}_D$	Dish rate error
K_s	Stabilization gain
G_{gyro}	Rate gyro transfer function
K_g	Rate gyro gain
ξ	Damping ratio
ω_n	Natural frequency
\hat{x}_n	Current state estimation
\hat{x}_{n-1}	Previous state estimation
$\hat{\dot{x}}_n$	Current state rate estimation
$\hat{\dot{x}}_{n-1}$	Previous state rate estimation
$\hat{\ddot{x}}_n$	Current rate of state rate estimation
$\hat{\ddot{x}}_{n-1}$	Previous rate of state rate estimation
x_n^*	Current state measurement
β	Filter memory length
T_s	Sampling rate
G_F, H_F, K_F	Constant filter gains
w	Random number

w_g	Gaussian noise
C_g	Gaussian noise multiplier constant
σ_g	Standard deviation of Gaussian noise for glint
\bar{w}	Mean of w
σ_w	Standard deviation of w
w_{lap}	Laplacian noise
M_{lap}	Laplacian noise multiplier variable
C_{lap}	Laplacian noise multiplier constant
σ_{lap}	Standard deviation of Laplacian noise
w_{Glint}	Glint noise
ρ_G	Glint probability
σ_R	Standard deviation of Gaussian noise for receiver angle tracking noise
τ_C	Cyclic time
N_{sin}	Sinusoidal noise
A_{sin}	Amplitude of sinusoidal noise
w_{sin}	Frequency of sinusoidal noise
P_{sin}	Phase of sinusoidal noise
B_{sin}	Bias term for sinusoidal noise
$N_{Gaussian}$	Gaussian noise
μ	Mean of Gaussian noise
σ^2	Variance of Gaussian noise
ε_{bse}	Radome-boresight error
K_R	Slope of the dome
P_o	Initial covariance matrix
\hat{y}_k	Current target position estimation
$\hat{\dot{y}}_k$	Current target velocity estimation
\hat{n}_{T_k}	Current target acceleration estimation
\hat{y}_{k-1}	Previous target position estimation

\hat{y}_{k-1}	Previous target velocity estimation
$\hat{n}_{T_{k-1}}$	Previous target acceleration estimation
$n_{c_{k-1}}$	Previous commanded missile acceleration
y_k^*	Current target position measurement
K_{1k}, K_{2k}, K_{3k}	<i>Kalman</i> gains
M_k	Covariance matrix of errors in the estimates after updates
P_k	Covariance matrix of errors in the estimates before updates
Q_k	Process noise matrix
R_k	Variance of the measurement noise
K_k	<i>Kalman</i> gain matrix
Φ_k	Fundamental matrix
H	Measurement matrix
N'	Effective navigation constant
N	Navigation ratio
$A_{M_{PNGL}}$	Lateral missile acceleration calculated by PNGL
y	Relative missile-target separation
t_{go}	Time to go
A_T	Estimated target acceleration
$A_{M_{APNGL}}$	Lateral missile acceleration calculated by APNGL
LOS_I	Initial line of sight
LOS_F	Final line of sight
R_I	Range before blind flight
R_F	Final range
β_I	Look angle before blind flight
β_F	Final look angle
λ_I	LOS angle before
λ_F	Final LOS angle
B_I	Body attitude before blind flight
B_F	Final body attitude

M_I	Missile position before blind flight
M_F	Final missile position
ϕ	Relaxation angle
S	Lateral distance
$V_{M_{LOS}}$	Missile velocity along LOS axis
$A_{M_{LOS}}$	Missile acceleration along LOS axis
TTG_{est}	Time-to-go estimation
V_{C_I}	Closing velocity before blind flight
TF_{AC}	Autopilot control system transfer function
τ_{AC}	Autopilot control system time constant
V_{M_X}	Missile velocity along X_{ref}
V_{M_Y}	Missile velocity along Y_{ref}
V_{M_Z}	Missile velocity along Z_{ref}
D	Drag force
L	Lift force
T	Thrust force
C_D	Drag coefficient
ρ	Air density
A_{cs}	Cross-sectional area of the missile
C_L	Lift coefficient
$C_{L\alpha}$	Lift coefficient per angle of attack
β_s	Sideslip angle
g	Gravitational acceleration
m	Mass of the missile
X_{int}	X axis of the intermediate frame
Y_{int}	Y axis of the intermediate frame
Z_{int}	Z axis of the intermediate frame
\hat{R}_Y	Rotation matrix for rotation about Y_{int}
\hat{R}_Z	Rotation matrix for rotation about Z_{ref}

$\hat{T}_{IRF-LOS}$	Transformation matrix from inertial reference frame to line of sight frame
$\hat{T}_{LOS-IRF}$	Transformation matrix from line of sight frame to inertial reference frame

LIST OF ABBREVIATIONS

ABBREVIATIONS

BMW	Bayerische Motoren Werke
E/O	Electro-Optical
IR	Infrared
RF	Radio Frequency
LOS	Line of Sight
IMU	Inertial Measurement Unit
PNGL	Proportional Navigation Guidance Law
INS	Inertial Navigation System
IRF	Inertial Reference Frame
M	Missile
T	Target
O	Origin of the Inertial Reference Frame
PN	Proportional Navigation
FoV	Field of View
FoR	Field of Regard
DoF	Degree of Freedom
EM	Electromagnetic
APNGL	Augmented Proportional Navigation Guidance Law
<i>BW</i>	Bandwidth
<i>NUM</i>	Number
<i>SNR</i>	Signal-to-Noise Ratio
<i>HE</i>	Heading Error
RCS	Radar Cross Section
Mr	Milliradian
USA	United States of America
ZEM	Zero Effort Miss

LATAX	Lateral Acceleration
BTT	Bank-to-Turn
STT	Skid-to-Turn
CW	Clockwise
CCW	Counter Clockwise

CHAPTER 1

INTRODUCTION

Science, on its own, is neither good nor evil; but can be used both ways.

1.1 A Brief Look at Homing Guidance and Its Historical Development

The main idea beyond the development of homing guidance technique is to guide the missile in order to intercept non-stationary targets that can handle evasive maneuvers in an unpredictable manner. In all types of homing guidance, an onboard sensor, namely a seeker, is utilized to provide target data so as to ensure target acquisition and tracking by the missile. The process of intercepting a highly maneuverable target requires continuous estimation regarding the target's location in space relative to the missile and a responsive attitude by the missile to any changes. In most cases, a target estimator plays a crucial role in post-processing of the sensed data to make reasonable predictions about the target's states. By the nature of homing guidance, as the missile gets closer to the target, the quality of the real time information obtained from the seeker related to the target states generally improves and, as a result, a superior intercept accuracy is likely to be achieved compared to any other form of missile guidance [1].

The origins of homing guidance date back to the end of World War II. At that time, the Germans were endeavoring to develop the first surface-to-air and air-to-air tactical guided missiles in history. For instance, the Hs. 298 was one of the air-to-air guided missiles developed by the Henschel Company and used radio-control as the guidance method [2]. It had a range of about one mile and required two crews on the launch aircraft in order to control its motion. One operator used a reflector-

type sight to aim at the target and the other controlled the missile via a joystick and another sight paired to the first one with a servo system [3].



Figure 1.1: Henschel Hs. 298 Missile [4]

The Ruhrstahl X-4, the successor of the Hs. 298, was another short range air-to-air guided missile designed by Germany during World War II. It implemented wire control mechanism as a guidance system and the range of attack was to be between 1.5 km and 3.5 km. A liquid rocket motor manufactured by BMW was integrated to the missile to provide thrust for 17 seconds. The warhead it carried was 20 kg with a lethal radius of about 8 m. Since the impact area was limited considering the relatively larger operational range of the missile, an acoustical proximity fuze, known as Kranich, with trigger range of 7 m was mounted into the nose of the missile in order to detonate the warhead to cause severe damage [5].

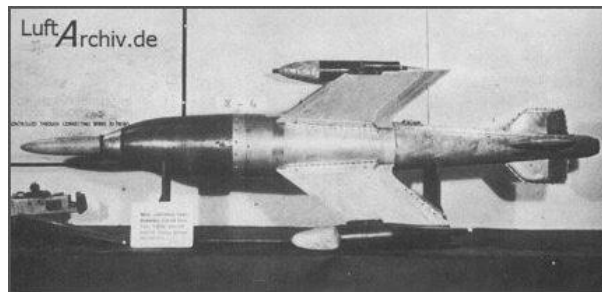


Figure 1.2: Ruhrstahl Kramer X4 Missile [4]

The two abovementioned missiles did not see any operational service and thus were not proven in air combat.

Rheintochter R-1, Enzian, Schmetterling, Wasserfall and Feuerlilie were all surface-to-air anti-aircraft missiles produced by Germany during World War II. Rheintochter R-1 missile was visually oriented and guided by an operator with the help of six flares located on the wingtips. Radio commands were used to control the path of the missile [6]. However, the Rheintochter R-1 missile was ineffective since R-1's intended targets flew above its 6 km range [2].

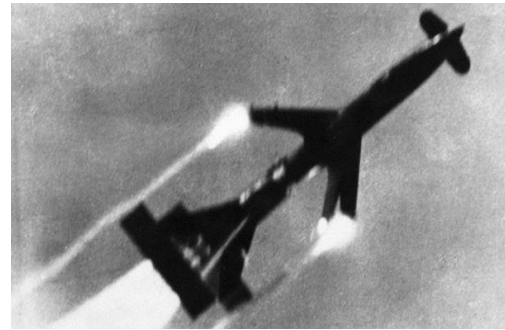


Figure 1.3: Rheintochter R-1 Missile [7]

Likewise, for the guidance and control of the Schmetterling missile, an operator used a telescopic sight and radio control to convey radio signals from a handheld joystick to the distant receiver located in the missile [8].



Figure 1.4: Schmetterling Missile [9]

The Enzian was the first missile that used infrared guidance system while carrying a gigantic 500 kg warhead having a lethal radius of 45 m [8].



Figure 1.5: Enzian Missile [10]

The supersonic Wasserfall was gyroscopically controlled in roll, pitch and yaw and guided by a ground operator who steered the missile by sending radio links [11].

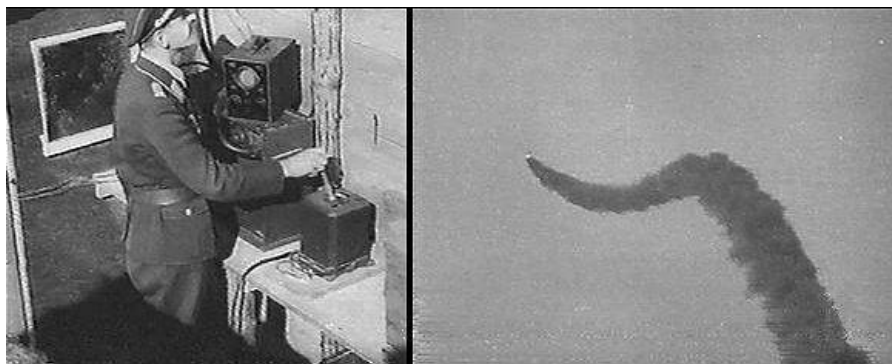


Figure 1.6: Radio Control of Wasserfall Missile [11]

Another anti-aircraft missile was the Feuerlilie which was designed to operate at supersonic speed levels by making use of radio command guidance, but due to unstable flight behavior and technical problems including with the controller and the drive section, it never became operational [11].

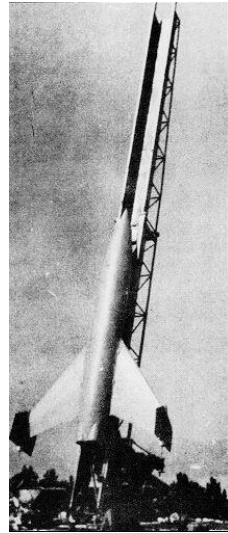


Figure 1.7: Feuerlilie Missile on Launch Bed [11]

Homing guidance technology has made a great deal of progress over the past seven decades and today's tactical guided missile designs involve much more complex engineering work in terms of inertial and targeting sensors together with guidance and autopilot control systems.

1.2 Homing Missile Guidance Types

Homing guidance is a term used to describe a guidance process that can determine the certain position parameters of the evader with respect to the pursuer and can formulate its own commands to guide itself to the target in order to achieve a successful interception [12].

Homing missile guidance is an autonomous, also called fire-and-forget, operation in which target motion is sensed by a seeker located on the pursuer missile, thus making the guidance performance prone to seeker noise and errors. Homing could be either used only for terminal phase guidance of missiles or for the entire flight, particularly for the cases where the target is positioned within the lock-on range of the seeker at the time of launch as so for the short-range missiles [12].

Homing systems may be classified into three general categories depending on the source of the identifying energy and how the target is being illuminated:

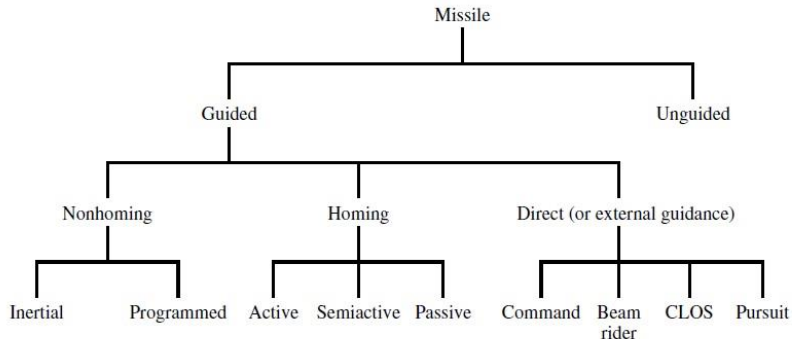


Figure 1.8: Missile Types and Classification [12]

1.2.1 Passive Guidance

In a passive homing system, the seeker detects the target by means of natural emanations or radiation such as heat waves, light waves or sound waves originated by the target [12]. Passive guidance is commonly exemplified by electro-optical (E/O) and infrared (IR) seekers. It is obvious that visual seekers are to be effective only if the target has adequate contrast with the background. Apparently, infrared homing is suitable for use against targets that present large temperature differentials with respect to their surroundings [12]. Passive seekers measure the angular direction of the target relative to the missile. Unfortunately, they do not readily provide any information about range-to-target or closing velocity (range rate) and should rely on other means for obtaining such data if necessary [1]. Most of the time, due to the fact that the energy is emitted by the target and not by the seeker, it is almost impossible for the target to determine if it is being tracked by a missile. On the other hand, it is easier for the target to deceive a passive seeker unit by dispensing flare decoys once it somehow realizes that it is being pursued by a missile. If deployed in the right way, such countermeasures may mislead a passive seeker to lock-on them instead of the target of interest.

1.2.2 Semi-Active Guidance

Semi-active guidance systems refer to cases where the target is being illuminated by an external beam of light, laser, IR or RF energy source. In semi-active guidance systems, usually an off-board tracking radar which may be ground-based, ship-borne or airborne, radiates energy to the target and the RF seeker in the nose of the missile senses the reflected energy and thus homes on the target [12]. In contrast to passive guidance, semi-active guidance technique makes range rate information, which is proportional to Doppler frequency, available to the tracking receiver while still providing the angular direction of the target in azimuth and elevation directions for three dimensional engagements. Another benefit of semi-active homing is that significantly huge amount of illuminating power can be transmitted to designate the target without adding to the size, weight and cost of the missile. Furthermore, inspite of comprising more complex and bulky equipment compared to the passive homing systems, it is possible to provide homing guidance over much greater ranges in semi-active guided systems [12].

1.2.3 Active Guidance

In active guidance systems, the missile both emits and senses the energy via its seeker. For instance, in active radar homing applications, both the transmitter and receiver devices are contained within the missile making it self-sufficient [12]. Above all, RF seekers are capable of supplying instantaneous range-to-go and closing velocity data in addition to the angular direction of the target and therefore, leading to an improvement in overall guidance accuracy [1]. Nevertheless, active homing missiles weigh and cost more. Besides, they are susceptible to jamming since their presence are revealed due to the energy they radiate. Power and weight considerations are the top-priority reasons beyond restriction of the use of active homing to terminal phase of guidance after the missile is brought to end-game with the help of other forms of guidance [12].

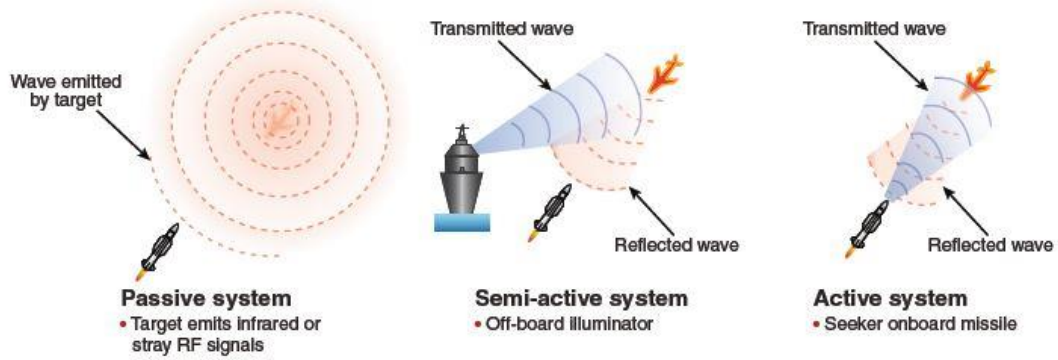


Figure 1.9: Basic Types of Homing Missile Guidance [1]

1.3 The Aim and Scope of the Study

This thesis aims to research how the homing guidance performance is being affected by the presence of challenging target maneuver together with the inevitable noise and error sources encountered in seeker data while elaborating on stochastic noise types.

The main focus is the active guidance systems where the relative missile to target range and closing velocity measurements are readily accessible in spite of being corrupted by the random error sources. Flight scenarios treated in this thesis represent distinct cases where the seeker is locked-on the target at the instant of launch and stays so for the entire flight until interception as well as the ones where the missile goes blind during some portion of its flight or the missile gets homed on the target only at the final section of its cruise, that is at the terminal phase of the whole guidance process. Remarkably, a novel, simply implemented and effective guidance algorithm is developed for the missile to get rid of the blind flight predicament so that the target appears in the field of vision of the seeker again and as soon as possible. For the purpose of studying highly maneuverable targets, several target maneuver models are proposed in the generated guidance scenarios. Due to imponderable nature of target maneuvers, the motion of the target being chased needs to be estimated to some extent and done so within the scope of this

study by employing filtering techniques that exist in literature. For the sake of completeness, *Monte Carlo* simulations wherein random noise models and different target maneuver models together with varied guidance scenarios were involved are also applied to test the performance of the mathematically modeled homing guidance loop.

1.4 The Outline of the Thesis

So far an effort was made to introduce the concept and types of homing guidance technique along with the historical background. Then, the purpose and scope of the study are presented in depth.

In Chapter 2, missile guidance system is treated as a closed-loop feedback loop in which all the necessary subsystems are embedded. The logic behind the closed-loop control system modeling is discussed and the significant roles of subsystems that take part in the homing guidance loop are explained by making a few introductory remarks.

Chapter 3 presents multiple realistic maneuver models for an air target. The acceleration of the target is assumed to obey any one or combination of these models that appear in the literature.

Chapter 4 starts by illustrating the relative kinematics between the pursuer and evader for three-dimensional engagements. Later, a review of seekers is made to provide information about the missions and the types of target sensors. Besides, models of gimbaled and strapdown seekers are demonstrated. Finally, the noise and error models are covered to show how the seeker data is corrupted by such effects. Detailed information about the noise and error sources is given in addition to their mathematical models.

Chapter 5 discusses the issue of target state estimation and LOS (line of sight) rate noise filtering with main emphasis on digital fading memory filters. It is

shown that the target acceleration can be estimated with sufficient precision for different target maneuver models provided that range measurements are available.

Chapter 6 focuses on the well-known “Proportional Navigation Guidance Law” while addressing to a special form of this guidance technique named “Augmented Proportional Navigation Guidance Law”. It is also noteworthy to state that a novel supportive algorithm for blind flight scenarios is mentioned comprehensively, which may be regarded as a contribution to the literature. In “Autopilot Model” section, instead of a detailed autopilot representation consisting of aerodynamics and airframe models, the relationship between the commanded and the achieved lateral acceleration is demonstrated via a 1st order transfer function since the main aim of this study is to focus on designing a seeker and a guidance system rather than an autopilot design. “Missile Maneuver Model” is also mentioned to indicate how the flight path of the pursuer is derived from the lateral acceleration outputs of the autopilot model which requires a proper transformation between the line of sight and inertial reference frames for simulation purposes.

Chapter 7 illustrates the end-game plots of the pursuer and the evader for challenging guidance scenarios. Furthermore, multiple-run *Monte Carlo* simulations are conducted to judge guidance system performance based on statistical approach since the aforementioned noise models represent random processes. Repeated simulation trials are also prepared to compare assumed target maneuver models, random noise models, designed seeker models, suggested target estimator models and implemented guidance law models in terms of the acquired final miss distance values.

Chapter 8 eventually wraps up the discussion of homing missile guidance system design by evaluating the simulation results and summarizing the outcomes of the whole study. Recommendations are also advised for the avid reader by making decent remarks on specific sections of the study that indeed represent an opportunity for further work.

CHAPTER 2

OVERVIEW OF MISSILE GUIDANCE SYSTEMS

2.1 Missile Guidance System Representation as a Closed-Loop Feedback System

In contrast to open loop control systems, closed-loop feedback control systems are capable of measuring the output and feeding it back for comparison with the desired reference input. In this sense, a missile homing guidance loop can be formulated as a feedback control system that regulates the line of sight angle rate to zero. In a missile guidance system, all the necessary measurements to ensure homing of the missile are provided via seeker and inertial measurement unit.

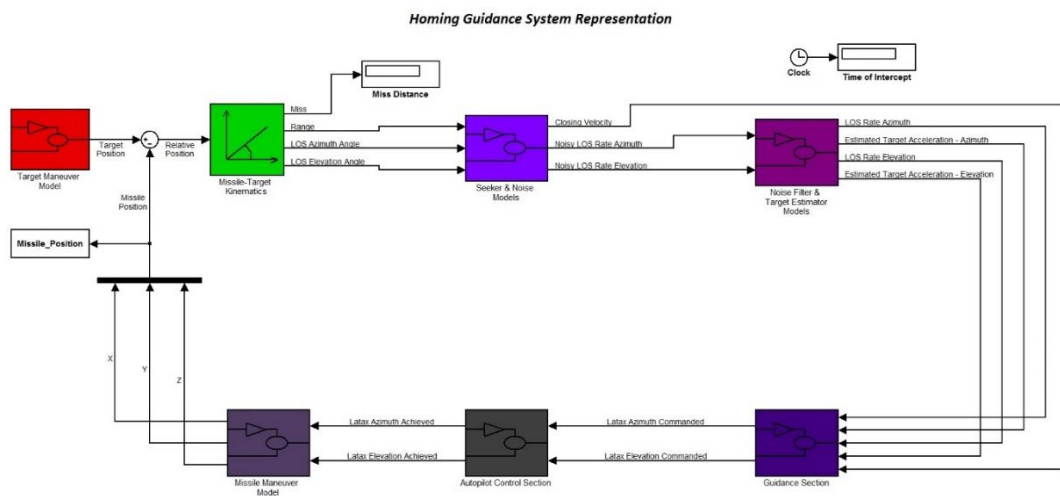


Figure 2.1: Missile Homing Loop Simulink Diagram

In the homing loop illustrated above, missile position is subtracted from target position to form a relative position which will come out to be the resultant

miss distance at the end of the flight simulation. Relative position could be formed in a similar way by integrating the difference between the target acceleration and the missile acceleration twice while taking the initial conditions related to velocity and position into consideration. In any case, the final relative distance between the missile and the target is desired to be close to zero for a successful interception. Here, target maneuver is considered as a disturbance rather than noise and the lateral acceleration commands of the missile as calculated by the mechanization of an approved guidance law can be regarded as the control inputs that try to keep LOS rate variation as small as possible by nulling out the effects of target maneuver which aim to alter the line of sight in order to avoid a collision.

2.2 Subcomponents of the Overall Missile Guidance Loop

As can be noticed from the missile homing loop block diagram shown in Figure 2.1, a missile guidance loop consists of several sections each of which plays a key role in pursuit-evasion scenarios. At this stage, the relationship between each of these subsystems is going to be explained briefly without going into too much detail.

To begin with, a realistic target model is needed. Since this study aims to develop a homing loop in which a highly maneuverable target is to be tracked, stationary or non-accelerating (constant velocity) targets are not taken into account.

Target and missile motion as resolved in inertial frame are combined mathematically to form the relative geometric relationships expressed in spherical-coordinate system for simplicity.

Afterwards, a terminal target sensor, typically an RF or IR seeker, measures the angles formed between the inertial reference frame and the missile-to-target line of sight vector. For three-dimensional engagements, pursuit action is scrutinized separately in two planes that always remain perpendicular to each other, hence leading to two LOS angles to be measured in azimuth and elevation directions. Range and range rate information can also be obtained based on the capabilities of

the seeker in use. Of course, the acquired seeker data is not perfect but noisy. Numerous noise types can be mathematically modeled to be added to the output signals of the seeker. Noisy LOS angle measurements are filtered continuously by a state estimator to determine the LOS rates in both azimuth and elevation directions.

Simultaneously, developed target estimator performs estimates of the target states, including the three acceleration components of the target along each inertial reference axis. Relative position and relative velocity estimates are also handled in a similar way, thus yielding nine estimated states in total. By the incorporation of the data taken from the precise Inertial Measurement Unit (IMU) with the relative state estimations, the position and velocity components of the target along inertial frame axes can as well be predicted with quite satisfactory accuracy.

Target acceleration estimations together with seeker measurements are all fed into the guidance law so that the required lateral acceleration components of the missile can be determined and commanded in two directions lying in azimuth and elevation planes and being perpendicular to the instantaneous missile-to-target line of sight.

Autopilot control system forces the missile to track the lateral acceleration guidance commands. By the effective use of aerodynamic control surfaces, the missile is steered towards the target for an interception, which is called the achieved missile motion.

Resulting missile motion and maneuvers of the target alters the relative spatial geometry which is sensed and processed by the missile seeker once again to ensure the continuity of the homing loop. Homing loop continues to operate until the closest point of approach between the pursuer and the evader is satisfied, whether or not a successful interception occurs.

Further details on each subsystem will be presented and discussed fully and sequentially in the forthcoming chapters.

CHAPTER 3

TARGET MANEUVER MODELS

From the viewpoint of pursuer, target maneuver is of a random nature and it is introduced to the homing loop as a disturbance contributing to the final miss distance. Mostly, a pursuer is needed to have an acceleration advantage over the evader of about three times in order to capture the target by the implementation of the Proportional Navigation Guidance Law (PNGL) [13].

The target may be maneuvering at the instant the missile is launched provided that it is aware of being locked-on by the missile seeker. The target may as well realize the pursuer after a while and start maneuvering arbitrarily a few seconds later than the missile launch time. Both cases will be demonstrated in this work.

Basically, there seem two possible engagement scenarios, namely head-on and tail-chase engagements, to encounter depending on how the missile and the target are situated at the beginning of the engagement and how the relative motion between the evader and the pursuer is likely to take place during the pursuit.

In head-on engagements, the target keeps flying towards the attacker while gaining altitude or nose diving with acceleration unknown to the pursuer. This situation makes it harder for IR homing missiles to be guided for a successful collision since hot engine exhaust emitted from the nozzle of the air target points away from the pursuer. Also for head-on engagement of active radar guided missiles, the radar cross section area of the target is much smaller so the seeker may not be able to track the target properly at its maximum lock-on range. Most notably from the kinematics perspective, missiles are likely to have a lower chance of hitting a target in this case due to the very high closure rates resulting from the combined speeds of the evader and the pursuer. Because of high approach rate, the missile

usually requires large lateral acceleration values to achieve which entails the risk of saturating the autopilot controllers. Moreover, target estimator gets very limited time to make reasonable state predictions corresponding to the motion of the target. The main advantage of the head-on engagement over the tail-chase engagement is the increased effective-use range of the missile.

In tail-chase engagements, also called rear-aspect engagements, the target flies away from the attacker while employing countermeasures and making evasive maneuvers to fool and get rid of the chaser. In this case, hot engine exhaust fumes are pointed directly at the pursuer and the infra-red seeker can track the target in a much simpler way. Furthermore, due to the reduced closure rate, the missiles have adequate time to sense and respond to any sudden evasive maneuvers, hence having a higher chance of hitting the target. Typically, missiles have much higher maneuvering capability compared to the aircrafts, and in a tail-chase engagement, the purposeful strategy of the evader could be to fly away from the missile fast enough to reduce the overtake rate while maintaining evasive maneuvers to force the missile to follow and run out its residual energy. From the point of view of the pursuer, the only disadvantage of the tail-chase engagement seems to be the relatively restricted effective-use range [19].

Both of the abovementioned engagement scenarios will be illustrated later in “Simulation Results” section.

The coming topics are going to exemplify the typical target acceleration models from the literature. The names of these models are also referred to the time rate of the acceleration which is denoted as jerk.

3.1 Constant Step Maneuver – Zero Jerk Model

A target may make constant magnitude step maneuver along one or multiple directions to escape from the pursuer. Due to constant acceleration, this model is referred to as “Zero Jerk Model”. Currently, aircrafts are capable of pulling a hard-turn maneuver of magnitude up to $10g$ temporarily and they can handle sustained $5g$ maneuvers. Pilots may be exposed to the risk of disorientation, dizziness and even fainting on condition that these acceleration values are to be exceeded.

$$a_T(t) := \begin{cases} 0, & \text{for } t \leq t_m \\ C, & \text{for } t_m < t \leq t_f \end{cases} \quad \begin{matrix} C \text{ is a nonzero constant} \\ t_m \text{ is the maneuver time} \\ t_f \text{ is the final flight time} \end{matrix} \quad (3.1)$$

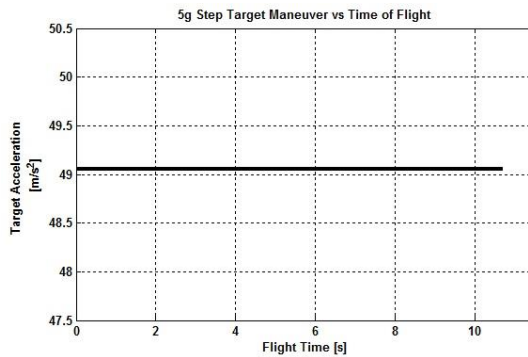


Figure 3.1: 5g Step Target Maneuver

3.2 Piecewise Continuous Step Maneuver

A target can change the magnitude of its acceleration periodically along one particular direction so that less time would be available for the target estimator to anticipate the maneuver behavior of the target with acceptable certainty. The figure below illustrates this situation as the target alters the magnitude of maneuver in between $-5g$ and $8g$ in 3 seconds time periods.

$$a_T(t) := \begin{cases} 0, & \text{for } t \leq t_{m1} \\ A, & \text{for } t_{m1} < t \leq t_{m2} \\ B, & \text{for } t_{m2} < t \leq t_{m3} \\ C, & \text{for } t_{m3} < t \leq t_f \end{cases} \quad \begin{matrix} \text{where } A, B, C \text{ are nonzero constants} \\ t_{m1}, t_{m2}, t_{m3} \text{ are the maneuver times} \\ t_f \text{ is the final flight time} \end{matrix} \quad (3.2)$$

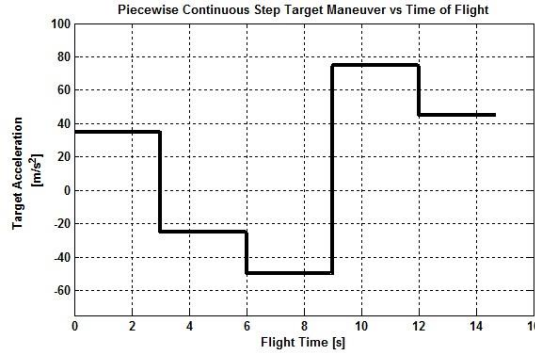


Figure 3.2: Piecewise Continuous Step Maneuver

3.3 Ramp Maneuver – Constant Jerk Model

Applying linearly increasing acceleration along one particular direction would be another strategy for an air target to evade from a pursuer. This kind of maneuver is known as “Constant Jerk Model” in literature. A target could perform such a maneuver model if it is boosting to attain a certain amount of speed during the engagement. Likewise, boost-phase ballistic missile defense could necessitate the examination of such models to engage and destroy the enemy missile while it is still boosting. The plot given below shows how the acceleration of the target varies linearly as it accelerates from $3g$ to $10g$ during the engagement.

$$a_T(t) := \begin{cases} 0, & \text{for } t \leq t_m \\ K \cdot t, & \text{for } t_m < t \leq t_f \end{cases} \quad \begin{matrix} \text{where } K \text{ is a nonzero slope constant} \\ t_m \text{ is the maneuver time} \\ t_f \text{ is the final flight time} \end{matrix} \quad (3.3)$$

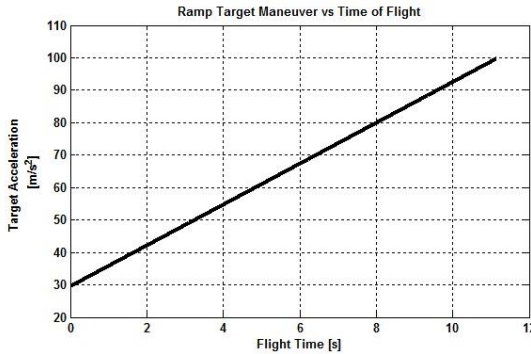


Figure 3.3: Ramp Target Maneuver

3.4 Weaving Maneuver – Variable Jerk Model

Low hit ratios coupled with large miss distances can be induced by the target if a weaving maneuver is initiated at a proper time before intercept. Since the acceleration of the target changes sinusoidally during this action, the model is entitled as “Variable Jerk Model”. Periodic maneuver sequences present a great deal of challenge for the target estimator being implemented as a part of the missile guidance system since the weave frequency in addition to maneuver amplitude is unknown to the pursuer. Accordingly, an increase in target weaving frequency usually yields larger miss distance values. It is also worthy to note that an increase in homing time does not guarantee a decline in the miss distance. In general, the safest and most effective method for improving miss distance performance against weaving targets is to reduce the flight-control system time constant, thus ending up with a more agile and responsive guidance system.

Acceleration capability and effective navigation ratio can be counted as the other major factors that play important role in determining guidance system performance against weaving targets as an increase in them favors the pursuer in most cases. Figure 3.4 shows the variation in acceleration of a weaving target with maneuver amplitude of $3g$ and a weave frequency of 1 rad/s .

$$a_T(t) := \begin{cases} 0, & t \leq t_m \\ A_m \sin w_t \cdot t, & t_m < t \leq t_f \end{cases} \quad \text{where } \begin{aligned} A_m &\text{ is maneuver amplitude} \\ w_t &\text{ is the weave frequency} \\ t_m &\text{ is the maneuver time} \\ t_f &\text{ is the final flight time} \end{aligned} \quad (3.4)$$

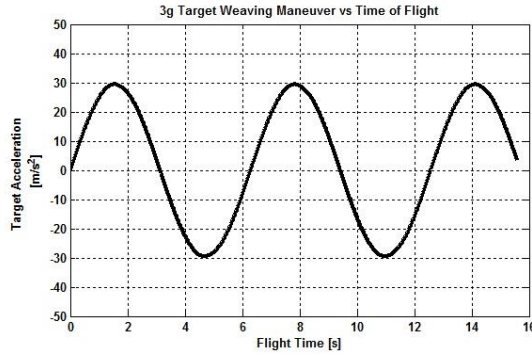


Figure 3.4: Weaving Target Maneuver

Once the target maneuver is modeled, it can be integrated twice with respect to time to obtain target velocity and target position in space. In order to carry out integration operations, initial velocity and initial position of the target are introduced to the equations of motion given in equations (3.5) and (3.6), respectively.

$$\text{Target Velocity} \rightarrow v_T(t) = v_{T_0} + \int_0^t a_T dt \quad (3.5)$$

$$\text{Target Position} \rightarrow R_T(t) = R_{T_0} + \int_0^t v_T dt \quad (3.6)$$

Resulting target position components are fed into homing loop to be considered in missile-target engagement kinematics calculations.

$$a_T \rightarrow \int_0^t \xrightarrow{\text{target velocity}} \int_0^t \xrightarrow{\text{target position}}$$

Figure 3.5: Derivation of Position from Acceleration

CHAPTER 4

MISSILE-TARGET KINEMATICS, SEEKER MODELING AND NOISE MODELS

4.1 Missile-Target Relative Spatial Kinematics

4.1.1 Inertial Reference Frame

An inertial reference frame is a reference frame that is neither accelerating nor rotating and in which *Newton's* laws of motion are valid. An Earth-fixed coordinate system can be regarded as an inertial reference frame for many problems of interest in missile dynamics under the assumption that the rotational velocity of the Earth is neglected [12]. An inertial reference frame can be arbitrarily positioned anywhere on the Earth. The choice of the reference frame is usually a matter of convenience for analytical investigation. All motion states of a dynamic model can be specified with respect to a reference frame. The origin of the reference frame is the stationary point from which the related states are measured. The axes of the reference frame are used to define the directions of measurements.

In this thesis, a right handed and orthogonal Cartesian reference frame is used to observe the kinematic relationships between the missile and the target. For instance, the position, velocity and acceleration states of the target are estimated with respect to a Cartesian reference frame by making use of a Cartesian guidance filter and then converted to a more suitable form to be readily used by the guidance algorithm. This conversion process is handled with the help of coordinate transformation methods. Equivalently, components of relative position, relative velocity and the acceleration of the target could be determined with respect to a

reference frame. Likewise, the Inertial Navigation System (INS) provides the motion states of the missile precisely, which include the position, velocity, acceleration, angular orientation and angular velocity of the missile. The provided states are also expressed in terms of reference frame of interest and act as supportive data for functionality of guidance and flight control systems. For the sake of simplicity, the origin of the inertial frame of reference is attached to the initial position of the missile at the time of launch. Figure 4.1 illustrates a tail-chase engagement and an inertial reference frame used to define motion states. The missile is launched from point O, the origin of the inertial reference frame, and directed towards the target.

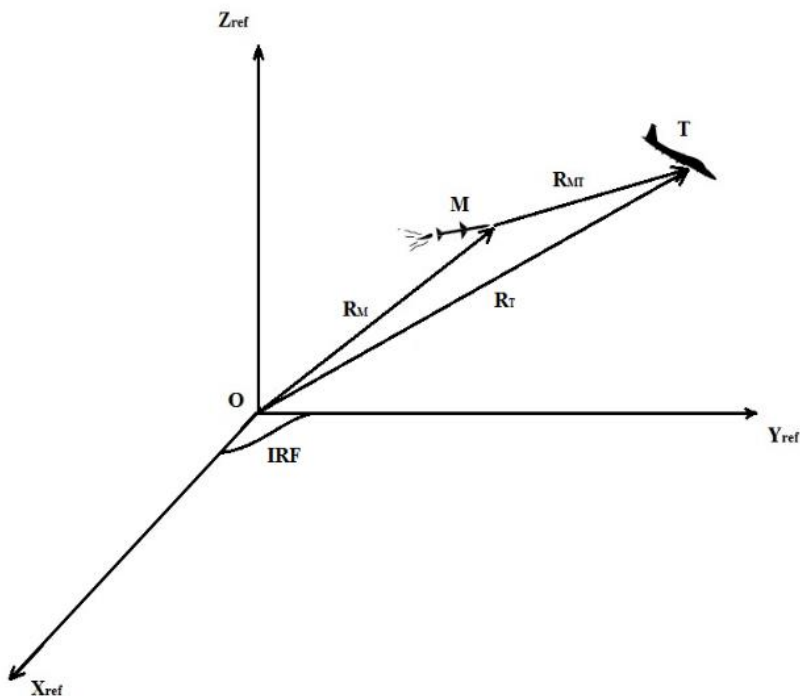


Figure 4.1: The Representation of Inertial Reference Frame in Air Engagement

4.1.2 Line of Sight Frame

Line of sight (LOS) frame is another useful frame considered in guidance applications during the formulation of the guidance rules. In contrast to inertial reference frame, line of sight frame is a non-stationary frame and its orientation in space changes continuously throughout the missile-target engagement. Line of sight frame can be regarded as a moving and rotating frame attached to the pursuer. It moves in accordance with the motion of the missile and rotates due to unsteady relative motion between the pursuer and the evader.

Line of sight frame is closely associated with the inertial reference frame and can be constructed from the launcher-fixed reference frame with two successive rotations of the reference frame. One rotation takes place about the Z_{ref} by an angle which is called azimuth angle (ψ) followed by another rotation about rotated axis - Y_{ref} by an angle called as elevation angle (θ) so that the X_{ref} axis becomes aligned with the X_{LOS} after two consecutive axis rotations. The rotations are carried out counterclockwise as suggested by the right-hand rule. It can be mathematically proved that the rotation sequences are interchangeable, that is the same line of sight frame is to be obtained if the rotation sequence is switched. Therefore, line of sight frame can be correlated with the inertial reference frame at every instant of an engagement and coordinate transformations can be handled in between the two frames of interest whenever required.

Appendices A.1 and A.2 cover the coordinate transformation operations from inertial reference frame to line of sight frame and vice versa, respectively. As can be seen from the Figure 4.2, the resultant X_{LOS} axis is directed from the missile right towards the target and similar to the inertial reference frame, LOS frame is right handed and orthogonal.

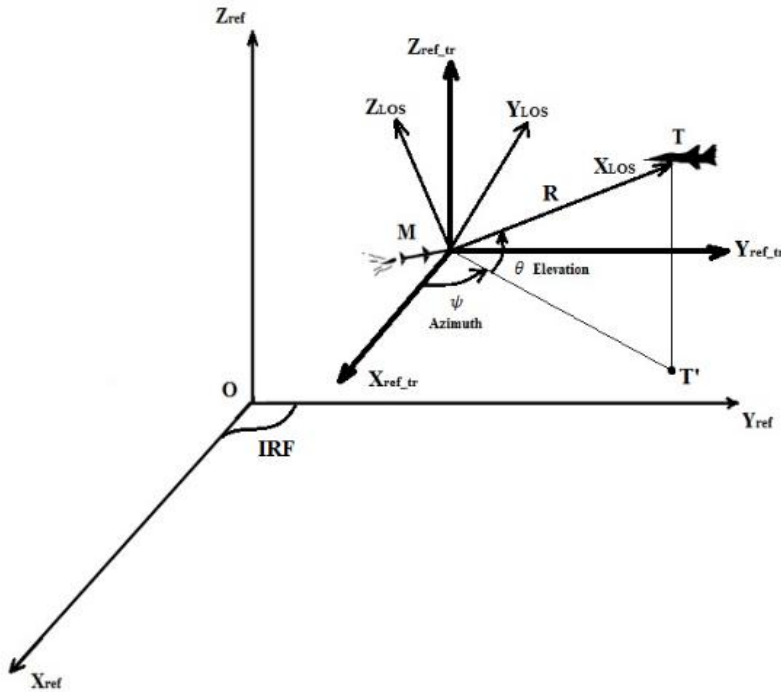


Figure 4.2: Line of Sight Frame

In order to present the relationship between the inertial and LOS frames conveniently, a reference frame, whose axes are marked as X_{ref_tr} , Y_{ref_tr} and Z_{ref_tr} , identical to the inertial reference frame is translated to coincide with the instantaneous missile position.

4.1.3 The Use of Line of Sight Concept in Missile Guidance Applications

There are plenty of guidance methods which employ line of sight concept as a primary source of guidance information. In this thesis, a special modified version of the well-known and widely used proportional navigation guidance is used wherein the LOS concept forms the basis for the development of the guidance law. Although the Proportional Navigation Guidance Law will be examined in detail later in Chapter 6, it is essential to point out the importance of the line of sight notion at

this stage with a few remarks which will assist during the discussion of the following topics.

In order to figure out why line of sight concept is helpful in an engagement, two moving bodies having different velocities and orientation can be considered. If two bodies are lying on the same plane and closing on each other, it can be concluded that they will eventually intercept if the sightline between the two does not rotate with respect to the inertial reference frame. By making use of similar triangles theorem, this fact can be proved with ease.

For three-dimensional engagements, the motion takes place in two planes, in azimuth and elevation planes, that are perpendicular to each other. This implies that the rates of azimuth and elevation LOS angles, $\dot{\psi}$ and $\dot{\theta}$, need to be forced to remain around zero. Equivalently, both of the LOS angles should be kept almost constant.

For an ideal case where nonmaneuvering bodies approach each other with constant velocities, a collision is inevitable. Obviously, constant LOS angles will be maintained throughout the collision course leading to “Parallel Navigation”.

However, in real homing guidance scenarios, most probably the target will be a maneuvering one. Target may accelerate or decelerate in various directions so that its velocity vector will change both its magnitude and direction over time yielding an eventual change in its position. Such sudden maneuvers will try to alter the LOS angles intentionally to avoid collision. In this case, the pursuer will have to do a corrective maneuver, of course with a certain amount of lag, to stay on the collision course with the target.

Abovementioned cases are illustrated geometrically in Figure 4.3.

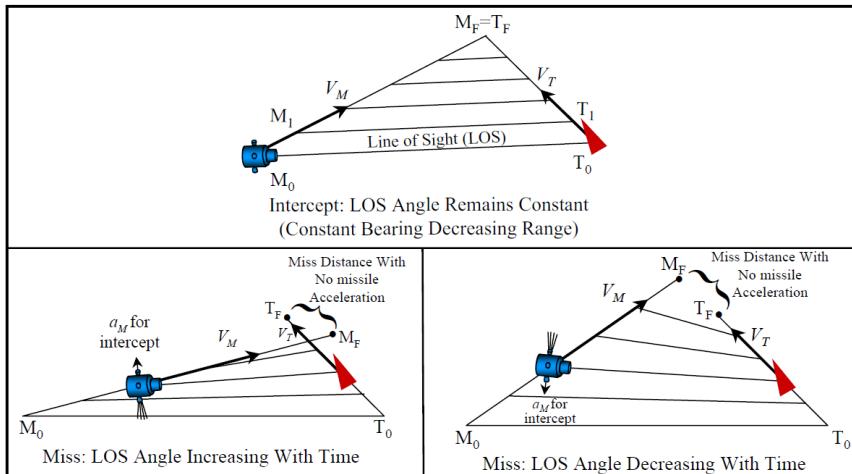


Figure 4.3: The Effect of LOS Angle in Missile Guidance [14]

4.1.4 Determination of Relative Range, Range Rate and Azimuth-Elevation LOS Angles

Not all seekers have the capability to measure range and range rate information. Active and semi-active RF seekers use Doppler frequency of the target return to make decent predictions of closing velocity. In pulsed radar systems, the range to a target is determined by using pulse-timing techniques. This is accomplished by measuring the time delay between transmission of an RF pulse and the reception of the pulse echo from the target [12]. Laser rangefinders can also be employed for the same purpose.

Relative range vector can be expressed either in fixed inertial reference frame or in moving line of sight frame as given below through equations from (4.1) to (4.5).

$$\vec{r}_{M/IRF} = x_M \vec{i}_{IRF} + y_M \vec{j}_{IRF} + z_M \vec{k}_{IRF} \quad (4.1)$$

$$\vec{r}_{T/IRF} = x_T \vec{i}_{IRF} + y_T \vec{j}_{IRF} + z_T \vec{k}_{IRF} \quad (4.2)$$

$$\vec{r}_{rel/IRF} = x_{MT} \vec{i}_{IRF} + y_{MT} \vec{j}_{IRF} + z_{MT} \vec{k}_{IRF} \quad (4.3)$$

$$\vec{r}_{rel} = \vec{r}_T - \vec{r}_M = \vec{r}_{MT} \quad (4.4)$$

$$\vec{r}_{rel/LOS} = R \vec{i}_{LOS} \quad (4.5)$$

Figure 4.4 demonstrates how relative range decreases quadratically with respect to time from 6020 meters to 1.297 meters in 10.83 seconds.

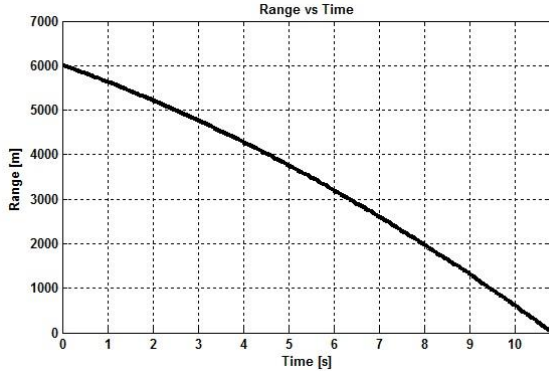


Figure 4.4: Range vs Time Variation for a Successful Interception

Similarly, closing velocity vector can be resolved in both abovementioned frames of interest. Since inertial reference frame has no rotating motion, the time rate of the unit vectors belonging to this frame is zero. However, due to the rotation of the line of sight frame with respect to an inertial reference frame, the time rate of change of LOS frame unit vectors are generally different than zero. This fact should be taken into consideration during the derivation of closing velocity vector from relative range vector in line of sight reference frame. Equations (4.6) to (4.8) represent the derived equations.

$$\vec{v}_{rel/IRF} = \frac{dx_{MT}}{dt} \vec{i}_{IRF} + \frac{dy_{MT}}{dt} \vec{j}_{IRF} + \frac{dz_{MT}}{dt} \vec{k}_{IRF} \quad (4.6)$$

$$\vec{v}_{rel/LOS} = \frac{dR}{dt} \vec{i}_{LOS} + R \frac{d}{dt} \vec{i}_{LOS} \quad (4.7)$$

$$\vec{v}_{rel/LOS} = V_c \vec{i}_{LOS} \quad (4.8)$$

Most of the time, it is more practical and meaningful to express the range rate information in line of sight frame. However, if the differentiation of the relative range vector is to be in LOS frame, as in the cases for missile guidance applications, and the relative velocity is desired to be observed in inertial reference frame, the Coriolis Theorem, i.e. Transport Theorem, is a useful method to establish the

relationship between the two frames. The corresponding correlation is given below in equation (4.9). In order to use this theorem, the angular velocity of the LOS frame with respect to the inertial reference frame as resolved in inertial reference frame is needed to be expressed. Equation (4.10) indicates the resolution of the LOS frame unit vector along which the range and range rate measurements are made, in terms of the inertial reference frame unit vectors.

$$\vec{v}_{rel/IRF} = \vec{v}_{rel/LOS} + \vec{\omega}_{LOS/IRF} \times \vec{r}_{rel/IRF} \quad (4.9)$$

$$\vec{i}_{LOS} = \cos \psi \cos \theta \vec{i}_{IRF} + \sin \psi \cos \theta \vec{j}_{IRF} + \sin \theta \vec{k}_{IRF} \quad (4.10)$$

Infrared (IR) and electro-optical (E-O) seekers are not able to provide range-dependent data for the time being and these information need to be periodically up-linked to the missile to facilitate PN guidance.

In passive seeker systems, the closing velocity is sometimes taken as the velocity of the missile if the speed of the missile is known to be much higher than the speed of the target.

Figure 4.5 illustrates a guidance scenario where closing velocity increases in magnitude with time. Range rate could also stay almost the same or decrease in amplitude with time depending on the initial velocities of the missile and the target, target maneuver as well as lateral acceleration and thrust capability of the missile.

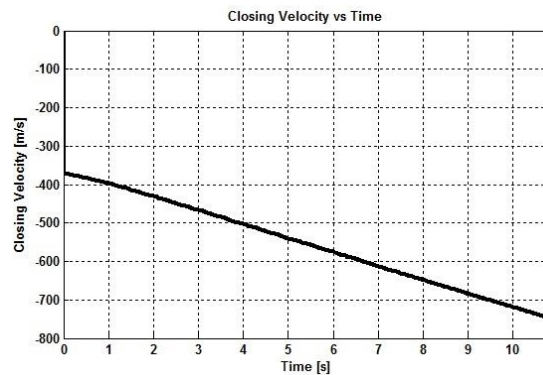


Figure 4.5: Closing Velocity vs Time Variation for a Successful Interception

LOS angle measurements are the fundamental elements of a guidance system that can be obtained by the sum of the missile body angles and gimbal angles relative to the airframe in yaw and pitch planes. .

These measurements are not perfect for sure and corrupted by a variety of noise and error sources each of which have a different impact on the quality of the acquired data. The resulting angular equalities can be written as follows in equations (4.11) and (4.12). With the current sensor technology having around 0.1 mrad resolution values, tracking systems assure quite good angular accuracy.

$$\theta = \theta_{m_{pitch}} + \theta_{g_{pitch}} + \varepsilon_{pitch} \quad (4.11)$$

$$\psi = \psi_{m_{yaw}} + \psi_{g_{yaw}} + \varepsilon_{yaw} \quad (4.12)$$

Figures 4.6 and 4.7 show LOS angle variations with respect to time for a surface-to-air engagement. It can be noticed that angle variations are kept below ± 10 degrees and no sudden increase or decrease is encountered. On the other hand, a gradual increase and decrease can be observed due to step target maneuver. Due to the smooth trend of LOS angle variations, LOS rate data is to be kept around zero which is a prerequisite condition for a successful hit.

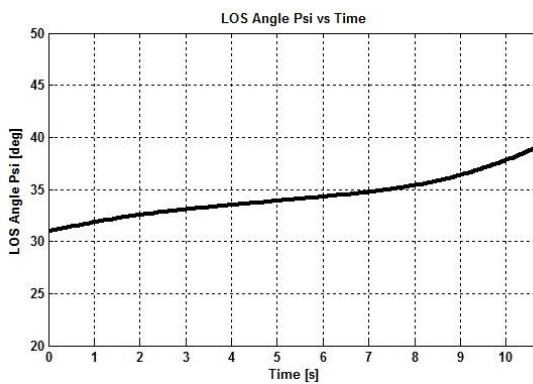


Figure 4.6: LOS Angle Psi vs Time Variation for a Successful Interception

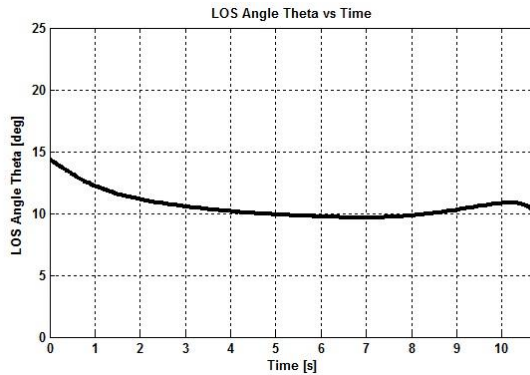


Figure 4.7: LOS Angle Theta vs Time Variation for a Successful Interception

By making use of relative position vector constructed from target-missile position components defined in Cartesian coordinate system, range to go, azimuth LOS angle and elevation LOS angles are computed and expressed as the elements of the spherical coordinate system simultaneously during the engagement simulation. This is accomplished by a proper coordinate transformation of the relative kinematics data from the Cartesian coordinate system to spherical coordinate system. The corresponding equations (4.13), (4.14), and (4.15) are presented below for convenience.

$$R = \sqrt{x_{MT}^2 + y_{MT}^2 + z_{MT}^2} \quad (4.13)$$

$$\psi = \text{atan2}(y_{MT}, x_{MT}) \quad (4.14)$$

$$\theta = \text{atan2}\left(z_{MT}, \sqrt{x_{MT}^2 + y_{MT}^2}\right) \quad (4.15)$$

Later an appropriate differentiator is applied to calculate closing velocity and related noise terms are introduced into the guidance system. Figure 4.8 illustrates how these range and angle quantities are defined with respect to the Cartesian coordinate system.

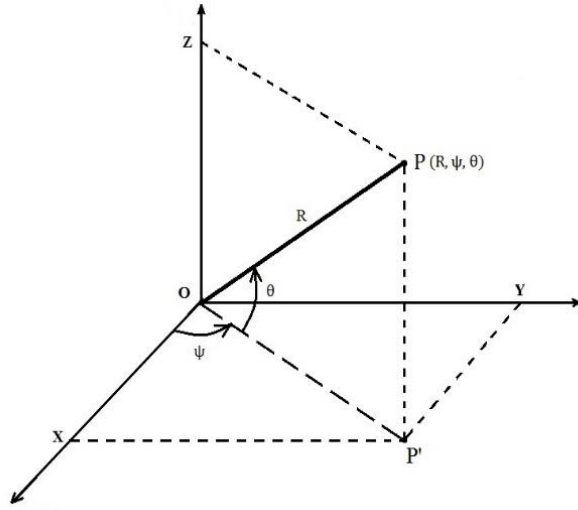


Figure 4.8: Spherical Coordinate System Representation

4.1.5 Definition of Miss Distance Concept

By definition, miss distance is the range between the pursuer and the evader at the instant the pursuer is at its closest position to the evader during an engagement. The goal of guidance is to reduce the miss distance which is analogous to the error in conventional control systems. Hence, miss distance values are a strong measure of guidance performance evaluation.

In literature, miss distance values less than 3 meters (i.e. 10 feet) are considered as successful interceptions [15]. Some sources state miss distance values up to 10 meters as satisfactory and acceptable [16]. With the help of a proximity fuze sensor, the warhead of the missile can be made to explode prior to collision to cause much severe damage. For such cases, the miss distance must be less than the warhead's lethal radius.

For simulation purposes, the sign of the relative range rate data is observed continually and the range between the missile and target is displayed as the final miss distance value whenever the simulation stops automatically as the range rate

data changes sign from negative to positive after crossing zero in the rising direction.

Target maneuver, noise and error sources, seeker models, target estimation and filtering techniques, implemented guidance laws and additional algorithms, selection of navigation constant, missile acceleration limits and autopilot time constant can be counted as the major factors having direct effect on the terminal miss distance values.

4.1.6 Definition of ‘Blind Flight’ and ‘Mid-Course Guidance’ Conditions

During an engagement, seeker may lose the track of the target due to target maneuver or noise effects. If the target suddenly disappears from the field of view of the seeker, range, range rate and LOS angle measurements are no longer provided to be used in the target estimations, guidance laws and the derivation of the LOS rates, respectively. This condition is stated as “Blind Flight”.

‘Blind Flight’ condition is valid if either of the following is true:

- Gimbal in yaw plane saturates as yaw gimbal angle reaches its maximum allowable limit
- Gimbal in pitch plane saturates as pitch gimbal angle reaches its maximum allowable limit

In some scenarios, the seeker of the pursuer may not be locked-on when the missile is launched due to relative range exceeding the seeker’s capability to sense the emitted energy, which refers to the mid-course phase of the interceptor guidance. In such cases, the aim in launching the missile could be to send the missile close enough to target by making use of the speed advantage of the missile over the target so that the seeker would get locked-on the target when the relative range drops below a certain value. By doing so, the seeker could have a chance to track the target and supply the required data to the other guidance subsystems and the missile could have an opportunity to hit the target.

Hence, “Mid-Course Guidance” condition is defined for cases where:

- Relative missile-target range is over the maximum lock-on range of the seeker being used

For simulation purposes, the real LOS angle computations are used at all times, in spite of being still unknown to the missile itself, in order to switch in between the inertial reference frame and the LOS frame while carrying out relevant missile and target acceleration vector transformations.

4.2 Seeker Modeling

4.2.1 Review of Seekers

4.2.1.1 Mission of the Seekers in Guidance

The seeker is the eye of a homing missile and plays an essential role in homing guidance technique. The mission of a homing missile seeker (i.e. *homing eye*) can be listed as follows [17]:

- Seekers are responsible for acquiring and tracking the target continuously after acquisition with an energy receiving device until the missile intercepts the target.
- Seekers provide LOS (line-of-sight) angular rates for both azimuth and elevation directions in order to mechanize the guidance law.
- Seekers provide the measurements of target motion including range-to-go R and closing velocity V_c which are possible with RF seekers.
- Gimbaled seekers should stabilize themselves against significant body rate motion (pitching and yawing rates) that may be much larger than the LOS rate to be measured [12].

Figure 4.9 shows an infrared seeker mounted on gimbals and housed in a radome.



Figure 4.9: Gimbaled Infrared Seeker of Short-Range Infrared IRIS-T Missile [18]

4.2.1.2 Description of Field of View and Field of Regard Concepts

Field of view (FoV) of a seeker can be defined as the conical angular region in space at which the seeker can observe at any given time. Seekers usually have small fields of view being at most a few degrees due to sensitivity considerations. This is one of the reasons why seekers are mounted on gimbals to increase the visible field [19]. This also helps to track targets that are capable of making agile maneuvers. For radar seekers, field of view is simply the beam width of the electromagnetic energy.

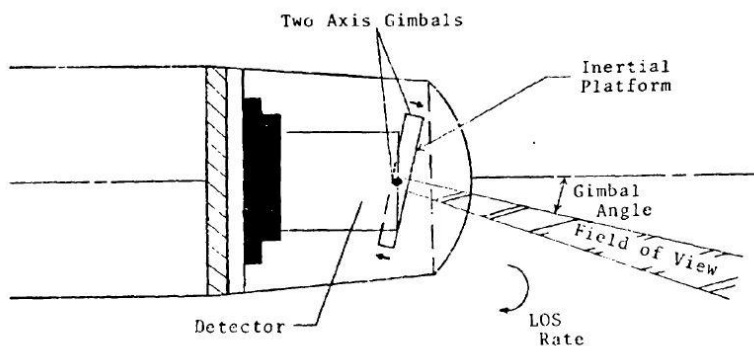


Figure 4.10: Gimbal and Field of View Angles of a Two-Axis Gimbaled Seeker [20]

Field of Regard (FoR) of a seeker is the total angular area that a seeker can view by moving the seeker aperture up and down and left to right on gimbals. For the tracking systems that do not require a large field of regard, the seeker is fixed to the body. In this case, the field of regard is the same as the field of view and such systems are called strapdown systems. Strapdown seekers are generally preferred against targets that are fixed or move with low speeds, anti-tank missiles serve as a model for strapdown systems. In particular, IR missile seekers typically have smaller fields of regard compared to RF seekers.

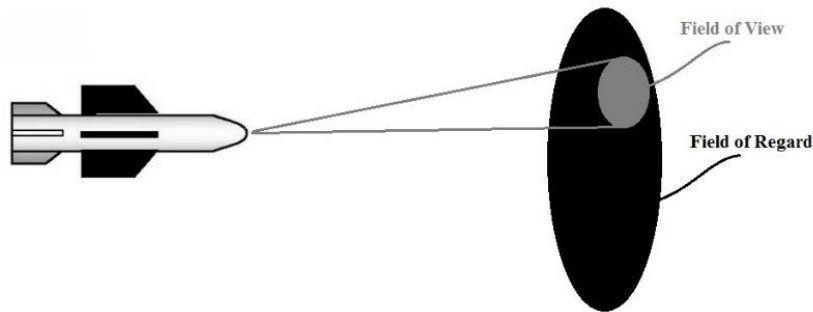


Figure 4.11: Field of View and Field of Regard Concepts

Like human eye, all seekers have field of regard limits within which they operate. These gimbal limits need to be incorporated into the simulation model to observe if the seeker is to saturate during proposed engagement scenarios. Due to the target maneuver, seeker may saturate and lose the target, which is described as the “Blind Flight” case.

Later in Chapter 6, a novel algorithm will be presented to support guidance law being implemented and aid seeker in locking on the target again once the target is in the blind zone.

4.2.2 Types of Seekers

Mainly, there are four seeker types each of which have superiority and drawbacks over each other.

Among them, heat seeking (IR) seekers are suited well for small missiles with short detection ranges. They make use of passive homing guidance techniques and they are quite effective in hitting the target precisely due to very small angular resolution. However, they do not readily provide range rate information and are prone to weather degradation. In addition, they can be deceived by countermeasures, such as flares deployed from the air target [21].

Microwave radar (RF) seekers are suitable for long range operations. They are not affected by weather conditions. Moreover, they provide range and range rate information. They make use of active or semi-active homing guidance techniques. On the other hand, they are equipped with large and heavy components. Therefore, they are suited for large missiles or ground based guidance systems. Also, the mechanical design and high precision production of microwave components together with electronic equipment involved in them make them considerably expensive. Besides, such microwave modules and filters are often gold or silver plated due to electrical loss and conductivity considerations, which contributes to the overall cost of the item significantly. Similar to IR seekers, they can be fooled by countermeasures, including jammers and chaffs [21].

Laser seekers are composed of small components and can yield small miss distance values. Furthermore, they can provide range and range rate information by the use of laser rangefinders which use laser beam to point at the target and determine the relative distance by sending a laser pulse in a narrow beam towards the target and measuring the time taken by the laser pulse to reach the target and return to the laser target sensor after being reflected off the target. Nevertheless, they cannot be used in cloudy and foggy weather and they are expensive. Above all, they have no fire-and-forget capability since the target needs to be illuminated continuously from an external designator until the missile reaches the target [21].

Lastly, visual (E/O) seekers are not preferred much anymore due to the lack of night vision. They also cannot operate in bad weather conditions. Relative range and closing velocity information are not attainable. Nonetheless, they comprise small components and it is possible to achieve small miss distances under optimal exterior conditions and at short range operations [21].

Figure 4.12 summarizes the advantages and disadvantages of each seeker type.

• Types of Seekers	Advantages	Disadvantages
• Heat Seeking (IR) Seekers	Small components Small miss distances	Weather degradation No range rate info Short range applications
• Microwave Radar (RF) Seekers	All weather Range rate info Long operating ranges	Large components High cost
• Laser Seekers	Small components Small miss distances Range rate info	Weather degradation High cost No fire & forget capability
• Visual (E/O) Seekers	Small components Small miss distances	Weather degradation No range rate info Can not operate at night

Figure 4.12: Seeker Types

The relationship between the wavelength and frequency of the waves can be expressed with the well-known formula below.

$$\lambda_w = \frac{c}{f} \text{ where } \begin{cases} \lambda_w \text{ is the wavelength} \\ c \text{ is the speed of light } (3 \times 10^8 \frac{m}{s}) \\ f \text{ is the frequency of oscillation} \end{cases} \quad (4.16)$$

Figure 4.13 demonstrates the corresponding frequency band ranges.

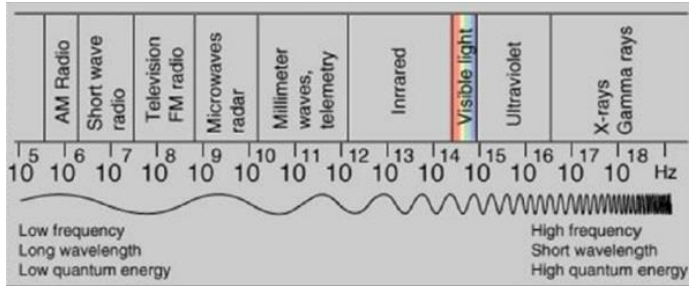


Figure 4.13: Seeker Frequency Bands [21]

4.2.3 Gimbaled vs Strapdown Seekers

Gimbaled seekers are isolated from the missile body motion through gimbals, servo motors and rate gyros mounted on each gimbal. 2 degree-of-freedom (DoF) gimbaled seekers are widely used for azimuth (yaw) and elevation (pitch) LOS angle measurements. The rotor of the gyro tends to remain fixed in space while spinning provided that no external force applies on it. Hence, the mechanical gyro resists gravity to change the direction of its spin axis. This phenomena can be explained by the principle of conservation of angular momentum.

$$\vec{L}_M = \vec{I} \times \vec{\omega} \text{ where } \begin{cases} \vec{I}: \text{moment of inertia} \\ \vec{\omega}: \text{angular velocity} \end{cases} \quad (4.17)$$

$$\vec{\tau}_{ext} = \vec{r} \times \vec{F} \text{ where } \begin{cases} \vec{r}: \text{lever arm} \\ \vec{F}: \text{applied force} \end{cases} \quad (4.18)$$

$$\vec{L}_{system} = \text{constant} \Leftrightarrow \sum \vec{\tau}_{ext} = 0 \quad (4.19)$$

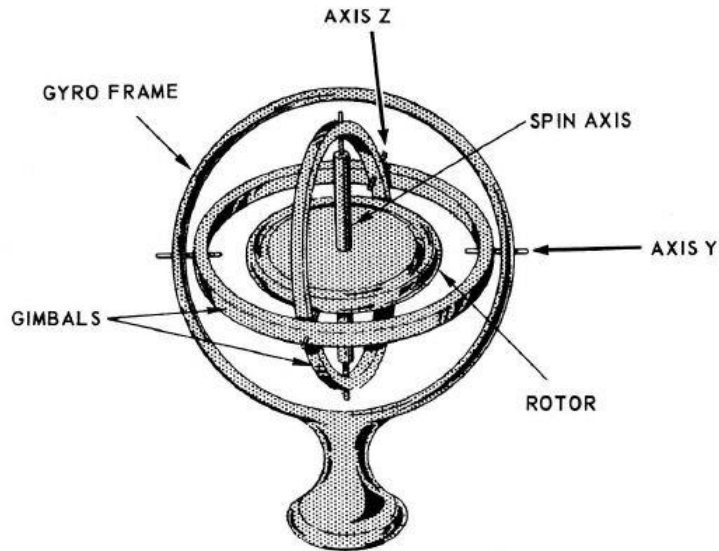


Figure 4.14: Two-Axis (2-DoF) Gyro Frame

Some seekers have the capability to make roll motion by making use of three-axis gimbals.

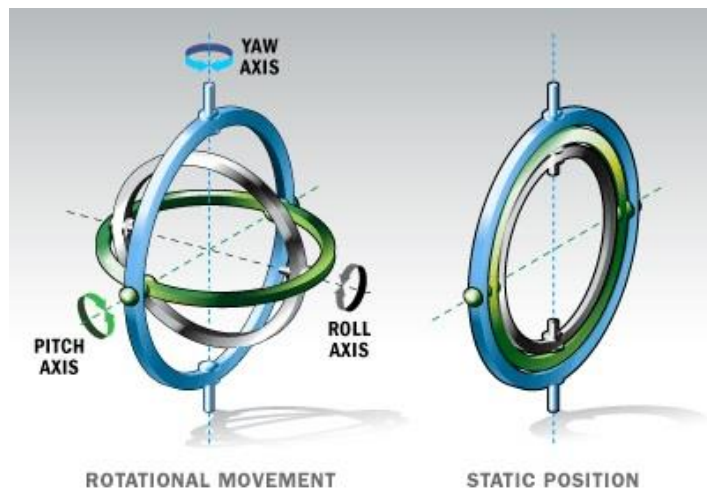


Figure 4.15: Roll-Pitch-Yaw Motion of a 3-DoF Gimbal Frame

A servomotor is used in each axis to accommodate seeker pointing. They require accurate rate gyros to determine inertial angular rate to provide boresight error tracking and stabilization against airframe motion. The seeker gimbal angle can saturate while pursuing a highly maneuverable target. As a result of this, the homing guidance loop becomes open and particularly if this happens in end-game, significant miss distance values can occur. Gimbaled seekers are more complex and cost more compared to the strapdown configurations. They also weigh more and are larger in volume than the strapdown seekers [21].

Strapdown systems use either a fixed target sensor position relative to the missile body, thus observing the same motion as the missile, or electronic beam steering by means of a phased-array radar antenna to increase the field of regard as illustrated in Figure 4.16. The spacing between the phase shifters determines the scan angle, that is how much the EM beam can be steered. Strapdown seekers do not have common use due to limited engagement geometries.

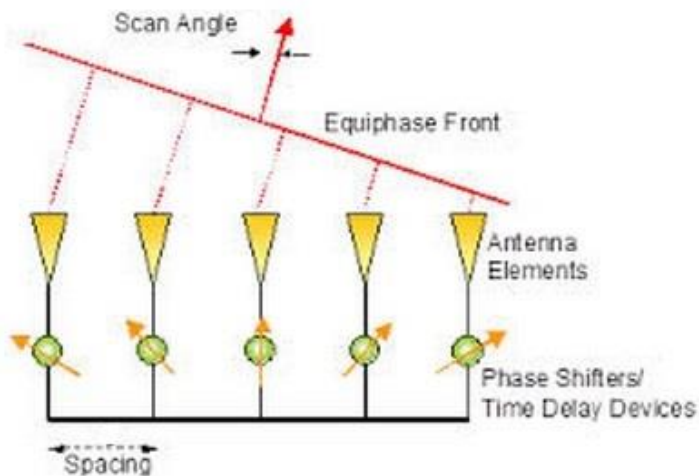


Figure 4.16: Phased Array Antenna Electromagnetic Beam Steering [22]

4.2.4 Gimbaled Seeker Model

4.2.4.1 LOS Rate Reconstruction Method

In order to derive the time rate of LOS angles and mechanize the guidance law, different approaches that appear in literature can be applied. One of them is LOS reconstruction method where a measured LOS angle is constructed in inertial frame of reference and then filtered to derive an estimate of LOS rate to be fed into guidance computer. LOS rate reconstruction method is another approach and a more direct way of obtaining LOS rate estimations from a gimbaled seeker [17].

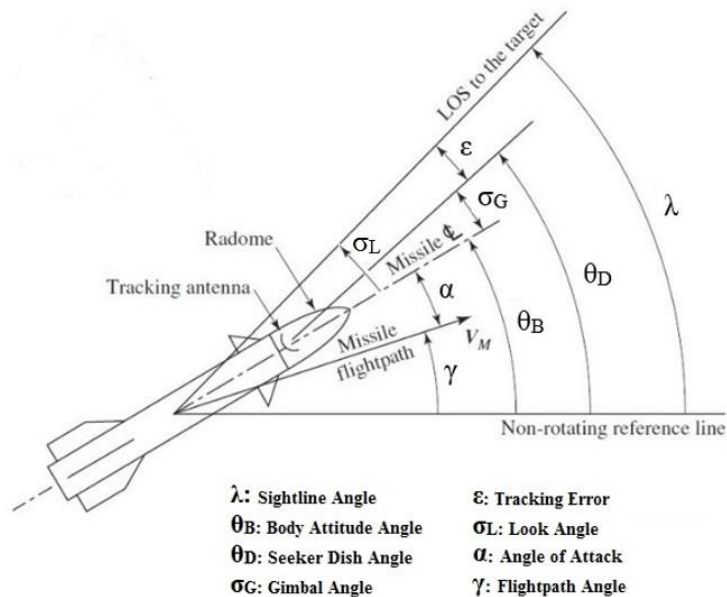


Figure 4.17: Angular Geometry of Missile Seeker [12]

The angles defined in Figure 4.17 will be helpful in the derivation of mathematical relationships and representing these relations in block diagram model of a gimbaled seeker as illustrated in Figure 4.18.

By making use of the angular geometry, the following relationships can be written:

$$\sigma_L = \lambda - \theta_B \quad (4.20)$$

$$\varepsilon = \sigma_L - \sigma_G \quad (4.21)$$

$$\dot{\theta}_D = \dot{\theta}_B + \dot{\sigma}_G \quad (4.22)$$

In order to track a target, seeker should point the sensor beam at the target continuously. Receiver measures the tracking error (ε_m) which is used by the seeker track loop to drive seeker dish angle in order to minimize the tracking error. Keeping the target in the field of view depends significantly on the minimization of the tracking error. As a consequence of the minimized tracking error, seeker dish rate ($\dot{\theta}_D$) becomes approximately equal to the inertial LOS rate ($\dot{\lambda}$). The relationship between the seeker dish angle and the inertial LOS angle can be approximated by the following first-order lag transfer function in Laplace domain:

$$\lambda(s) = \frac{1}{\tau_s s + 1} \theta_D(s) \quad (4.23)$$

This relationship can be represented as well by a differential equation in time domain assuming non-zero initial condition for the LOS angle.

$$\tau_s [\dot{\lambda}(t) - \lambda(t_0)] + \lambda(t) = \theta_D(t) \quad (4.24)$$

Here, τ_s is the seeker track-loop time constant. Therefore, seeker dish angle will lag the actual LOS angle. It should be noted that the commanded dish rate is proportional to the tracking error.

$$\dot{\theta}_{Dc} = \frac{1}{\tau_s} \varepsilon_m \quad (4.25)$$

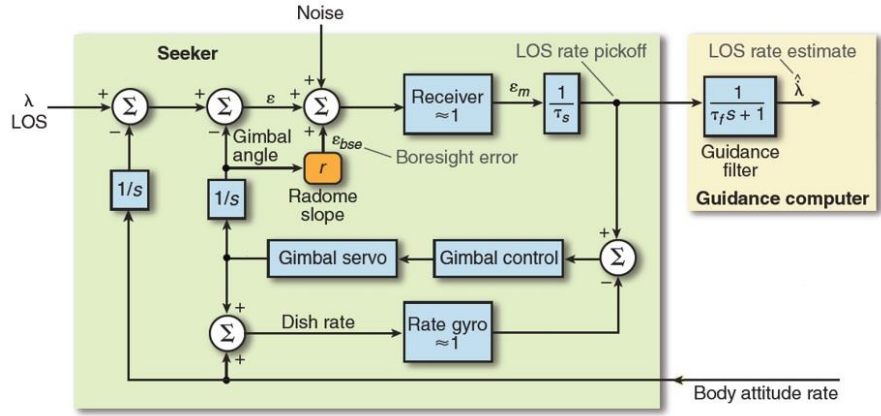


Figure 4.18: Block Diagram Model of a Gimbaled Seeker [17]

The difference between the commanded dish rate and the achieved dish rate is used to trigger the gimbal controller and a gimbal rate is produced via servomotor torquing of the gimbals [17]. In addition, body attitude angles and gimbal angles in pitch and yaw planes are determined by the integration of the time rates of these quantities and take part in the seeker model.

$$\dot{\varepsilon}_D = \dot{\theta}_{D_c} - \dot{\theta}_D \quad (4.26)$$

$$\theta_B = \int_0^t \dot{\theta}_B dt \quad (4.27)$$

$$\sigma_G = \int_0^t \dot{\sigma}_G dt \quad (4.28)$$

The measured LOS rate is filtered by an appropriate guidance filter to eliminate the measurement noise and then used to initiate the Augmented Proportional Navigation Guidance Law (APNGL).

4.2.4.2 Tracking and Stabilization Loops

Gimbaled seeker model as proposed by the LOS rate reconstruction method comprises two closed feedback loops, namely the tracking and stabilization loops. Corresponding Simulink block diagram illustrations are presented in Figure 4.19 and Figure 4.20.

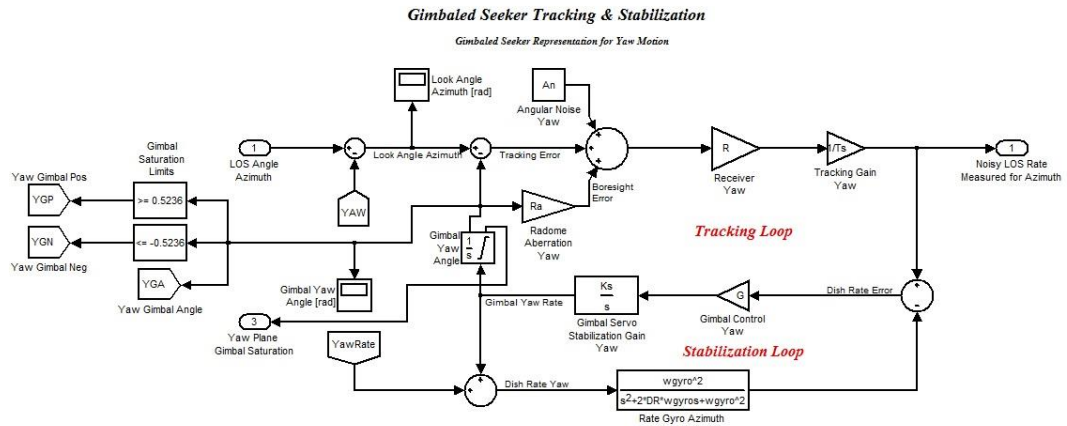


Figure 4.19: Gimbaled Seeker Representation for Azimuth

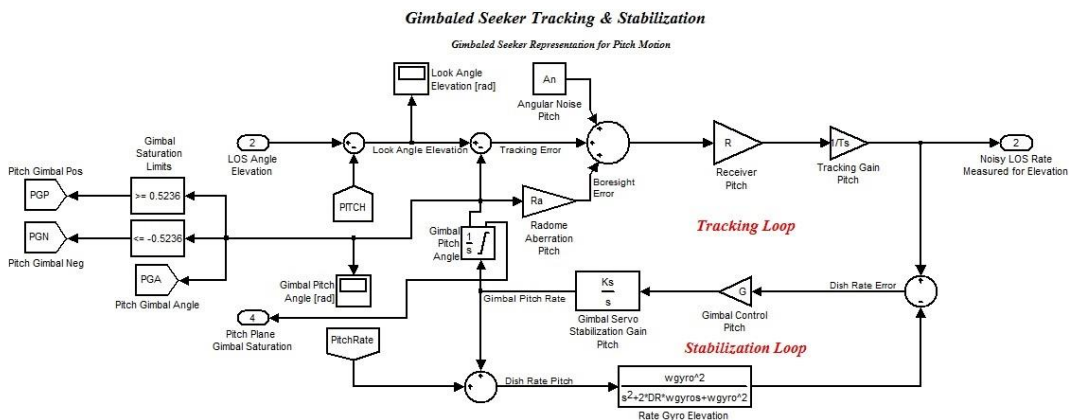


Figure 4.20: Gimbaled Seeker Representation for Elevation

In the tracking loops, gimbal angles are obtained and forced to follow look angles in order to keep tracking the target. Here, bias angular error and radome aberration error contribute to the resulting angular tracking errors. The selection of the tracking loop time constant τ_s is a compromise between enhancing the speed of response and mitigating the noise transmission to within acceptable limits and it is chosen to be 0.05 seconds as the default value during simulation studies.

Figures 4.21, 4.22, 4.23 and 4.24 show how gimbaled seeker having two degrees of freedom follows the corresponding look angles in each direction as a result of the tracking loop performed in the proposed seeker model. For this surface-to-air engagement scenario, gimbals do not saturate as can be seen from the graphs. However, both gimbals attain comparatively large values at the beginning of the flight as a combined consequence of heading error introduced at the launch and step target maneuver. Afterwards, the missile aligns itself with respect to the line of sight and starts making decent estimations regarding the target's acceleration thanks to the target estimator being implemented.

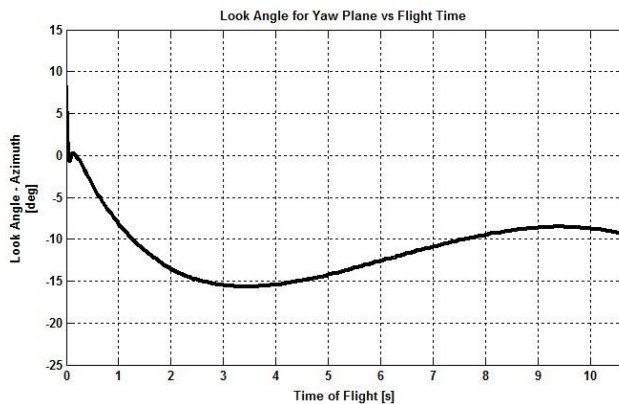


Figure 4.21: Azimuth Look Angle Variation with Flight Time

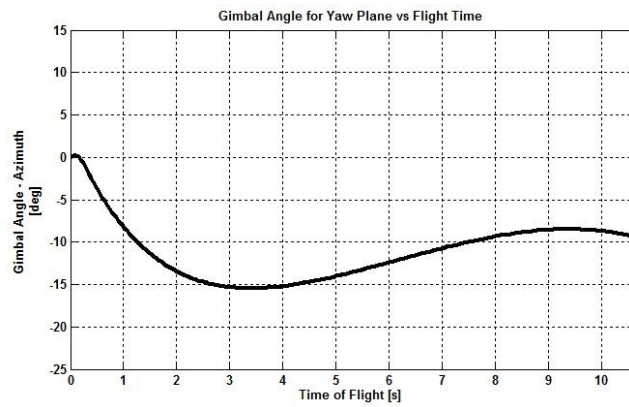


Figure 4.22: Azimuth Gimbal Angle Variation with Flight Time

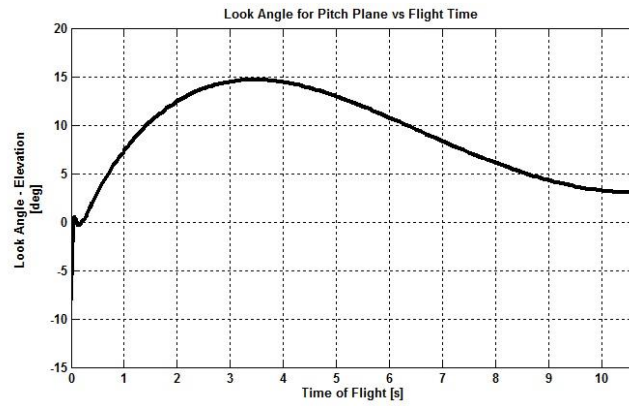


Figure 4.23: Elevation Look Angle Variation with Flight Time

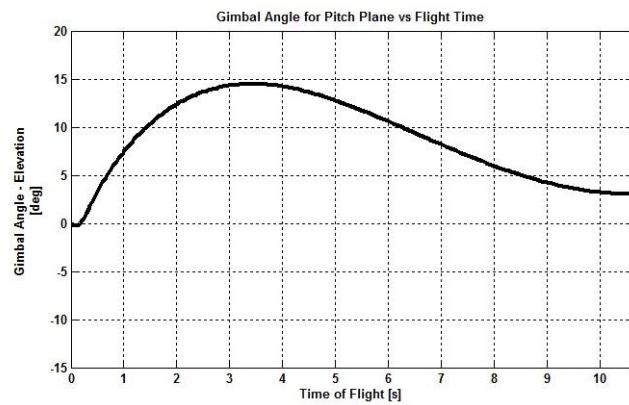


Figure 4.24: Elevation Gimbal Angle Variation with Flight Time

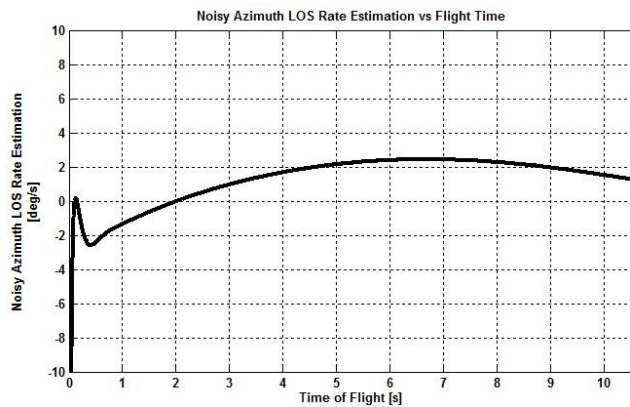


Figure 4.25: Noisy Azimuth LOS Rate Estimation

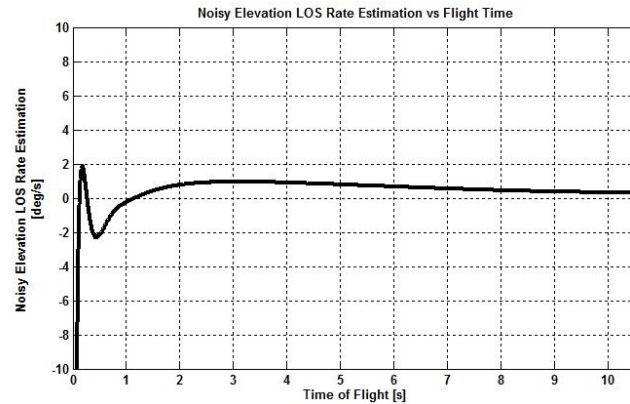


Figure 4.26: Noisy Elevation LOS Rate Estimation

Figures 4.25 and 4.26 demonstrate the LOS rate variation results in azimuth and elevation planes when LOS rate reconstruction method is applied as the gimbaled seeker model. It is noteworthy to state that the noisy LOS rate estimates are very close to zero having at most a value of 3 deg/s. These results are expected since the application of Proportional Navigation Guidance Law aims to enforce the LOS rate to be close to zero as possible for a successful collision to occur.

In the stabilization loops, two mutually perpendicular gimbals are employed along with rate gyros for space-stabilization of the seeker against significant missile body rate motion. Here, the difference between the commanded dish rate and

achieved dish rate, namely dish rate error, is fed to the gimbal controller where an integral control action is applied to derive an angular rate for the gimbal. The stabilization gain K_s is the loop crossover frequency and set as high as possible while being subject to bandwidth restrictions of the stabilizing rate gyro. Bandwidth gives an opinion about the system's susceptibility to noise. It is also a good indicator to see whether the system is responsive or not. It is a fact that the larger the bandwidth the faster the response. For simulation purposes, rate gyros are modeled as a second order system with a damping ratio (ξ) and a natural frequency (ω_n) as expressed in equation (4.29).

$$G_{gyro}(s) = \frac{K_g \omega_n^2}{s^2 + 2\xi\omega_n s + \omega_n^2} \quad (4.29)$$

Bandwidth (BW) of a second order dynamic system is given by the following formula in equation (4.30). For ξ values ranging from 0 to 1, the system is underdamped and the response is oscillatory where the amplitude of the oscillations gradually reduces to zero. For such systems, the bandwidth may take values from $0.64\omega_n$ to $1.55\omega_n$. Specifically, the bandwidth of a second order dynamic system exactly equals to the natural frequency of the system provided that the damping ratio of the system is designed to be 0.707.

$$BW = \omega_n \sqrt{1 - 2\xi^2 + \sqrt{2 - 4\xi^2 + 4\xi^4}} \quad (4.30)$$

4.2.4.3 Saturation Limits of Pitch and Yaw Gimbal Angles

It was previously mentioned that if any of the seeker gimbals reach to its maximum allowable limits in either azimuth or elevation direction, the corresponding gimbal cannot rotate anymore in that direction and the gimbal is said to be saturated.

Nowadays, modern missiles may have a total field of regard of 120° and more to avoid seeker from being saturated during a dynamic engagement. Therefore, a gimbaled seeker can slew its aperture $\pm 60^\circ$ in both azimuth and elevation directions to keep track of the target [19].

In strapdown systems, where electromagnetic beam steering can be applied, it is possible to attain a total field of regard angle of about 60° . Hence, EM energy can be steered $\pm 30^\circ$ in azimuth and elevation directions to stay locked on the maneuvering target.

In Chapter 6, the saturation of gimbal angles and actions that can be taken to get rid of ‘Blind Flight’ condition will be examined in further detail. A novel way of dealing with this issue will be addressed and proven via randomly repeated simulation trials called as *Monte Carlo* simulations.

4.2.5 Strapdown Seeker Model

This section covers the implementation of digital fading memory filters as a way of filtering noisy LOS angle measurements to obtain more accurate LOS angle data and later using them recursively in the derivation of LOS rates for azimuth and elevation directions. This method is used to represent an immovable seeker model that does not make use of gimbals for tracking and stabilization purposes. In this study, a two state fading memory filter is performed since the rates of the LOS angles are to be estimated together with the filtered LOS angle values.

4.2.5.1 Noisy LOS Angle Filtering by Second Order Fading Memory Filters

Digital fading memory filters are constant gain and recursive filters. In fading memory filter applications, new measurements are weighted more heavily than the older ones. Filter estimate is essentially the summation of the old estimate with the residual multiplied by a gain where residual is simply the difference

between the current measurement and the previous estimate [2]. The corresponding filter equations and gains are presented as follows.

$$\hat{x}_n = \hat{x}_{n-1} + \hat{x}_{n-1}T_s + G_F[x_n^* - (\hat{x}_{n-1} + \hat{x}_{n-1}T_s)] \quad (4.31)$$

$$\hat{x}_n = \hat{x}_{n-1} + \frac{H_F}{T_s}[x_n^* - (\hat{x}_{n-1} + \hat{x}_{n-1}T_s)] \quad (4.32)$$

$$G_F = 1 - \beta^2 \quad (4.33)$$

$$H_F = (1 - \beta)^2 \quad (4.34)$$

In these equations, filter gains G_F and H_F take constant values depending on the β parameter to which a constant between zero and unity is assigned. β parameter is closely associated with filter's memory length. An increase in β aims to decrease the bandwidth of the filter as well as allowing the filter to remember more about the previous measurements, thus ending up with smoother (noise-free) estimates. On the other hand, high β value leads to a sluggish filter and as a result of this; the estimates lag the actual signals. Decreasing β makes filter react faster, but tends to deteriorate noise transmission at the same time. In other words, the noisiness of estimate is the price paid for achieving a responsive filter. Moreover, increasing the sampling rate, thus decreasing T_s , helps to reduce delay and makes filter faster while it does not affect noise transmission at all.

Figures 4.27 and 4.28 illustrate azimuth LOS angle variations with respect to the time of flight. Blue lines show the actual LOS angles whereas green lines represent the measured LOS angles which are corrupted by zero mean Gaussian noise with 1 milliradian (Mr) variance. Red lines denote the estimated LOS angles as the noisy measurement data are filtered by the application of the fading memory filter. Here, β is selected to be 0.7 while T_s is chosen as 0.1.

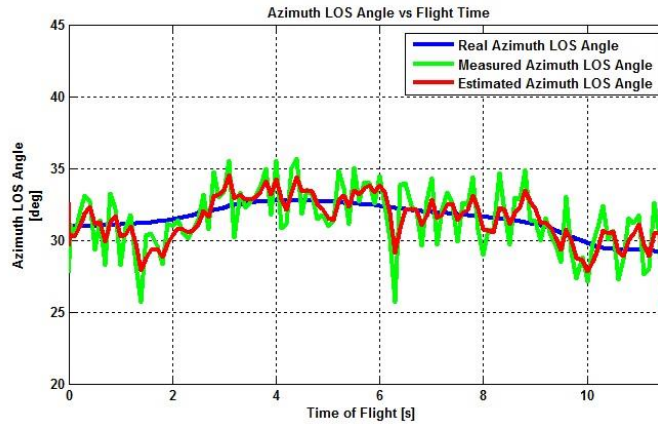


Figure 4.27: Azimuth LOS Angle vs Flight Time

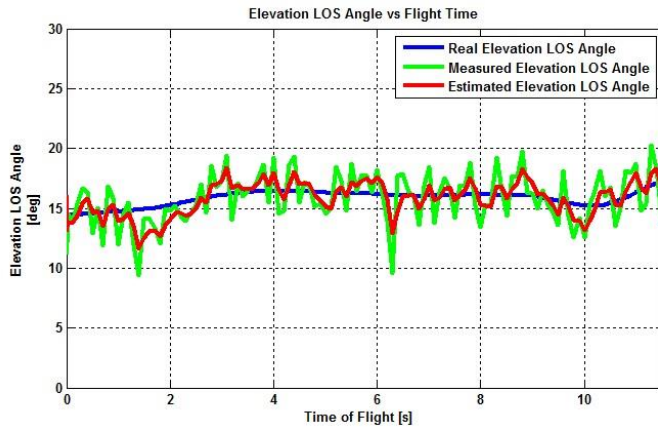


Figure 4.28: Elevation LOS Angle vs Flight Time

4.2.5.2 LOS Rate Estimation via Second Order Fading Memory Filters

Figures 4.29 and 4.31 demonstrate the implementation of recursive fading memory filter algorithms in Simulink in order to derive the LOS rates from noisy LOS angle measurements. Figures 4.30 and 4.32 clearly prove the benefits of two state digital fading memory filtering application. In these graphs, blue lines represent the real time rates of change of LOS angles whereas green lines indicate the LOS rate data obtained directly by differentiating the noisy LOS angle measurements. Red lines denote the LOS rates estimated by the fading memory filters being

applied. By looking at these plots, the implemented filtering application can be said to perform quite good since the estimated values are very close to the actual ones. Obviously, if the measured LOS rates as represented by green lines were to be used by a guidance system, the resulting miss distances would be totally devastating.

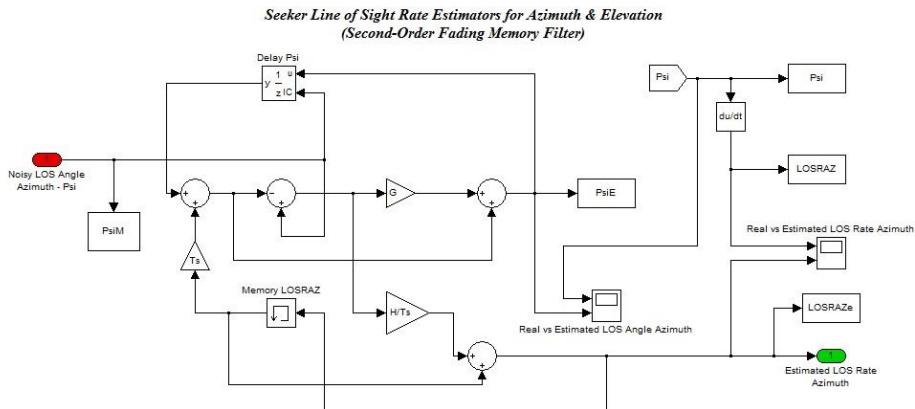


Figure 4.29: Second Order Fading Memory Filter Application for Azimuth

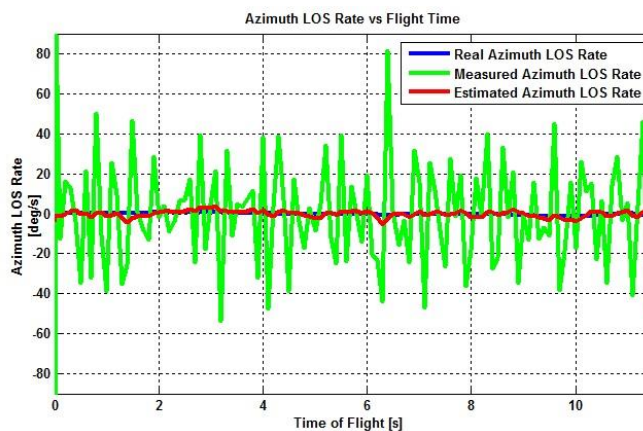


Figure 4.30: Azimuth LOS Rate vs Flight Time

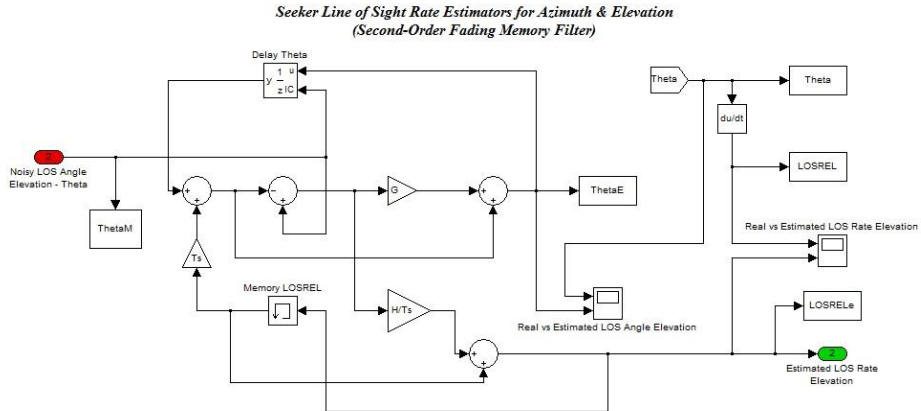


Figure 4.31: Second Order Fading Memory Filter Application for Elevation

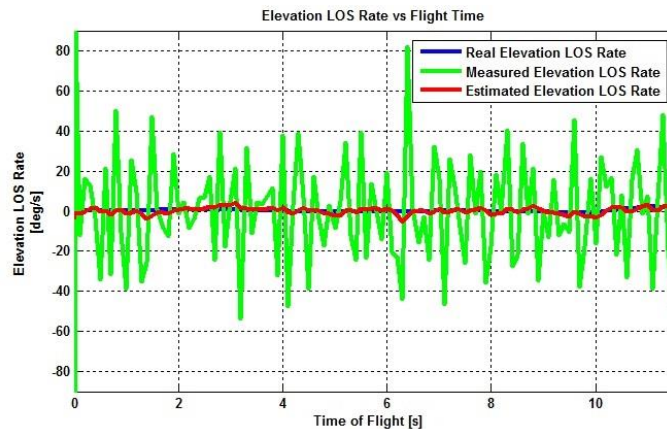


Figure 4.32: Elevation LOS Rate vs Flight Time

4.3 Noise and Error Models

4.3.1 Glint Noise

Each mechanical element on target has different scattering properties and reflections from those elements vary in amplitude and phase over time, hence seeker does not track a point but wanders randomly over or beyond the target cross section area [12]. This occurrence introduces an angular error in the target tracking system.

As a result of this, LOS angles become corrupted by noise and angle fluctuations are observed. Glint Noise is also called as ‘scintillation noise’ and it is a highly heavy-tailed, non-Gaussian, target-induced noise. It can be mathematically modeled as the combination of Gaussianly distributed noise and Laplacian noise [23]. Due to Laplacian distribution, glint spikes are observed in the generated glint noise models. The spiky pattern is indeed associated with the long-tailed non-Gaussian distribution of the glint noise model. As missile approaches to the target, glint noise increases and contributes to the final miss distance significantly. Glint noise is very dominant in all seeker types, especially in end-game. Glint noise generation as composed of Gaussian noise and Laplacian noise is accomplished by the following algorithm in Matlab software and then incorporated into the homing loop modeled in Simulink.

Gaussian Noise

$$\begin{aligned} & \text{for } k = 1, 2, \dots, \text{NUM} \\ & w(k) = \text{randn}(\text{NUM}, 1) \\ & w_g(k) = C_g \sigma_g (w(k) - \bar{w}) \sigma_w \end{aligned}$$

Laplacian Noise

$$\begin{aligned} & \text{for } k = 1, 2, \dots, \text{NUM} \\ & x(k) = \text{randn} \\ & y(k) = \sqrt{0.5} \log\left(\frac{x}{1-x}\right) \\ & z(k) = 2 \text{randn} - 1 \\ & \text{if } z > 0 \text{ then } y(k) = -y(k) \\ & w_{lap}(k) = M_{lap}(k) \sigma_{lap} y(k) \\ & M_{lap}(k) = C_{lap} k \end{aligned}$$

Glint Noise

$$w_{Glint}(k) = -\rho_G w_g(k) + \rho_G w_{lap}(k)$$

In glint noise characterization equations, σ_g and σ_{lap} are taken to be 1 and 4, respectively; whereas noise multiplier constants C_g and C_{lap} take values of 10^{-3} and 5×10^{-5} , respectively. In addition to these, 0.8 is assigned for glint probability ρ_G .

Figures from 4.33 to 4.36 show glint noise generation as a mixture of Gaussian and Laplacian distributions step by step. It can be easily seen from the figures that the formation of glint spikes are mainly due to Laplacian distribution. The number of spikes can be intentionally increased by assigning higher probability values for the Laplacian noise distribution.

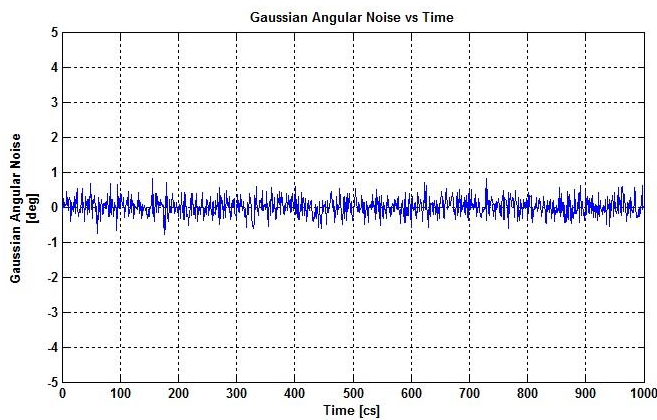


Figure 4.33: Gaussian Angular Noise Generation

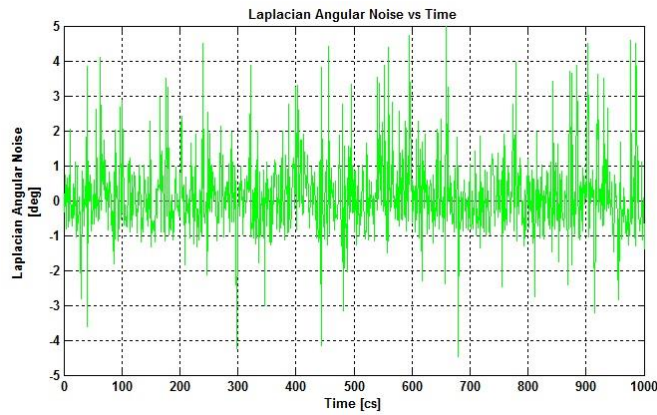


Figure 4.34: Laplacian Angular Noise Generation

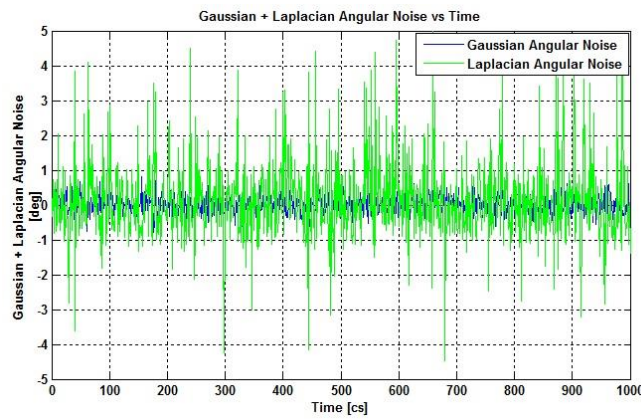


Figure 4.35: Gaussian + Laplacian Angular Noise Generation

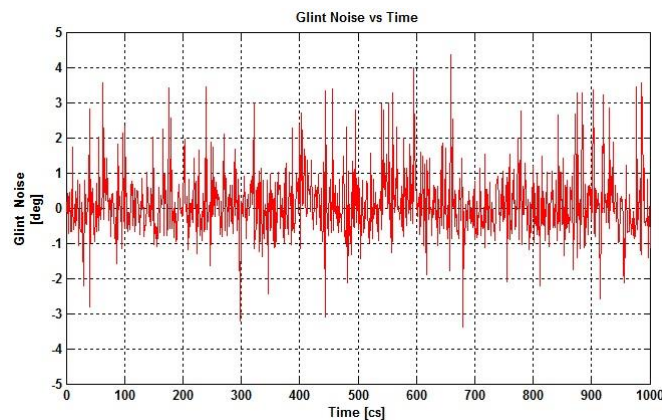


Figure 4.36: Glint Noise

Figure 4.37 represents a more realistic glint noise generation as the amplitude of the noise increases with the flight time while the relative range decreases continuously during a successful interception and the pursuer becomes closer to the target.

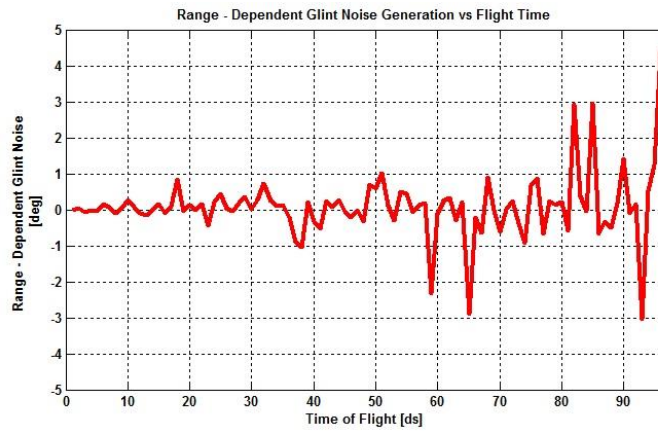


Figure 4.37: Range-Dependent Glint Noise Generation

Figures 4.38 and 4.39 illustrate how the quality of LOS angles in azimuth and elevation planes are being affected in an unfavorable way by the effect of glint noise.

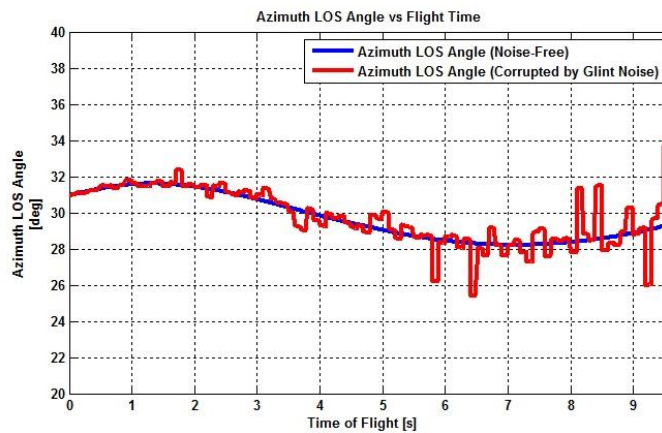


Figure 4.38: Azimuth LOS Angle Corrupted by Range-Dependent Glint Noise

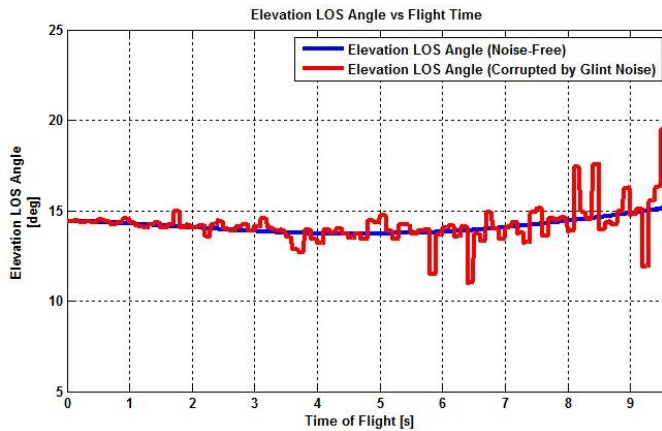


Figure 4.39: Elevation LOS Angle Corrupted by Range-Dependent Glint Noise

4.3.2 Receiver Angle Tracking Noise

Receiver angle tracking noise can be introduced to the tracking system as a contribution of two distinct noise types, namely radar cross section fluctuation and eclipsing effect [24]. These two noise types are typical angular error sources observed in RF seekers resulting in noisy LOS angle measurements which, in turn, affect the derivation of line of sight rates. In contrast to glint noise, receiver angle tracking noise is dominant at the beginning of the engagement. Therefore, it is not regarded as critical as the glint noise in terms of the resulting miss distances.

4.3.2.1 Radar Cross Section Fluctuation

In radar frequency (RF) seekers, Radar Cross Section (RCS) fluctuation occurs due to the anisotropic distribution of the reflected radar energy from target cross section area. It modulates the signal-to-noise ratio (*SNR*) and received signal quality. Similar to glint noise, the degree of effect depends on the range-to-go. However, unlike to glint noise, RCS fluctuations fade away as the pursuer approaches to the target. As a result of decreasing relative range, the quality of the received signal improves and high signal-to-noise ratios are achieved as well [24].

4.3.2.2 Eclipsing Effect

Eclipsing effect is an inevitable consequence of pulsed radar systems commonly used in missile guidance applications. This phenomenon is experienced as target return pulse arrives when transmitter is on and receiver is off. This results in periodic LOS data loss for RF seekers [24]. Maximum amount of noise is generated at the seeker lock-on range. As the missile gets closer to the target, the relative distance decreases and EM waves can travel the corresponding distance in shorter periods of time.

In order to avoid eclipsing effect in guidance applications, multi-pulse or continuous wave radar systems can be used. Special RF devices named as circulators are also utilized to separate the receiver channel from the transmitter so that EM waves can be not only transmitted but also received continuously and simultaneously. Figure 4.40 illustrates the eclipsing effect phenomena.

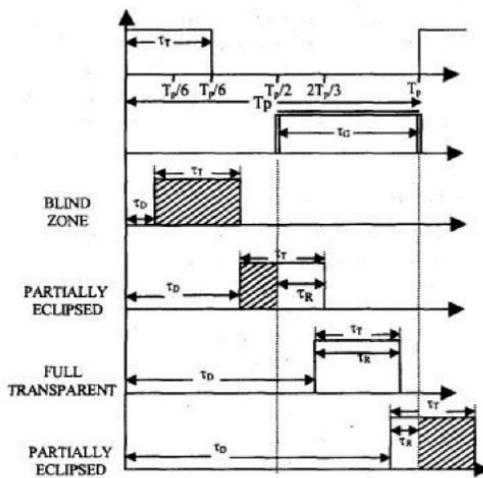


Figure 4.40: Eclipsing Effect

The following algorithm is implemented in Matlab in order to generate the Gaussian receiver angle tracking noise and then introduced to the homing loop modeled in Simulink.

Standard deviation of the Gaussian noise is represented as the function of the signal-to-noise ratio as follows.

$$\sigma_R = \frac{K_1}{\sqrt{SNR}} \quad (4.35)$$

Afterwards, signal-to-noise ratio is expressed in relation with the Radar Range equation.

$$SNR = \frac{K_R \tau_C^2}{R_{MT}^4} \quad (4.36)$$

τ_C is a cyclic time varying quantity and takes values between 0 and ε_{max} due to eclipsing effect where ε_{max} is related to the receiver gate mechanism of a specific seeker and chosen to be 0.25 in this study. τ_C can be taken as ε_{max} for no eclipsing effect cases and is taken to be 0.125 for modelling of the receiver noise [24].

$$\tau_C = \frac{\tau_R}{T_p} \quad (4.37)$$

After some mathematical manipulation of the abovementioned equations, the expression simplifies into the following form.

$$\sigma_R = \frac{K_1}{\sqrt{K_R}} \frac{R_{MT}^2}{\tau_C} = K_2 \frac{R_{MT}^2}{\tau_C} \quad (4.38)$$

Since σ_R is maximum, that is $\sigma_{R_{max}}$, when the relative distance is maximum, that is $R_{MT_{max}}$, the following equation holds true.

$$K_2 = \varepsilon_{max} \frac{\sigma_{R_{max}}}{R_{MT_{max}}^2} \quad (4.39)$$

Finally, the standard deviation of the zero mean Gaussian receiver angle tracking noise can be given by equation (4.40) for any instantaneous missile-target distance where $\sigma_{R_{max}}$ is chosen to be 1.8° .

$$\sigma_R = \sigma_{R_{max}} \left(\frac{R_{MT}}{R_{MT_{max}}} \right)^2 \frac{\varepsilon_{max}}{\tau_C} \quad (4.40)$$

Generated receiver angle tracking noise and its effect on azimuth and elevation LOS angles are displayed below. As opposed to glint noise, receiver noise fades away with increasing flight time and decreasing range-to-go.

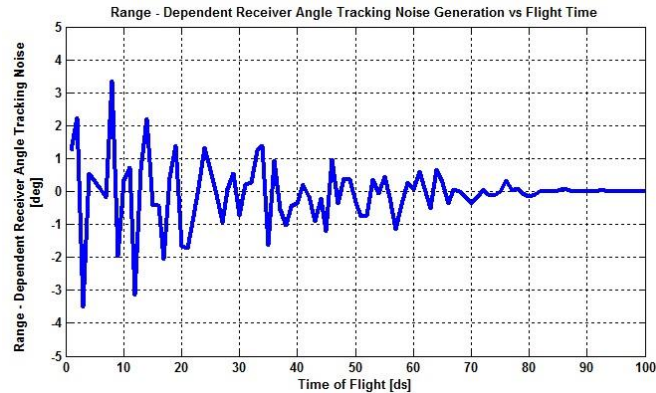


Figure 4.41: Range-Dependent Receiver Noise Generation

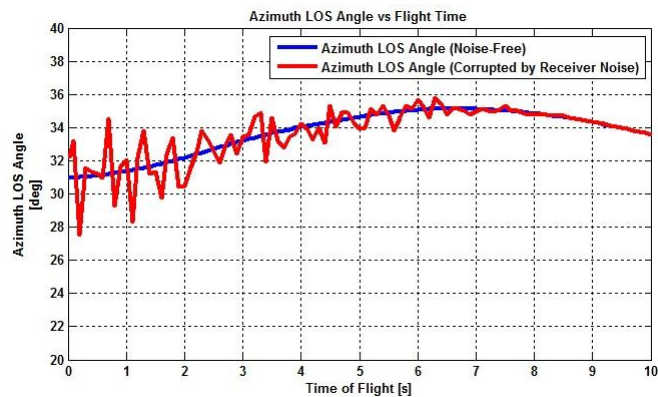


Figure 4.42: Azimuth LOS Angle Corrupted by Range-Dependent Receiver Noise

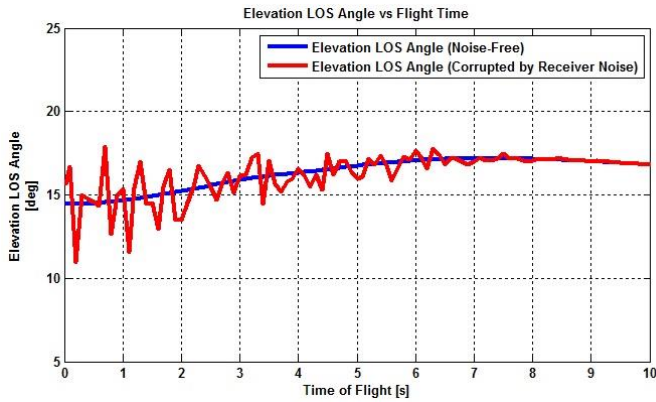


Figure 4.43: Elevation LOS Angle Corrupted by Range-Dependent Receiver Noise

4.3.3 Sinusoidal Noise

Sinusoidal noise is another form of error sources encountered in missile guidance applications. This type of noise is repetitive by its nature and may be added to the LOS angle or LOS rate measurements to judge its impact on homing guidance performances by the evaluation of the resulting miss distances. The following figures show how the LOS rates are being affected by the existence of sinusoidal noise. Equation (4.41) suggests a way of generating sinusoidal noise where A_{sin} is chosen to be 5×10^{-3} and w_{sin} is taken to be 0.5 rad/s for this study.

$$N_{sin} = A_{sin} \sin(w_{sin} t + P_{sin}) + B_{sin} \quad (4.41)$$

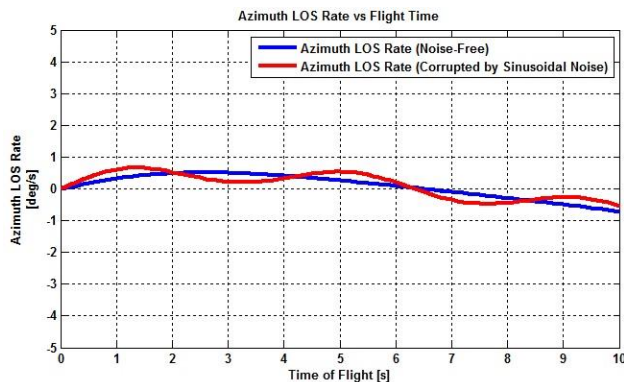


Figure 4.44: Azimuth LOS Rate Corrupted by Sinusoidal Noise

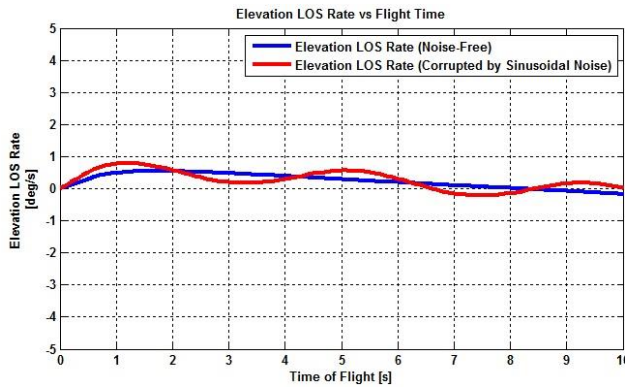


Figure 4.45: Elevation LOS Rate Corrupted by Sinusoidal Noise

4.3.4 Random Gaussian Noise

As its name suggests, random Gaussian noise is of stochastic nature and formed by generating different number sequences in each *Monte Carlo* simulation. Hence, this kind of noise is not reproducible. Range-to-go measurements are usually assumed to be corrupted by random Gaussian noise as is depicted in the figure below. There may exist high amount of noise related to the range measurements at the beginning of an engagement, however the magnitude of the random noises decays as pursuer comes closer to the target and seeker provides better range measurements. This decay can be modeled by reducing the variance of the Gaussian distribution as the missile-target range decreases.

$$N_{Gaussian} \sim N_G(\mu, \sigma^2) \quad (4.42)$$

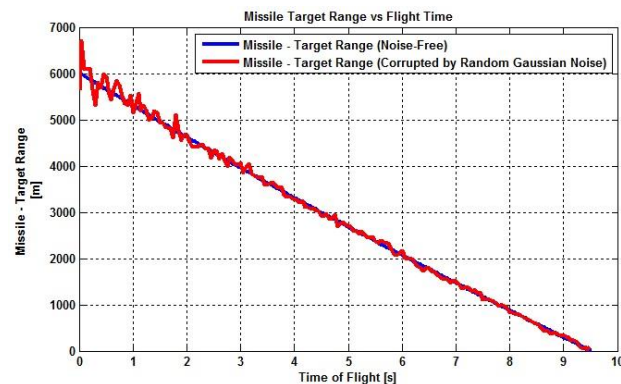


Figure 4.46: Missile-Target Range Corrupted by Random Gaussian Noise

4.3.5 Radome-Boresight Errors

Radome-boresight errors are introduced to the guidance system due to radome refraction of the RF energy or Irdome distortion of the IR energy as they pass through the protective material of an endoatmospheric missile. The degree to which extent the refraction error occurs is based on many factors such as shape, size, thickness and material of the dome, temperature and operating wave frequency, so it is not easy to model and compensate for this kind of error a priori. For practical purposes, the slope of the radome which is unsteady throughout the entire dome can be used to characterize the attitude of error [17]. Since radome-boresight error varies with gimbal angle, for this study, a linear relationship between the achieved gimbal angles and resulting boresight error is assumed to examine the effects of such errors on guidance performance where the linearity constant K_R is simply the slope of the dome and is taken to be -0.01 during modelling of the radome aberration error.

$$\varepsilon_{bse} = K_R \sigma_G \quad (4.43)$$

Radomes are designed to convey the reflected energy with minimum loss while, at the same time, leading to minimum aerodynamic drag. This situation poses a contradiction in terms of design specifications, which is illustrated in the following figure. Most of the time, a compromise solution is sought in order to balance the advantages of both design requirements.

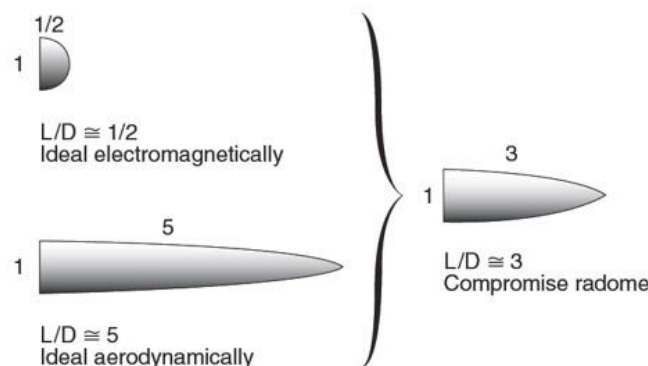


Figure 4.47: Compromise Radome Model [17]

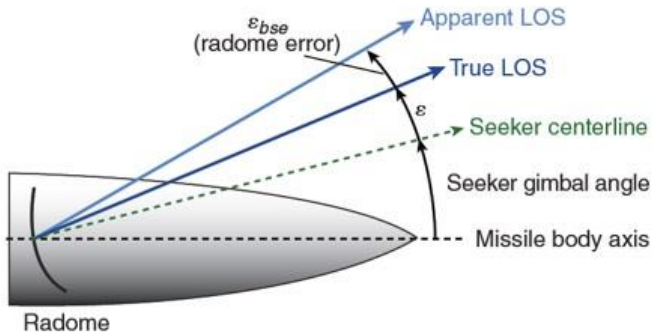


Figure 4.48: Radome-Boresight Error [17]

4.3.6 Bias Errors

Although the seeker gimbals are normally manufactured with high precision, no production is perfect and some mechanical problems may be encountered during the assembly stage of gimbals into radome. For this reason, a constant angular noise can be purposely added to the seeker tracking system as a bias error resulting from seeker gimbal misalignment provided that the angular misalignment error is measured beforehand by a proper measuring instrumentation.

4.3.7 Heading Errors

Heading error is introduced at the launch of the missile as missile's velocity vector is deviated from the line of sight. Hence, by proper selection of initial attitude of the missile at the time of launch, the effect of distinct heading error scenarios can be analyzed. Obviously, the lateral acceleration commanded by the missile is expected to attain higher values as heading error gets larger which entails the risk of lateral acceleration saturation. The use of Proportional Navigation Guidance Law aims to null out the undesired effects of heading errors in order to achieve a successful interception as will be explained in further detail in Chapter 6.

CHAPTER 5

NOISE FILTER AND TARGET ESTIMATOR MODELS

As discussed in previous chapters, noise and error sources accompanied by target maneuver are likely to play a crucial role in engagement scenarios and they can yield large miss distances by directly influencing the measured LOS rates. Augmented Proportional Navigation Guidance Law relies on the LOS rate measurements and estimations belonging to the states of the target motion. Hence, the mission of filtering of excessive noise present in LOS rate measurements and satisfactory estimation of target states need to be fulfilled to achieve a successful interception. This section begins with the implementation of first order digital fading memory filters used as a filtering technique for noisy LOS rate measurements. The discussion continues with the presentation of a target estimator model used to estimate time-varying position, velocity and acceleration states of a maneuvering target along each direction in three dimensional space, thus yielding nine states to be estimated in total. Step and weaving target maneuvers are taken into consideration to judge the performance of the estimator and corresponding estimation results are presented.

5.1 LOS Rate Noise Filtering by First Order Fading Memory Filters

First order fading memory filters may be applied as a simple but effective way of coping with noisy LOS rate data. The aforementioned characteristics of fading memory filters are also valid for this case. The corresponding filter and gain equations are given below [2].

$$\hat{x}_n = \hat{x}_{n-1} + G_F[x_n^* - \hat{x}_{n-1}] \quad (5.1)$$

$$G_F = 1 - \beta \quad (5.2)$$

The representation of these equations in Simulink environment is presented as follows.

Fading Memory Filter Design for Noisy Azimuth LOS Rate

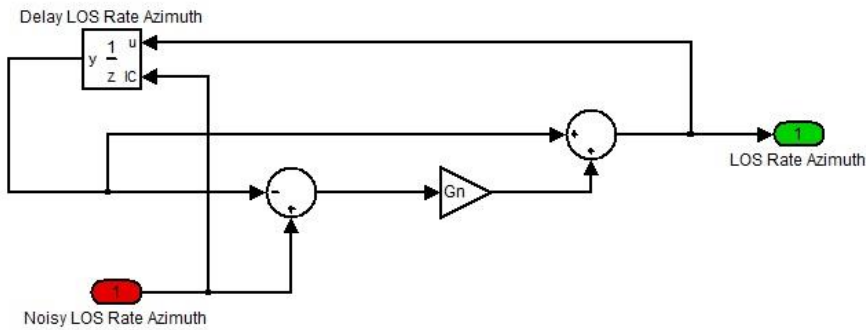


Figure 5.1: First Order Fading Memory Filter Application for Azimuth LOS Rate
Noise Filtering

LOS rates corrupted by noise and filtered LOS rate data are plotted in the following figures. For this case, random zero mean Gaussian noise of 1 Mr/s variance is applied. Filtered LOS rate variations are kept within $\pm 2^\circ$ degrees whereas the noisy LOS rate data fluctuates between 6° and -6° . Hence, it can be concluded that the results are quite satisfactory.

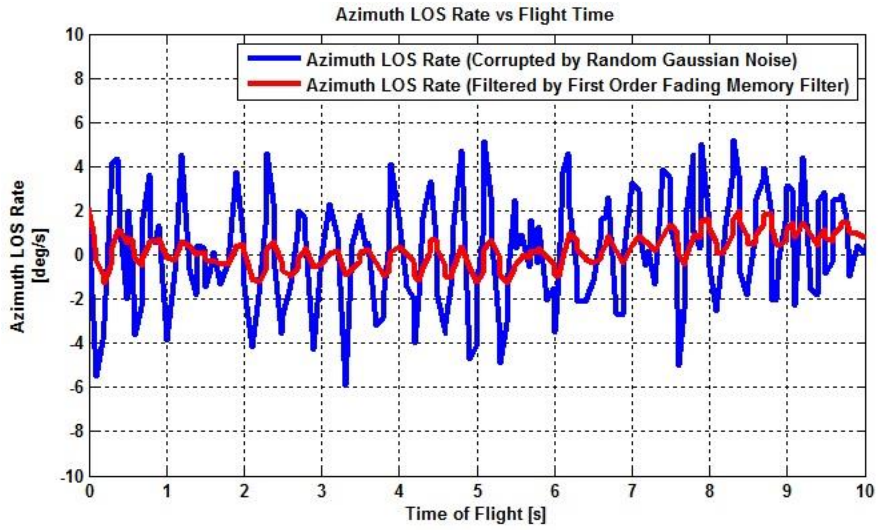


Figure 5.2: Azimuth LOS Rate Filtered by First Order Fading Memory Filter

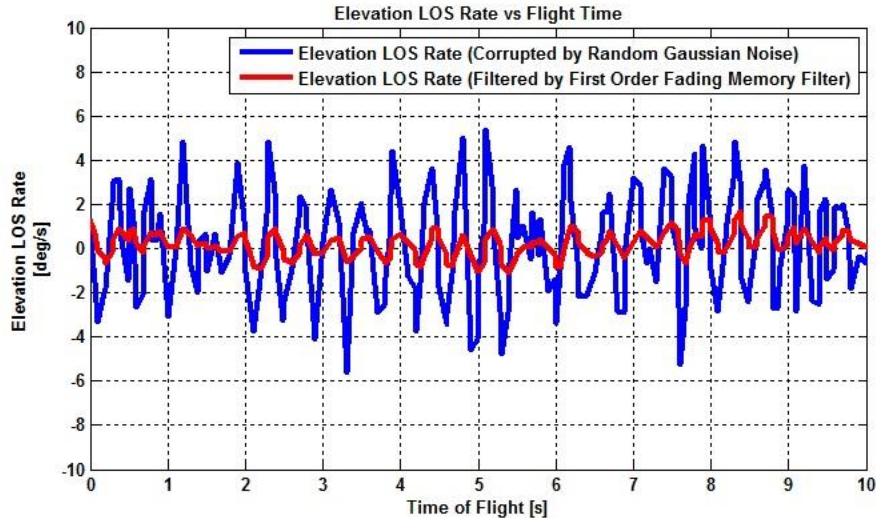


Figure 5.3: Elevation LOS Rate Filtered by First Order Fading Memory Filter

5.2 Target State Estimation via Third Order Fading Memory Filters

Since three target states are to be estimated along each axis of the inertial reference frame, a third order fading memory filter implementation is required. Digital fading memory filters use noisy position measurements belonging to the

target in order to make reasonable estimations. Filtering and estimation processes take place at the same time to predict the actual instantaneous position of the target in space over the entire pursuit scenario. Later, velocity and acceleration components of the target are intended to be derived and predicted as accurate as possible. Noisy target position measurements are acquired by making use of a precise Inertial Measurement Unit (IMU) and fundamental seeker measurements, namely LOS angles for azimuth and elevation directions and missile-target range.

By making use of recursive filter equations and the relevant gains as well as selecting appropriate filter parameters β and T_s , it is possible to obtain decent estimations regarding target position, target velocity and even target acceleration that is to be used in Augmented Proportional Navigation Guidance Law during the determination of the lateral acceleration components required by the missile to chase the target effectively. Corresponding filter equations and gains are presented below for convenience [2].

$$\hat{x}_n = \hat{x}_{n-1} + \hat{x}_{n-1}T_s + 0.5\hat{x}_{n-1}T_s^2 + G_F[x_n^* - (\hat{x}_{n-1} + \hat{x}_{n-1}T_s + 0.5\hat{x}_{n-1}T_s^2)] \quad (5.3)$$

$$\hat{\dot{x}}_n = \hat{x}_{n-1} + \hat{x}_{n-1}T_s + \frac{H_F}{T_s}[x_n^* - (\hat{x}_{n-1} + \hat{x}_{n-1}T_s + 0.5\hat{x}_{n-1}T_s^2)] \quad (5.4)$$

$$\hat{\ddot{x}}_n = \hat{x}_{n-1} + \frac{2K_F}{T_s^2}[x_n^* - (\hat{x}_{n-1} + \hat{x}_{n-1}T_s + 0.5\hat{x}_{n-1}T_s^2)] \quad (5.5)$$

$$G_F = 1 - \beta^3 \quad (5.6)$$

$$H_F = 1.5(1 - \beta)^2(1 + \beta) \quad (5.7)$$

$$K_F = 0.5(1 - \beta)^3 \quad (5.8)$$

Simulink block diagram representation of the recursive fading memory filtering algorithm used to estimate target states along X axis of the inertial reference frame is presented below.

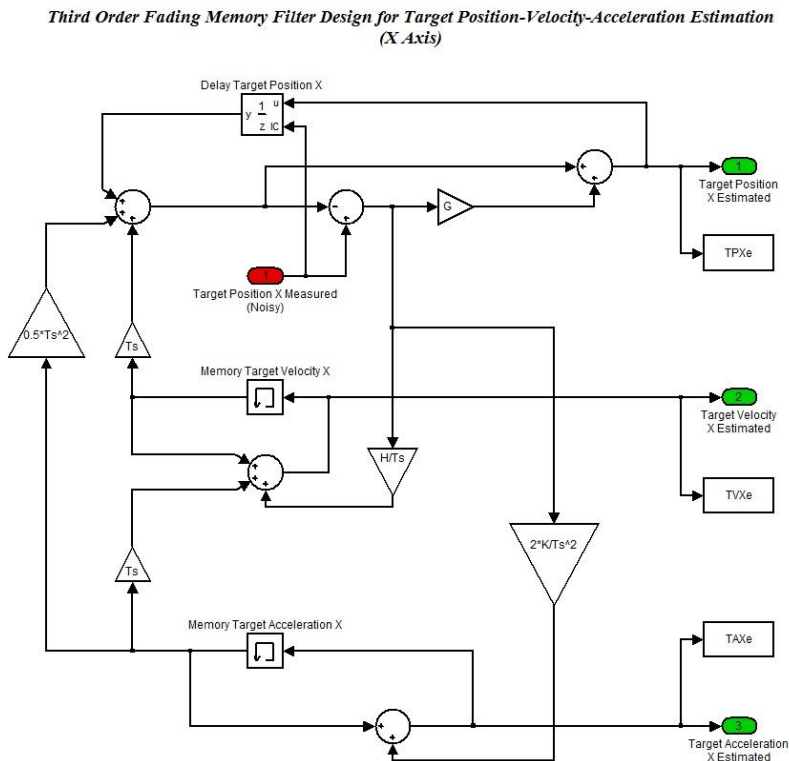


Figure 5.4: Third Order Fading Memory Filter Application for Target Estimation

Due to the fact that the estimation process takes place with respect to inertial frame of reference, coordinate transformation from inertial reference frame to LOS frame as included in depth in Appendix A.1 needs to be handled at the same time. Consequently, estimated target acceleration components are resolved in LOS frame and the two components normal to the sightline play the role in determination of the required missile lateral acceleration in azimuth and elevation planes.

Another method mostly used in filtering and estimation problems is the well-known *Kalman* filtering. *Kalman* filter proposes optimal solution for linear

estimation problems. However, due to ease of implementation and less computing capability requirement, fading memory filtering technique is preferred in this study. In *Kalman* filtering technique, noisy target position is measured and position, velocity and acceleration of the target are attempted to be estimated, similar to the fading memory filters. What distinguishes the *Kalman* filter from the fading memory filter is that the *Kalman* filter computes the time varying *Kalman* gains via a set of recursive equations known as the matrix *Riccati* equations [2]. In order to start the *Riccati* equations, an initial diagonal covariance matrix P_o is used. Selection of a proper P_o matrix is a critical step to ensure that the filter is to work as desired. The statistical distribution of process and measurement noises must be incorporated into the *Kalman* filter model and most of the time, a fine tuning is needed to make the filter ready for practical guidance applications. *Kalman* filter equations are represented in state-space form below for the sake of completeness and recursive *Riccati* equations in addition to initial covariance matrix are also included.

$$\begin{bmatrix} \hat{y}_k \\ \hat{\dot{y}}_k \\ \hat{n}_{T_k} \end{bmatrix} = \begin{bmatrix} 1 & T_s & 0.5T_s^2 \\ 0 & 1 & T_s \\ 0 & 0 & 1 \end{bmatrix} \begin{bmatrix} \hat{y}_{k-1} \\ \hat{\dot{y}}_{k-1} \\ \hat{n}_{T_{k-1}} \end{bmatrix} + \begin{bmatrix} -0.5T_s^2 \\ -T_s \\ 0 \end{bmatrix} n_{c_{k-1}} + \\ \begin{bmatrix} K_{1k} \\ K_{2k} \\ K_{3k} \end{bmatrix} \left[y_k^* - [1 \ 0 \ 0] \begin{bmatrix} 1 & T_s & 0.5T_s^2 \\ 0 & 1 & T_s \\ 0 & 0 & 1 \end{bmatrix} \begin{bmatrix} \hat{y}_{k-1} \\ \hat{\dot{y}}_{k-1} \\ \hat{n}_{T_{k-1}} \end{bmatrix} - [1 \ 0 \ 0] \begin{bmatrix} -0.5T_s^2 \\ -T_s \\ 0 \end{bmatrix} n_{c_{k-1}} \right] \quad (5.9)$$

$$M_k = \Phi_k P_{k-1} \Phi_k^T + Q_k \quad (5.10)$$

$$K_k = M_k H^T [H M_k H^T + R_k]^{-1} \quad (5.11)$$

$$P_k = (I - K_k H) M_k \quad (5.12)$$

$$P_o = \begin{bmatrix} \sigma_{noise}^2 & 0 & 0 \\ 0 & \left[\frac{V_{MHE}}{57.3} \right]^2 & 0 \\ 0 & 0 & n_T^2 \end{bmatrix} \quad (5.13)$$

5.2.1 Target Position Estimation

Target position estimation results are illustrated in the following figures for three distinct target maneuvers. Target is considered to take different evasive maneuvers along each axis of the inertial reference frame.

For this specific scenario, target is making;

- $3g$ weaving maneuver along X_{ref} with 0.5 rad/s frequency and an initial velocity of 150 m/s,
- $-5g$ step maneuver along Y_{ref} with an initial velocity of 300 m/s,
- Piecewise continuous step maneuver by changing its step maneuver amplitude in every 3 seconds along Z_{ref} with no initial velocity.

During the estimation stage, noise and error models affecting the range-to-go as well as LOS angles are involved in the homing loop. Random Gaussian noise decaying with relative range is introduced to affect range-to-go data. Besides, sinusoidal noise is added intentionally to the LOS angle measurements. These noise sources directly affects the target position measurements. Corresponding noisy measurements of the target position are plotted in the graphs too. Actual target positions are also given for comparison purposes.

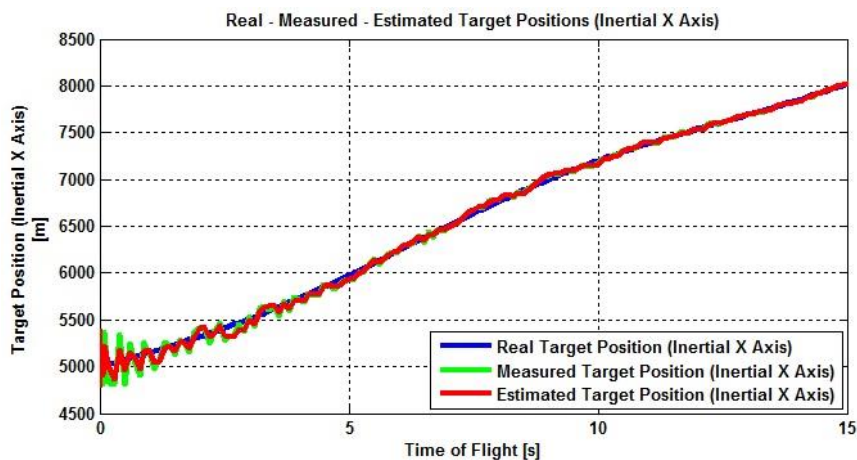


Figure 5.5: Target Position Estimation along X_{ref} by 3rd Order Fading Memory Filter

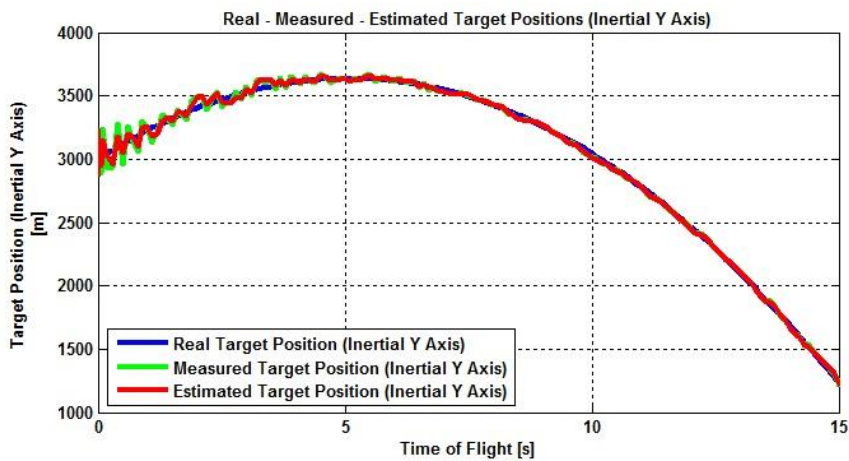


Figure 5.6: Target Position Estimation along Z_{ref} by 3rd Order Fading Memory Filter

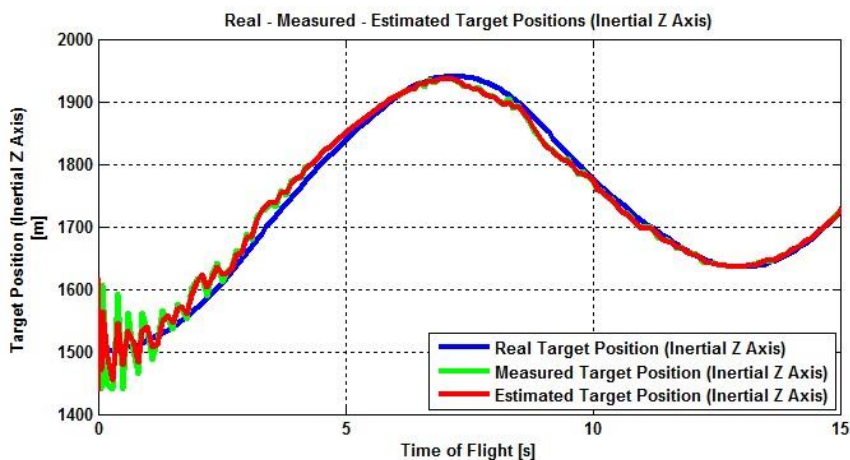


Figure 5.7: Target Position Estimation along Z_{ref} by 3rd Order Fading Memory Filter

The effect of random Gaussian noise can be seen from the graphs above. It is dominant at the beginning and diminishes as the pursuer approaches the target.

5.2.2 Target Velocity Estimation

Target velocity estimation results are illustrated in the following figures for three distinct target maneuvers. Actual target velocities are also included for comparison purposes. The filters are started with an initial condition of 0 m/s velocity along all directions assuming that closing velocity information is not available at the beginning of the engagement.

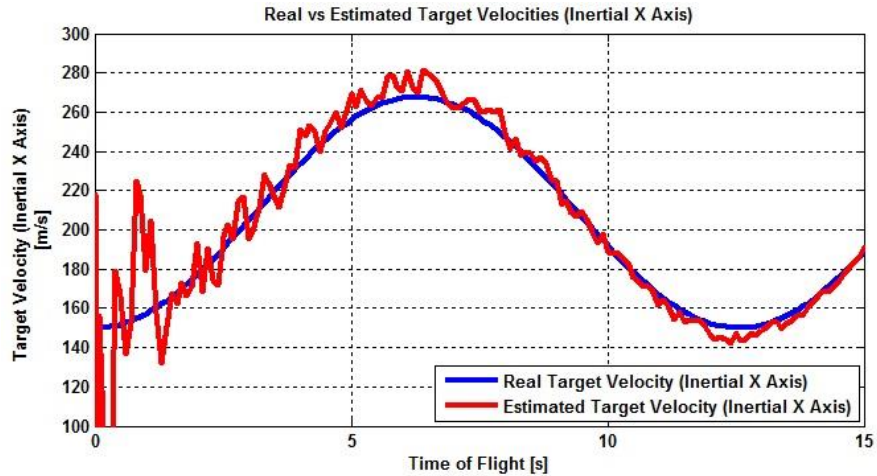


Figure 5.8: Target Velocity Estimation along X_{ref} by 3rd Order Fading Memory Filter

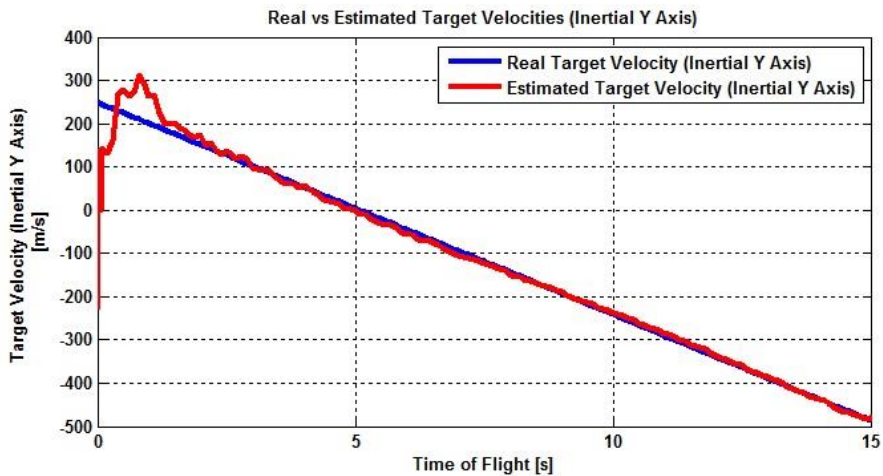


Figure 5.9: Target Velocity Estimation along Y_{ref} by 3rd Order Fading Memory Filter

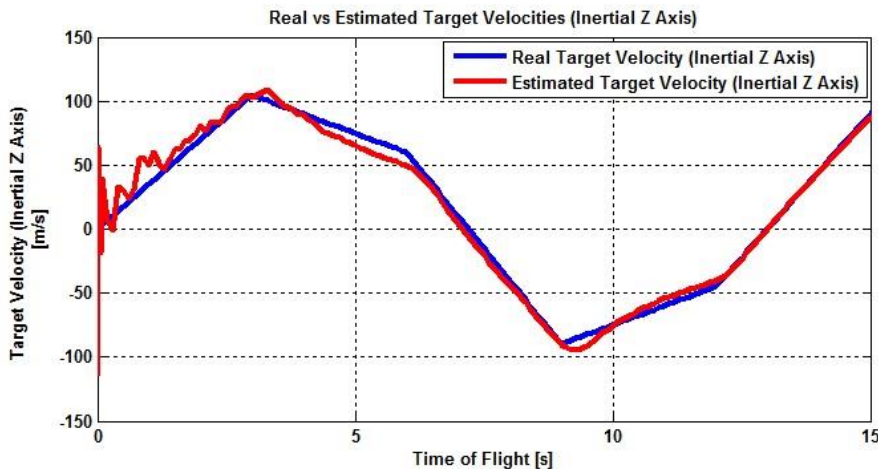


Figure 5.10: Target Velocity Estimation along Z_{ref} by 3rd Order Fading Memory Filter

High noise effects can also be seen in velocity estimations. For low noise case, the estimations would be much smoother. Similarly, if the filters were to be started with initial velocities around the actual initial velocities of the target by assuming that the closing velocity and LOS angle data are already available just before the estimation begins, the estimations would be much more accurate.

5.2.3 Target Acceleration Estimation

Target acceleration estimation results are illustrated in the following figures for two different targets taking step and weave maneuvers. Actual target accelerations are also indicated for comparison purposes. Magnitude of step maneuvers and weaving amplitude-frequency are also stated for convenience. There is a trade-off regarding the estimations between the smoothness and speed of response of weaving acceleration. Depending on the level of noise and target weaving frequency expected in engagement scenarios, a compromise filter design can be established.

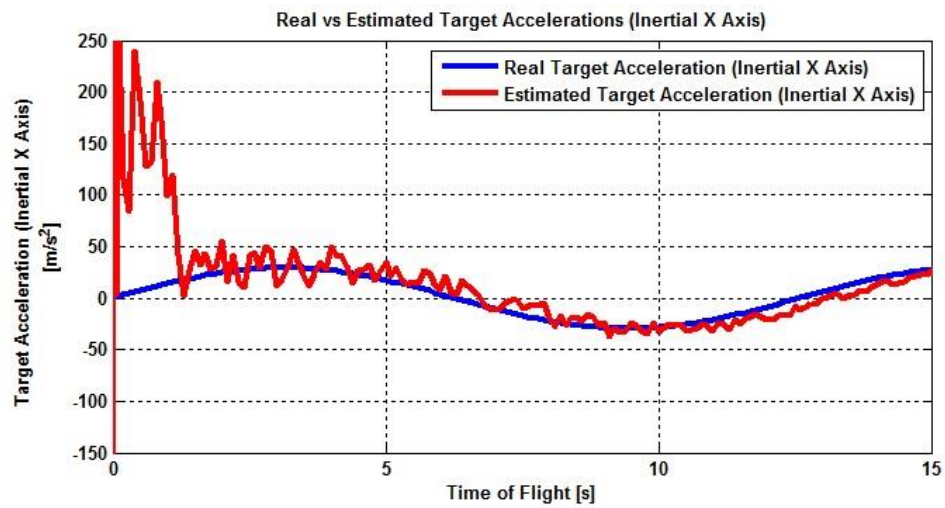


Figure 5.11: Target Acceleration Estimation along X_{ref} by 3rd Order Fading Memory Filter

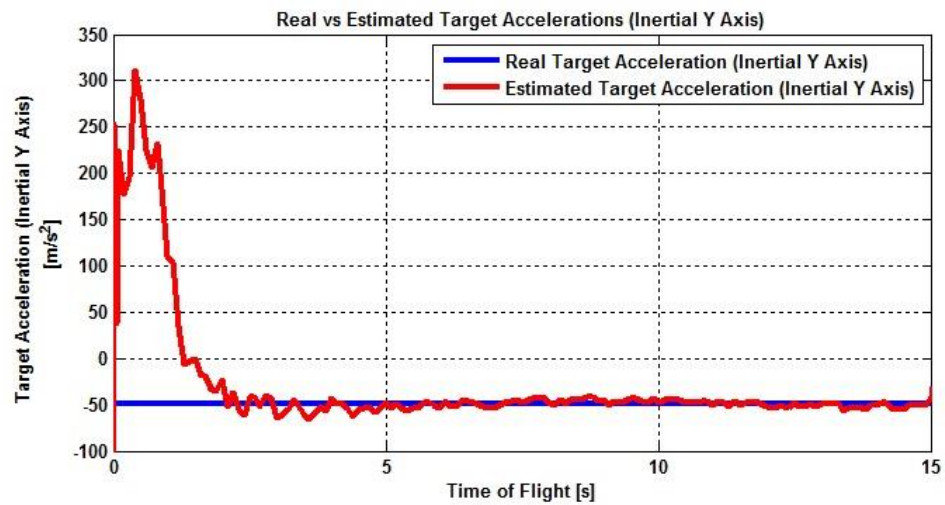


Figure 5.12: Target Acceleration Estimation along Y_{ref} by 3rd Order Fading Memory Filter

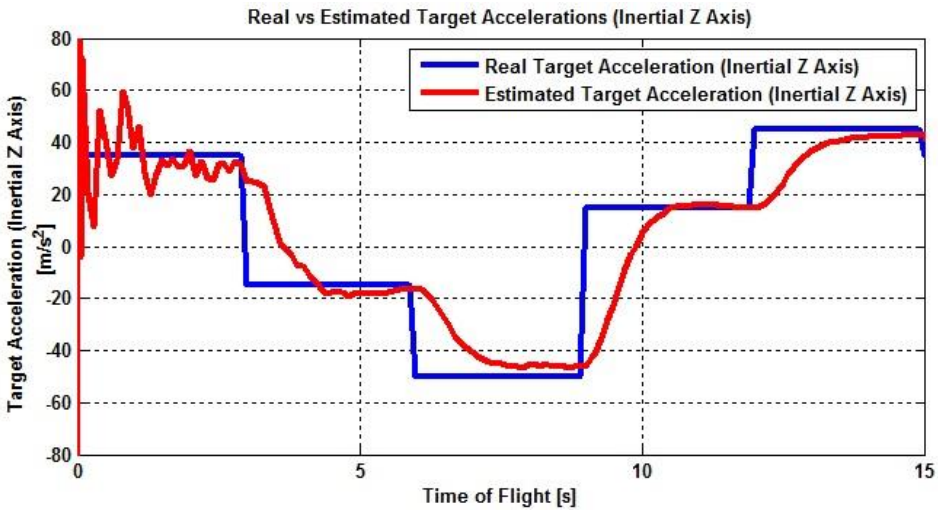


Figure 5.13: Target Acceleration Estimation along Z_{ref} by 3rd Order Fading Memory Filter

Since the filters are started with initial conditions of 0 m/s velocity, a high jump regarding the acceleration estimations along X_{ref} and Y_{ref} can be noticed. This results from the significant gap between the actual initial velocity of the target and the initial velocity condition set for the filter. Filter tries to catch the real target velocity as quickly as possible, within almost 2 seconds for the case in hand, hence a huge velocity differential is experienced in a very short time by the filter. Consequently, this differential directly affects the acceleration components estimated by the filter.

The fading memory filter performs with quite good precision against step and weaving target maneuvers as can be recognized from the figures above. The acceleration of the target in all three directions are predicted with pretty good accuracy within just 3 seconds.

The figures also imply that piecewise continuous step maneuver can be a smart strategy for the evader to deceive the pursuer due to the lags introduced at every instant the pursuer changes its acceleration magnitude. Weaving maneuver can also be regarded as a wise strategy compared to the step maneuver from the standpoint of the evader since estimations usually lag the actual target acceleration values.

CHAPTER 6

GUIDANCE, AUTOPILOT AND MISSILE MANEUVER MODELS

6.1 A Brief Introductory Background on Proportional Navigation

The origins of Proportional Navigation dates back to antiquity. The ancient mariners realized that a collision would occur eventually if a constant bearing angle is maintained with another ship and the speeds of the two ships stay constant. This fact is known as the Parallel Navigation rule which forms the basis for the development of Proportional Navigation and was used by some mariners to avoid a collision by changing the bearing angle, and thus line-of-sight, intentionally. Others used this technique to rendezvous each other at sea and sea pirates used it to catch merchantmen in old times [19]. This geometrical rule is also used by animals in order to catch their prey effectively [25].

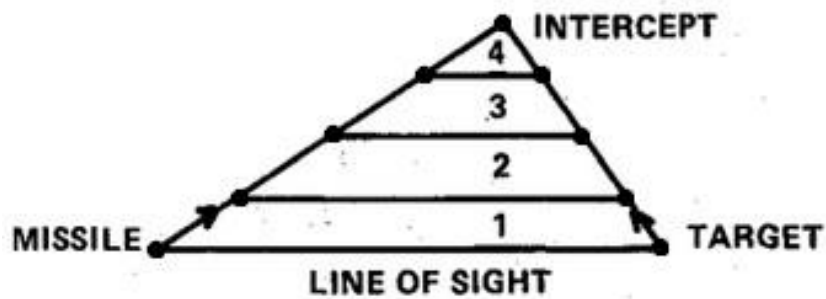


Figure 6.1: Parallel Navigation [26]

Some sources claim that the principles and equations of Proportional Navigation were developed by the German scientists at Peenemunde during the Second World War [27]. However, no proof of this assertion exists. Proportional Navigation is assumed to be invented in 1948 by C. L. Yuan at the RCA Laboratories in the USA. The first PN guided missile, Lark missile, was developed by Raytheon in the USA and intercepted a pilotless aircraft successfully in December 1950 [19]. It used a continuous wave active radar sensor to track the target [26]. Since that time, the Proportional Navigation technique is applied in plenty of homing guided weapons and proven to be reliable, effective and robust over the last six decades in many practical surface-to-air and air-to-air operations. It is mostly preferred due to its ease of implementation and robustness.

6.2 Proportional Navigation Guidance Law

As previously mentioned, in parallel navigation, a constant bearing angle is satisfied. Hence, the LOS rate is equal to zero under the assumption that the speeds of the evader and the pursuer are constant and the evader does not maneuver. However, in reality, the LOS rate is likely to differ from zero and Proportional Navigation Guidance Law aims to null out the effects of any LOS rate that may be developing during an engagement. This compensation is achieved by commanding lateral acceleration values that are normal to the line-of-sight to turn the missile accordingly at a rate that is proportional to the rate of LOS angle changes. The proportionality constant is called as the Effective Navigation Constant (N') which is a fixed value to be determined during the guidance system design stage.

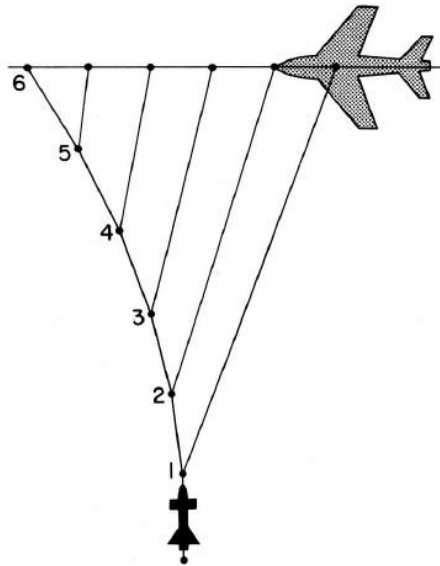


Figure 6.2: Proportional Navigation Guidance for a Planar Engagement

In Proportional Navigation, the angle the velocity vector of the missile makes with the inertial reference axis is proportional to the rate of change of LOS angle [26]. Here, the proportionality ratio, referred to as Navigation Ratio (N), is a time-varying dimensionless number.

$$\dot{\gamma} = N \dot{\lambda} \quad (6.1)$$

Two special values of N leads to specific forms of guidance laws. For $N = 1$, pure pursuit takes place whereas, for $N = \infty$, parallel navigation is observed [19].

There is a relationship between the navigation ratio and the effective navigation constant as follows.

$$N = N' \left(\frac{V_c}{V_M} \right) \quad (6.2)$$

Substitution of (6.2) into (6.1) yields the following equation.

$$\dot{\gamma} = N' V_c \dot{\lambda} / V_M \quad (6.3)$$

Lateral acceleration of the missile required for proper implementation of Proportional Navigation Guidance Law can be stated as below.

$$A_{M_{PNGL}} = V_M \dot{\gamma} \quad (6.4)$$

Finally, the Proportional Navigation Guidance Law can be expressed by the following equation.

$$A_{M_{PNGL}} = N' V_c \dot{\lambda} \quad (6.5)$$

Proportional Navigation Guidance Law is highly effective against not only stationary but also non-accelerating (constant velocity) or non-maneuvering targets.

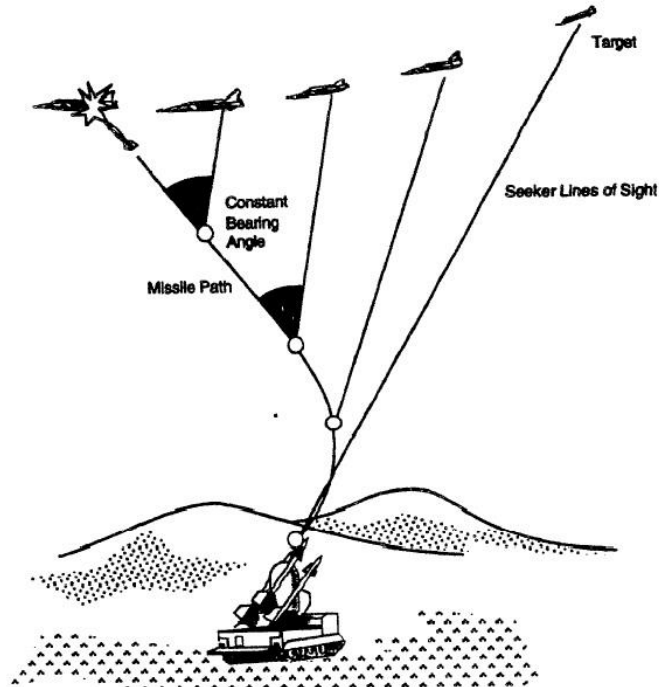


Figure 6.3: Proportional Navigation Guidance for a Spatial Engagement

6.3 Effects of Effective Navigation Constant on Guidance Performance

The effective navigation constant is usually selected to be between 3 and 5. The lateral acceleration commanded by the missile increases as a higher value is assigned as the effective navigation ratio, as a result the missile possesses more agility and there is a possibility of reducing hit time although more control effort and energy are to be spent. Besides, the lateral acceleration of the missile is not limitless and increasing the effective navigation ratio entails the risk of saturating the controllers which would not be desired especially during a thrilling end-game. On the other hand, high N' may recover larger heading errors as the capability of the missile to accelerate laterally increases. This fact is depicted in Figure 6.4.

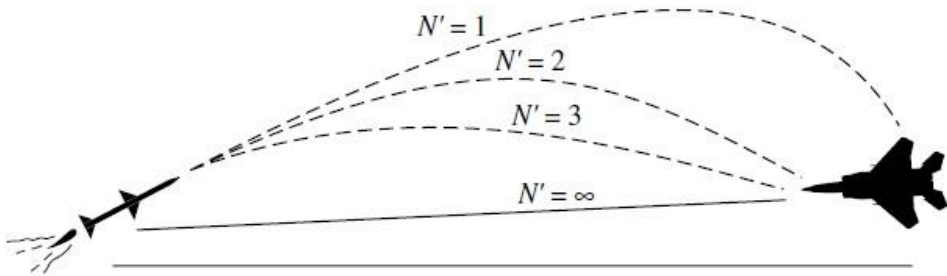


Figure 6.4: Effect of N' on Missile Flight Path [12]

However, as in most design works, with every advantage comes a drawback. Due to the fact that the LOS rate and closing velocity data are not perfect and corrupted by noise, the noise within the guidance system is also amplified by the selection of high effective navigation constant. As a result, the guidance system becomes more susceptible to high noise levels and the guidance performance is degraded.

It can be concluded that the maneuverability of the missile can be improved by selecting higher N' values unless the system is foreseen to be exposed to high levels of measurement noise.

6.4 Augmented Proportional Navigation Guidance Law

Augmented Proportional Navigation Guidance Law (APNGL) is a modified version of the well-known Proportional Navigation Guidance Law (PNGL). This advanced guidance law includes an additional term which compensates for the target maneuver. The derivation of APNGL is given below step by step.

To begin with, LOS angle can be stated as follows.

$$\lambda = \frac{y}{R_{MT}} = \frac{y}{V_C(t_F - t)} \quad (6.6)$$

Here, y stands for the relative missile-target separation in the corresponding engagement plane.

Using the quotient rule, the LOS rate can be expressed by taking the derivative of both sides in equation (6.6).

$$\dot{\lambda} = \frac{y + \dot{y}(t_{go})}{V_C t_{go}^2} \quad (6.7)$$

Here, t_{go} denotes the time to go until intercept and is explicitly defined in equation (6.8).

$$t_{go} = t_F - t \quad (6.8)$$

Hence, the Proportional Navigation Guidance Law can be equivalently expressed as follows.

$$A_{M_{PNGL}} = N' V_C \dot{\lambda} = \frac{N'(y + \dot{y}t_{go})}{t_{go}^2} \quad (6.9)$$

The expression in the parentheses of the above equation is the future separation between the pursuer and the evader. In other words, it represents the miss distance that would occur provided that the target did not maneuver and the missile did not make any further corrective maneuvers, which is also referred to as the Zero Effort Miss (ZEM) [12].

For a maneuvering target, the zero effort miss is augmented by an additional term and takes the following form.

$$ZEM_{APNGL} = y + \dot{y}t_{go} + 0.5A_T t_{go}^2 \quad (6.10)$$

Consequently, the Augmented Proportional Navigation Guidance Law is derived.

$$A_{M_{APNGL}} = \frac{N' ZEM_{APNGL}}{t_{go}^2} = N' V_C \dot{\lambda} + \frac{1}{2} N' A_T = N' \left(V_C \dot{\lambda} + \frac{A_T}{2} \right) \quad (6.11)$$

The level of target maneuver is predicted by a target estimator model to take role as an augmentation term in APNGL. Therefore, accurate target estimation is mandatory if APNGL is chosen as the guidance law. Unlike PNGL, APNGL can be used against targets that are accelerating and making maneuvers. Missiles implementing APNGL demand less lateral acceleration at the end of the engagement, which is a more critical phase of the flight, when compared to the missiles utilizing PNGL for the same final miss distance. However, more lateral acceleration is required at the beginning of an engagement if APNGL is used instead of PNGL. For $N' = 3$, APNGL requires the half of the acceleration it would demand with PNGL and an optimal guidance law is obtained, which means an increase in N' will result in larger miss distances. Another benefit of APNGL is the reduction of the total control effort spent during a pursuit since an extra information regarding the target maneuver is available. This additional knowledge lets the missile maneuver in a more efficient way. Thus, APNGL can be concluded to be superior to PNGL. A missile making use of APNGL usually requires about three times more lateral acceleration than the evader to capture the maneuvering target [13]. Although the APNGL is derived under the assumption of constant step target maneuver, it is pretty effective against all types of maneuvering targets. Therefore, it is a popular guidance law against maneuverable targets and used by many guidance systems including US air-defense Patriot missile system [19].

6.5 A Novel Supportive Guidance Algorithm to be Applied in Blind Flight Scenarios

Guidance laws are quite helpful in guiding the missile when the target appears in the field of regard of the seeker. Lateral acceleration values to be commanded by the missile in order to pursue the target successfully can be determined by the application of the guidance laws provided that the seeker is locked-on the intended target. However, guidance laws do not propose any way of dealing with predicaments wherein the evader gets rid of the vision of the tracking target sensor. Hence, when the target gets into the blind zone, missile has no idea about what to do while being supposed to chase and hit the target as quickly and accurately as possible. Yet, some precautions can be taken at the design stage of homing system to help missile in deciding on its future motion whenever it is unable to acquire the up-to-date information from the seeker regarding the range rate, LOS angles and the states of the target. At the instant the seeker loses track of the target as a result of any gimbal angle reaching to its maximum allowable limit, there seems a couple of actions a missile can take in order to position itself in such a way that the target appears in the field of vision of the missile seeker again and as soon as possible. In this section, a trivial attitude control method supported by a simple but effective novel algorithm that can be used in “Blind Flight” conditions is presented.

6.5.1 Attitude Control of Missile Airframe in Blind Flight

With the lack of LOS rate and closing velocity information as well as target acceleration estimations from the seeker, an easy and effective reaction would be to adjust the body attitude rates, namely pitch and yaw rates, so as to correct the attitude of the missile frame in space. In this study, target loss due to gimbal saturation is handled by triggering pitch and yaw rates to increase and/or decrease depending on which gimbal limit is being exceeded and in which direction it is being saturated. For instance, if the gimbal that provides information about the

motion that takes place in the azimuth plane is saturated after reaching to its maximum allowable limit in the positive CCW direction, say $+30^\circ$, the yaw rate of the missile is forced to increase by an amount, say 0.1 rad/s , by the yaw autopilot so that the corresponding gimbal angle will decrease and will no longer be saturated. Hopefully, the missile body will be directed towards the target after this corrective maneuver and seeker will be able to sense the target again and supply measurements to the guidance section. At this point, an analogy between the missile seeker and human eye can be posed to clarify the situation. Like missile seeker, field of vision of human eye is limited in vertical and horizontal directions. When an object does not lie inside the field of vision of the eye, a head movement in the corresponding direction would be necessary to make the object visible by the eye. The abovementioned method is tested on mathematically modeled guidance system and proved to be quite successful in reducing the gimbal angles and capturing of the target once again.

6.5.2 Geometric Illustration of the Developed Novel Algorithm

A new and feasible algorithm is developed to play a supportive role in acquiring the target via seeker again, once gimbal saturation is observed. The reason of declaring this method as having a supportive role is that it is not applicable on its own due to physical considerations, but acts as a complementary solution to the one discussed in Section 6.5.1. Figure 6.5 will aid in defining and explaining the method.

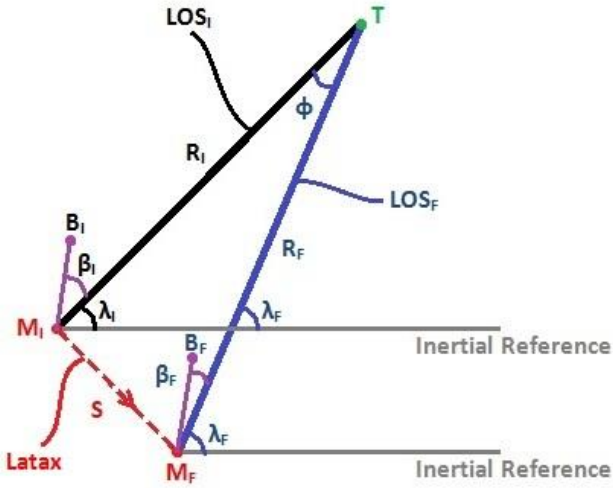


Figure 6.5: Geometric Illustration of the Novel Method

Here, a planar engagement geometry is depicted. The plane of interest can be considered as being either the azimuth plane or the elevation plane. Point T and M_I represent the instantaneous position of the target and the initial position of the missile, respectively, at the instant the related gimbal angle reaches to its maximum allowable limit and the seeker loses the track of the target. LOS_I , R_I and λ_I stand for the initial line-of-sight, missile-target range and LOS angle measured with respect to an inertial reference axis or a plane formed by two mutually perpendicular inertial reference axes. β_I is the initial look angle formed between the body frame of the missile and the instantaneous line-of-sight. Due to the fact that gimbal angles follow the look angles in order to keep track of the target, β_I can also be regarded as the corresponding gimbal angle reaching to its limit. In fact, there will be very small difference between these two quantities since the length of the missile is negligible compared to the relative range, except for the last meters of the pursuit, which is likely to take less than 10 per cent of a second.

It has been previously stated that Proportional Navigation Guidance Law aims to keep LOS angles almost constant for a successful intercept, but when the target disappears from the seeker's field of regard, guided flight condition does not

exist and guidance laws are not valid anymore. In contrast to PNGL, the object of the newly formulated method is to change the line of sight intentionally by an angle ϕ so that the look angle will decrease and the gimbal angle will be less than its maximum value by the same angle ϕ . By the application of a lateral acceleration being perpendicular to LOS, LOS angle can be changed to have a narrower look angle, which is denoted by β_F in the above figure. LOS_F , R_F and λ_F stand for the final line-of-sight, relative range and LOS angle, respectively. M_F is the new position of the missile after accelerating laterally. According to Figure 6.5, the following equalities and expressions can be written to prove these statements.

$$\lambda_F = \lambda_I + \phi \quad (6.12)$$

$$\lambda_F > \lambda_I \quad (6.13)$$

$$-\beta_I = -\beta_F + \phi \quad (6.14)$$

$$|\beta_F| < |\beta_I| \quad (6.15)$$

The minus signs in Equation (6.14) come from the adapted sign convention since the angles measured along CW direction are assumed to be negative and vice versa. In writing these equations, the body attitude of the missile is assumed to stay constant despite the lateral acceleration, which is not realistic. However, the proposed method can only be applicable when the missile's attitude is taken into account. At this point, the two methods recommended so far actually do not contradict, but supports each other. In order to realize a lateral acceleration along a certain direction, a missile is expected to adjust its body rates accordingly via its autopilot and lean towards the intended direction so that the drag is minimized. Otherwise, the motion would be against physical laws of nature and would not be possible.

Consequently, the missile is expected to accelerate laterally in order to change the line of sight and while doing so, the body motion should take place accordingly to facilitate the lateral motion.

6.5.3 Explicit Explanation of the Method from Mathematical Point of View

After introducing the geometrical relations that lead to the formation of the novel method, mathematical relationships can be presented to further scrutinize the technique. The novel algorithm is based on the fundamental equations of motion, but a couple of parameters need to be set as will be mentioned later. The corresponding equation of motion is given first.

$$S = V_{M_{LOS}} t + \frac{1}{2} A_{M_{LOS}} t^2 \quad (6.16)$$

Here, S is the lateral distance to be covered by the missile by the application of the lateral acceleration. This distance will be approximated by the following relationship.

$$S = R_I \phi \quad (6.17)$$

Obviously, the real S value will be slightly less than the one calculated by the formula above. The outcome of this fact will be acknowledged soon. It should be recalled that R_I is the relative range between the missile and the evader measured by the seeker just before the gimbal saturation is observed. Hence, R_I is a known quantity in spite of being corrupted by noise and can be directly used. Likewise, $V_{M_{LOS}}$ is the missile's velocity along the corresponding direction that is normal to the instantaneous line of sight and along which the lateral acceleration is to be applied. This direction will simply be along Y_{LOS} or Z_{LOS} as illustrated in Figure 4.2. Missile knows its velocity components along inertial reference axes throughout the engagement by the use of a precise Inertial Measurement Unit (IMU), however LOS angles are needed to be measured by the seeker to resolve the velocity vector of the missile in the LOS frame. Since LOS angles are available during the guided flight, missile's velocity can be resolved in the LOS frame simultaneously and the last

derived velocity components just before the target gets into the blind zone can take part in the equation of motion given in (6.16). $A_{M_{LOS}}$ is the quantity to be determined. It can turn out to be a positive or a negative quantity.

In equation (6.16), only two parameters are needed to be set in order to calculate the required lateral acceleration value. One of the parameters is the angle ϕ and it is set to be 30 per cent of the maximum allowable limit of the gimbal which is 30° for the case in hand. If the saturation limit of the gimbal is very big such as $+60^\circ$, use of smaller percentage values like 10 per cent seems to be logical. The other parameter to be decided on is the time t , in other words how long should it take for the missile to travel the lateral distance S . Assuming that a typical engagement will last between 10 to 15 seconds, 20 to 30 per cent of the time to go estimation can be assigned to t so that the missile will try to capture the target again in about 3 seconds. A practical way of estimating the remaining flight time until intercept is included below.

$$TTG_{est} \approx R_I / V_{C_I} \quad (6.18)$$

If t is selected to be more than 3 seconds, it may be very hard for the pursuer to acquire the target again since the target can handle different maneuver types along different directions in this time period. Selecting very small values for t such as 0.5 seconds is also hazardous since this will yield very large lateral acceleration values and there will be a risk of saturating autopilot controllers. Previously, it has been said that the distance S to be covered is less than the one calculated by (6.17). This fact yields lateral acceleration values slightly more than needed and as a result, it takes a little bit shorter time to cover the distance S , which usually has a positive influence on improving the guidance performance.

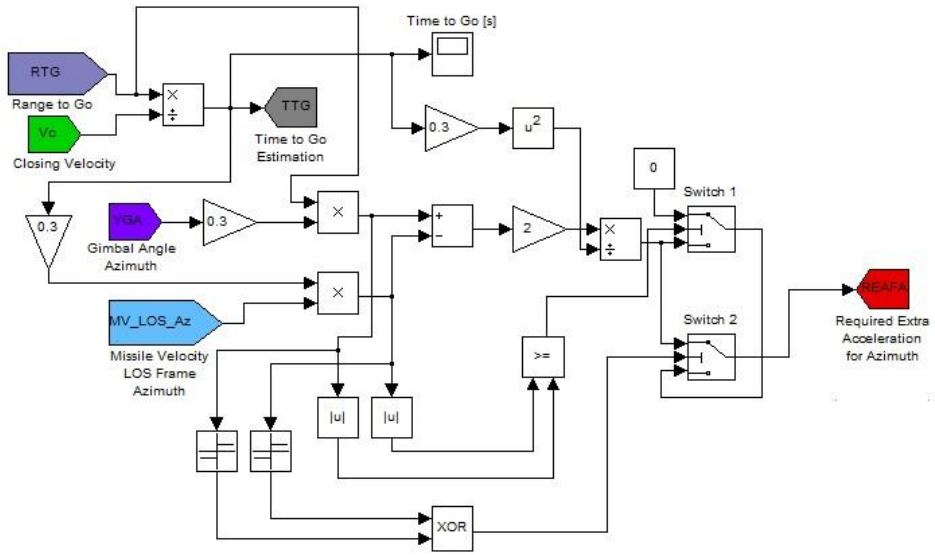


Figure 6.6: Simulink Representation of the Novel Algorithm for Azimuth

If the signs of the S and $V_{M_{LOS}}$ are the same and the absolute value of $V_{M_{LOS}}t$ term is bigger than the absolute value of S , then the implementation of the novel algorithm is not useful anymore. Because, for such a case, the missile will have a lateral velocity component adequate to catch up the target within a time period less than the specified time t . Hence, the novel algorithm will try to slow down the missile along the corresponding direction by the application of a lateral acceleration in the opposite direction. In this case, the missile will spent more energy and control effort due to the commanded lateral acceleration and it will last longer to capture the target. Indeed, for such cases, the missile does not have to accelerate laterally since the velocity of the missile will be sufficient to acquire the target again within the specified time period. In order to prevent this unwanted situation, two switches are added to the Simulink model in order to control the output of the novel algorithm.

The aforementioned analogies can be extended further at this point. The analogy between human eye and missile seeker was mentioned. Furthermore, the body attitude of the missile was associated with the head motion of a human. In addition to these analogies, the novel algorithm proposed can be associated with the lateral movement of a human accompanied by a head motion to see the object that initially lies outside the field of vision of the human.

6.5.4 Discussion on Benefits of the Novel Algorithm

The developed algorithm is run 100 times in *Monte Carlo* simulations wherein random noise models were involved, ending up with promising results. *Monte Carlo* simulations showed the improved performance of the guidance system with the novel algorithm as the average miss distance values has decreased while higher hit ratios are achieved as well. Since the time spent for capturing the target is expected to be less with the application of the developed algorithm, an improvement in the average engagement times can also be observed.

6.6 Autopilot Model

The required lateral acceleration values in azimuth and elevation directions computed by the guidance system are commanded to the autopilot section. Yaw and pitch autopilots take the guidance signals and aim to achieve the lateral acceleration values accurately and with minimum lag in order to ensure a successful collision. Nowadays, advanced autopilot models are responsible for the accomplishment of these duties and the effect of autopilot section on guidance performance in terms of obtained miss distances are considered to be negligible compared to other overwhelming effects including target maneuver and noise sources. In this study, as mentioned earlier, instead of a detailed autopilot model consisting of aerodynamic effects and dynamic models of missile airframe, the relationship between the commanded and achieved lateral acceleration values is demonstrated via a 1st order transfer function as given below since the main aim of this study is to focus on designing a seeker and a guidance system rather than an autopilot control system.

$$TF_{AC} = \frac{1}{\tau_{AC}s + 1} \quad (6.19)$$

With the use of 1st order transfer functions for yaw and pitch channels, time constants can be varied to introduce lag and adjust the responsiveness of the autopilot model. For simulation studies, τ_{AC} is chosen to be 0.3 seconds for both yaw and pitch channels. The smaller the time constant is, the faster the system responds, and thus an improvement in the guidance performance in terms of miss distances is expected to be observed for small autopilot time constants. A perfect response autopilot can also be assumed for simulation purposes if the effect of autopilot lag is beyond the scope of the study.

Another important subject that needs to be addressed at this point is the saturation limits of the lateral acceleration values. Of course, the required lateral acceleration values calculated by the guidance laws cannot be achieved all the time due to finite lateral acceleration capabilities of the missile. In this study, a limit of $35g$ is set to observe the effect of lateral saturation on guidance performance.

Lastly, the body angle and body rate of the missile in elevation plane are approximated by the assumption of resulting lift and drag forces that apply on the missile body frame and aim to cancel the effect of gravitational force. The body angle is simply the sum of the flight path angle (γ) of the missile and the angle of attack (α).

$$\theta_{m_{pitch}} = \gamma + \alpha \quad (6.20)$$

Here, flight path angle (γ) is the angle formed between the missile's velocity vector and the horizontal plane formed by inertial reference axes X_{ref} and Y_{ref} .

$$\gamma = \text{atan2}\left(V_{M_Z}, \sqrt{V_{M_X}^2 + V_{M_Y}^2}\right) \quad (6.21)$$

In addition, the time rates of each term in Equation (6.20) yield the following equality.

$$\dot{\theta}_{m_{pitch}} = \dot{\gamma} + \dot{\alpha} \quad (6.22)$$

By definition, the angle of attack is the angle between a reference line that can be selected to be longitudinal axis of the missile and the resultant relative wind which is directed opposite to the movement direction of the body frame relative to the atmosphere. Drag force (D) acts in the opposite direction to the relative motion and a lift force (L) perpendicular to the relative air flow direction arises due to the angle of attack. The coefficient of lift is assumed to vary linearly with the angle of attack until the critical angle of attack value is attained. Stall is experienced after the angle of attack exceeds the critical value.

Drag force is given by the following formula where the drag coefficient C_D is an even function of the angle of attack and can be assigned a fixed value for small angles of attack depending on the shape of the body exposed to air flow. ρ is the air density and equals 1.225 kg/m^3 at sea level and at 15°C . V_M is the speed of the missile and A_{CS} is total area exposed to oncoming air flow which can be approximated by the cross-sectional area of the missile body frame for small angles of attack.

$$D = \left(\frac{1}{2}\rho V_M^2\right) A_{CS} C_D \quad (6.23)$$

Lift force equation and the variation of lift coefficient with respect to angle of attack in degrees are also given below.

$$L = \left(\frac{1}{2}\rho V_M^2\right) A_{CS} C_L \quad (6.24)$$

$$C_L = C_{L\alpha} \alpha \quad (6.25)$$

Since an endoatmospheric missile is under consideration, a gravitational force resulting from the mass of the missile acts downward. Sideslip (β_s) angle is neglected since it usually takes very small values during flight of a missile having bank-to-turn (BTT) configuration. BTT configuration is suitable for highly maneuverable high-speed missiles and regarded as a decent choice for alleviating the difficulty experienced in attacking high-g targets which may be encountered by missiles having skid-to-turn (STT) configuration [12]. Therefore, BTT configuration can be considered as a reasonable assumption. Due to negligible sideslip angle, the body attitude of the missile in azimuth plane is directly taken to be coinciding with the missile's velocity component in azimuth plane.

$$\theta_{m_{yaw}} = \text{atan2} (V_{M_Y}, V_{M_X}) \quad (6.26)$$

$$\dot{\theta}_{m_{yaw}} = \frac{d}{dt} [\text{atan2} (V_{M_Y}, V_{M_X})] \quad (6.27)$$

Angle of attack and the forces that act on the missile body frame are illustrated on the Figure 6.7.

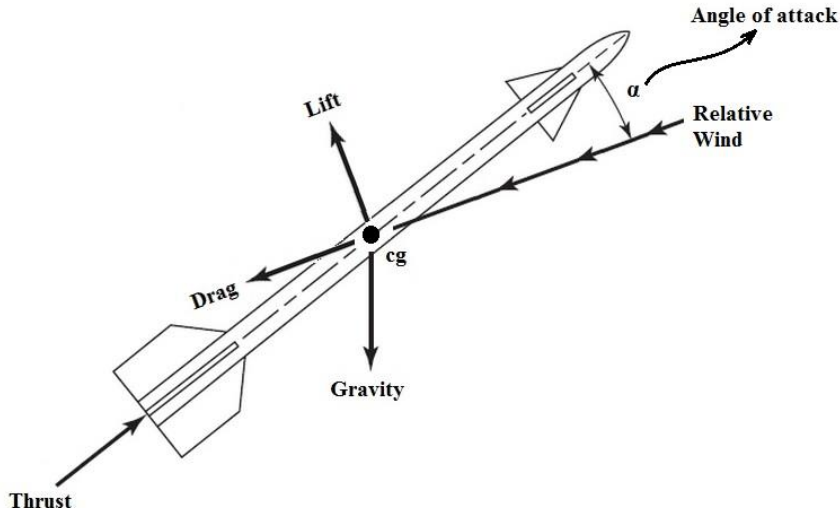


Figure 6.7: Angle of Attack and Forces Acting on Missile

In order to cancel out the effect of gravitational force by the developed drag, lift and thrust forces acting on the missile, the following equation must be satisfied which poses a trim condition for the flight simulation.

$$L \cos \gamma - D \sin \gamma + T \sin(\gamma + \alpha) - mg = 0 \quad (6.28)$$

As the mathematical substitutions and manipulations are handled in equation (6.28), the time-varying angle of attack can be expressed in radians by the following formula, except the boosting phase, and then, can be used in determination of the body pitch angle ($\theta_{m_{pitch}}$) and its rate ($\dot{\theta}_{m_{pitch}}$) as suggested by equations (6.20) and (6.22).

$$\alpha \approx \alpha_{trim} = \left[\frac{mg}{(1/2\rho V_M^2)A_{CS}C_{L\alpha} \cos \gamma} + \frac{C_D}{C_{L\alpha}} \tan \gamma \right] \frac{\pi}{180} \quad (6.29)$$

In this study, the mass of the missile is assigned to be 90 kg and the diameter of the missile's cross-section is taken as 15 cm while g is acting downward with a magnitude of 9.81 m/s². Drag coefficient (C_D) is taken as 0.3 and 0.1 deg⁻¹ is assigned for $C_{L\alpha}$.

Flight path angle and angle of attack variations together with body attitude angles are plotted in Figure 6.8. In this scenario, target is supposed to make $2g$ and $5g$ step maneuvers along in yaw and pitch planes, respectively. Figure 6.9 shows the variations of drag and lift forces with respect to time of flight. Lastly, the speed curve of missile is given in Figure 6.10. The speed of missile increases from 1.6 Mach to 3.4 Mach during the engagement which was completed in 11.17 seconds resulting in a miss distance of 0.3034 meters.

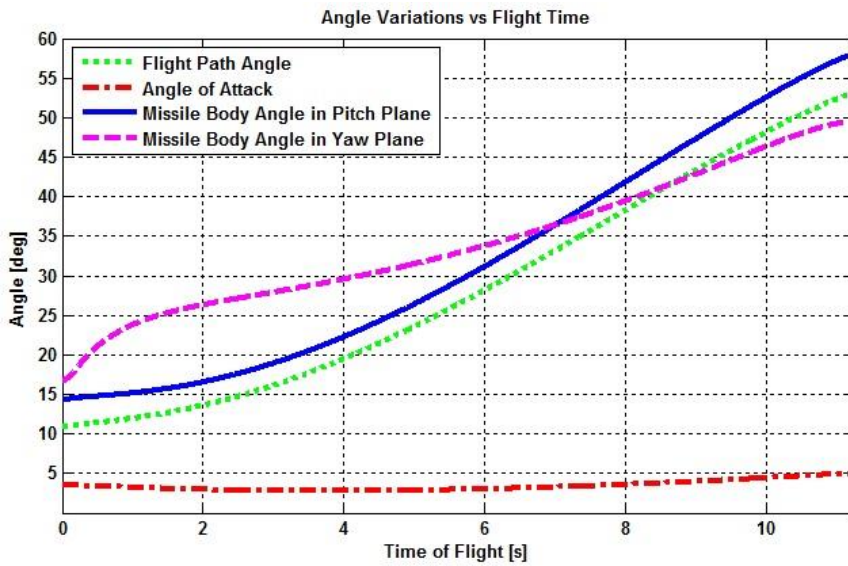


Figure 6.8: Angular Variations with Flight Time

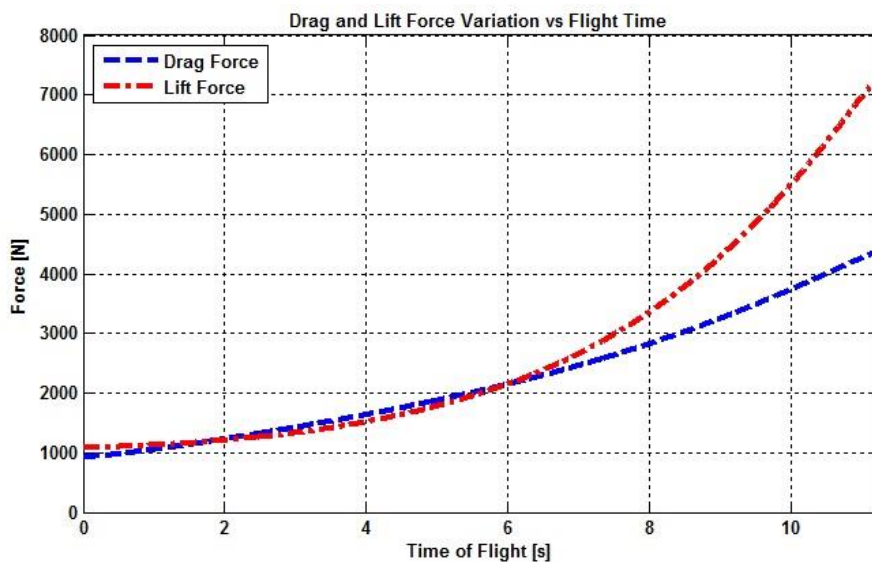


Figure 6.9: Drag and Lift Force Variation with Flight Time

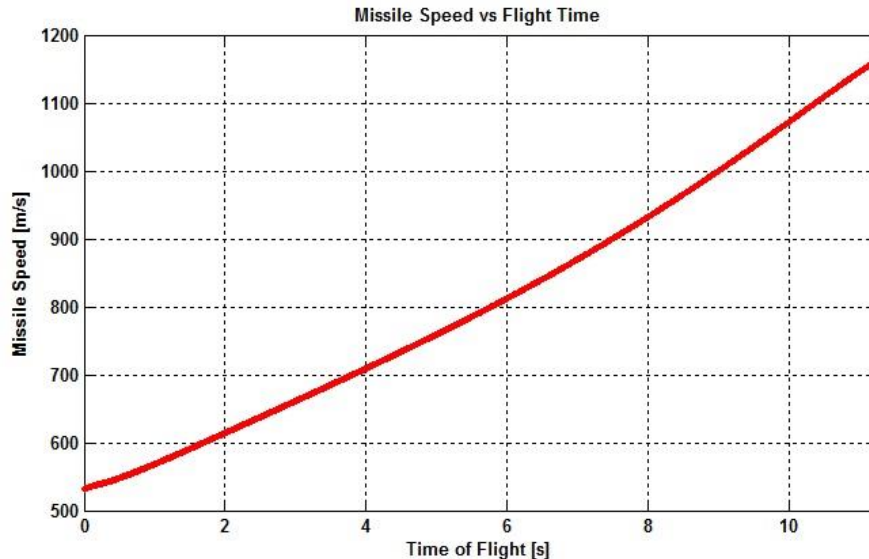


Figure 6.10: Missile Speed Variation with Flight Time

6.7 Missile Maneuver Model

For simulation purposes, the achieved lateral acceleration components are transformed from LOS frame to inertial reference frame as demonstrated in Appendix A.2 and then integrated twice to obtain, in turn, velocity components and the position of the missile in space. In real guidance engineering applications, this transformation process is not needed to be performed, since an acceleration vector can be resolved in any arbitrary frame of interest but will obviously lead to the same path of motion in space no matter it is resolved in LOS frame or in inertial reference frame.

PN guidance laws do not have a direct influence on the acceleration component along the LOS, in order to alleviate this issue, a thrust strategy is modeled to be applied in ‘Mid-Course Guidance’ conditions to provide ramp acceleration along the initial line of sight until the missile-target range reduces to seeker lock-on range and guided flight starts. An example illustrating this challenging scenario is included in the “Simulation Results” section.

CHAPTER 7

SIMULATION RESULTS

7.1 End-Game Plots of Pursuer and Evader for Distinct Target Maneuver Types and Guidance Scenarios

Figure 7.1 illustrates a target taking a $5g$ step maneuver along X_{ref} while gaining altitude in Z_{ref} . The simulation lasted 11.34 seconds with a miss distance of 1.185 meters.

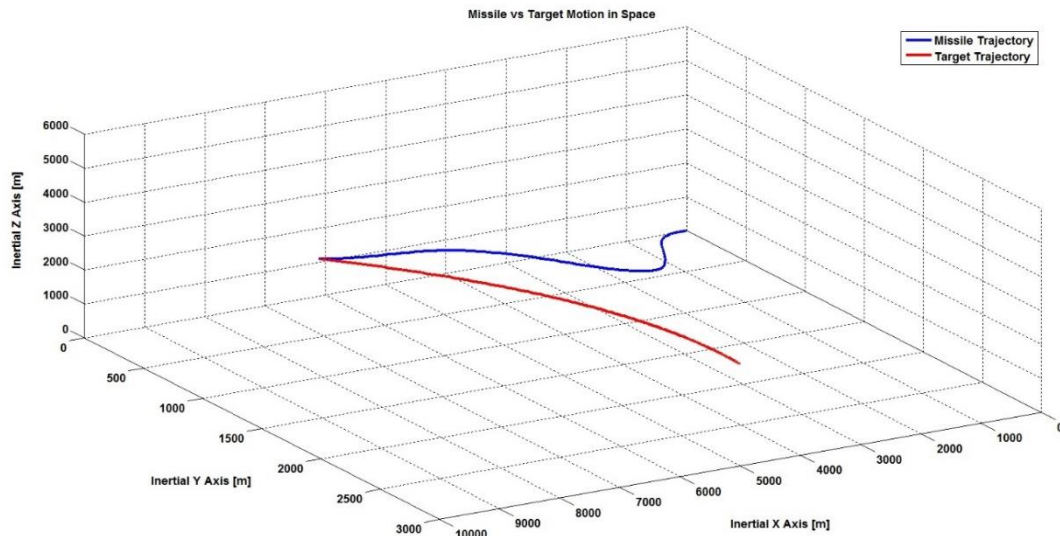


Figure 7.1: $5g$ Step Maneuvering Target

Figure 7.2 shows a target taking a hard pull return maneuver of $7g$ in horizontal plane while keeping its altitude. The engagement took 10.62 seconds resulting in a miss distance of 1.229 meters.

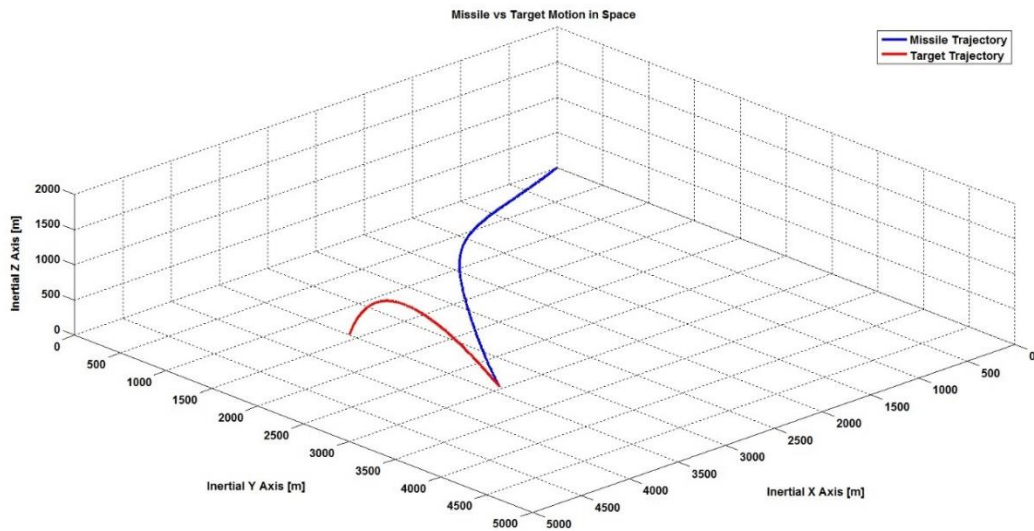


Figure 7.2: Hard Pull Return Target Maneuver

In Figure 7.3, target is making evasive maneuvers of $3g$ along X_{ref} , $7g$ along Y_{ref} and $5g$ along Z_{ref} to get rid of the chasing missile. A heading error of about 25° is introduced at the launch in order to cause “Blind Flight” condition at the beginning and pose a more challenging scenario. The saturation limits of the gimbals are set to $\pm 30^\circ$. Unfortunately, seeker loses the target at the beginning of the engagement, but achieves to lock onto the target again after 0.57 seconds, thanks to the supportive guidance algorithms being implemented. For this scenario, the miss distance was 1.915 meters and the simulation was completed in 11.37 seconds.

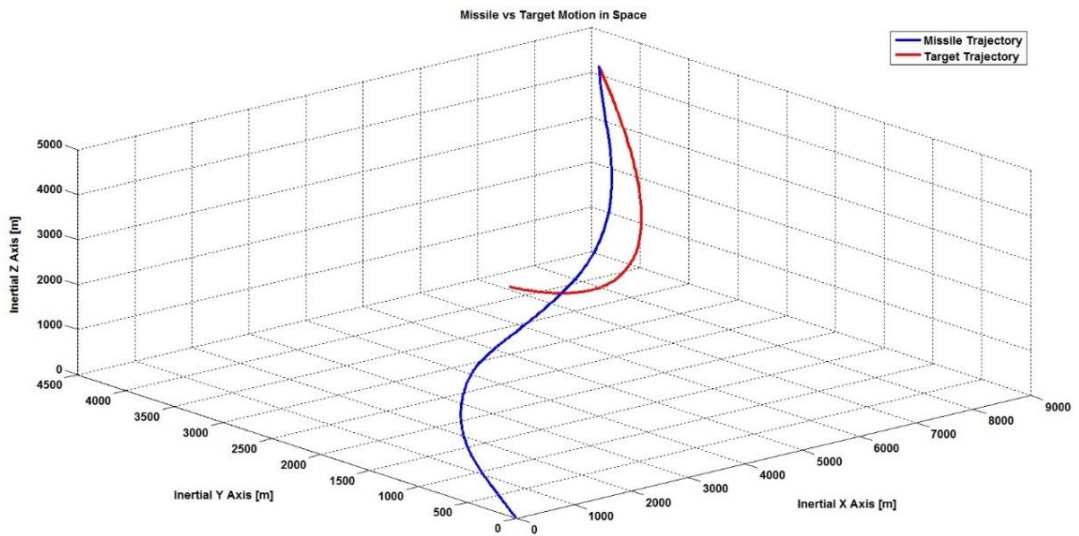


Figure 7.3: Target's Evasive Maneuver along all Directions

In Figure 7.4, a tail-chase engagement scenario is plotted. Here, target changes its acceleration every 3 seconds. Its acceleration values are $3.5g$, $-3.5g$, $-5g$, $4.5g$, $7.5g$, $-4.5g$ during the engagement. The corresponding miss distance was 2.18 meters and the total flight time was displayed as 15.89 seconds.

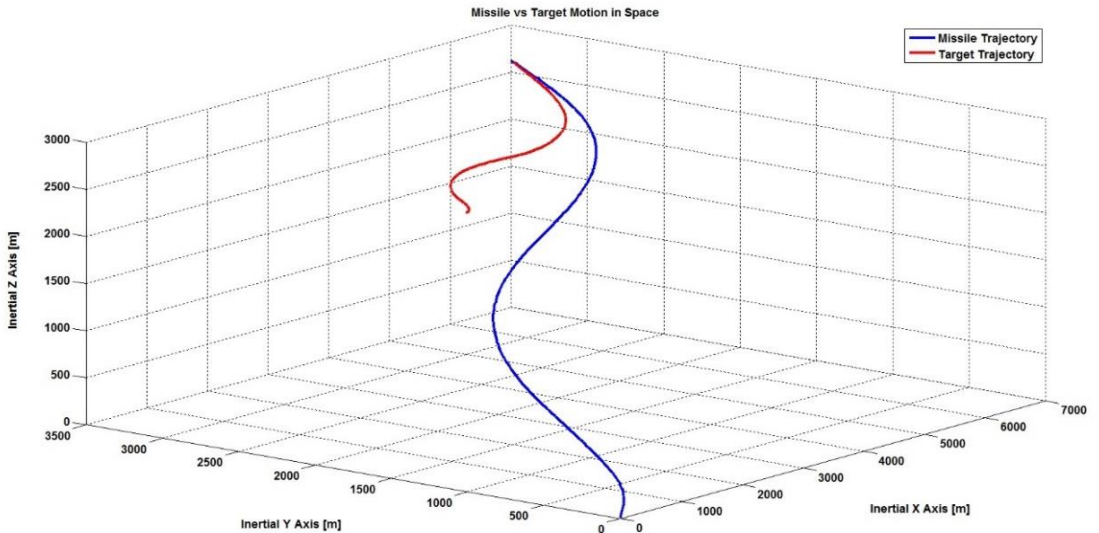


Figure 7.4: Piecewise Step Target Maneuver

Figure 7.5 demonstrates a target accelerating linearly from $1g$ to almost $10g$ along Z_{ref} direction before being hit at $t_f = 10.97$ seconds. The miss was recorded to be 0.9923 meters.

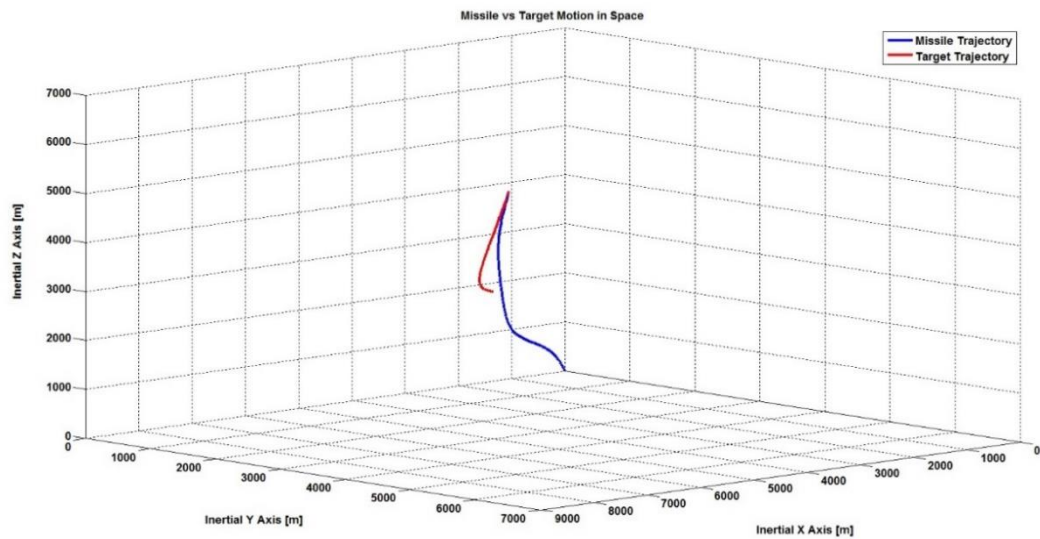


Figure 7.5: Altitude Gaining Target

In Figure 7.6, target dives with a negative ramp acceleration input attaining $4.5g$ along $-Z_{ref}$ at the instant of interception. The calculated miss was 0.573 meters and the missile hit the target after 10.75 seconds it has been launched.

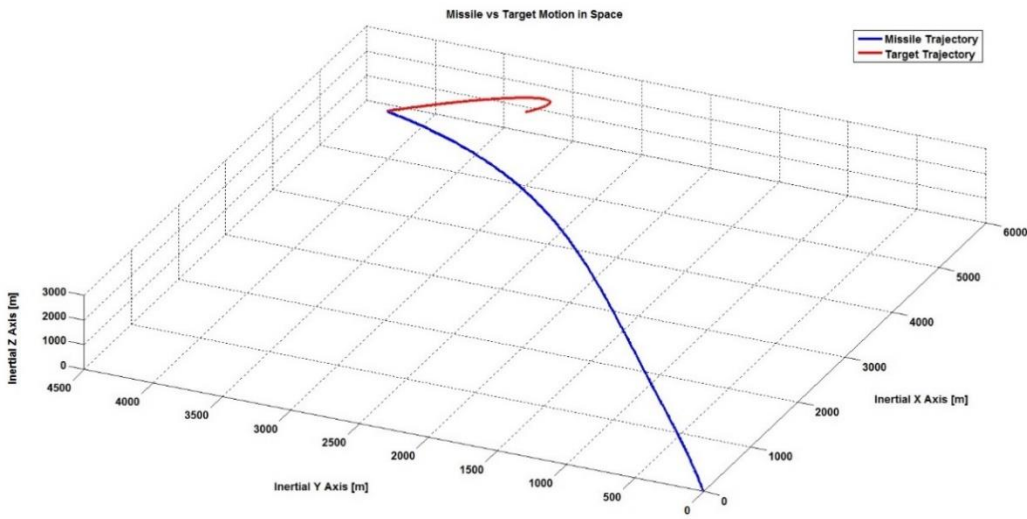


Figure 7.6: Target's Nose Dive Maneuver

In the figure below, target makes $5g$ weaving maneuvers with 0.8 rad/s weaving frequency in horizontal plane in order to deceive the missile. The weaving motion of the missile during the pursuit can be clearly seen. For this guidance scenario, miss distance happened to be 3.89 meters, which can be regarded as a miss rather than a successful hit. The whole simulation was completed in 14.97 seconds.

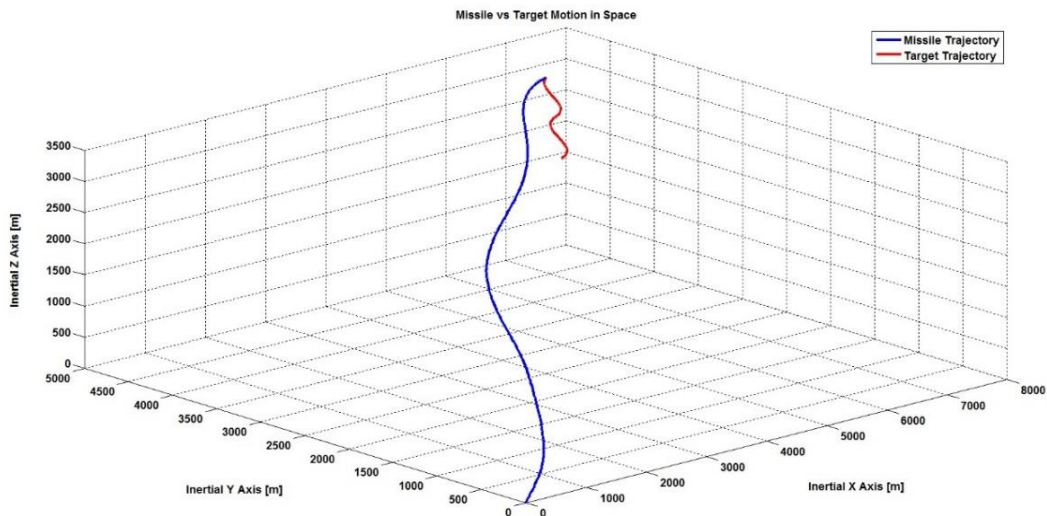


Figure 7.7: $5g$ Weaving Maneuver of the Target in Horizontal Plane

Weaving target maneuver of $3.5g$ magnitude at 0.5 rad/s frequency is depicted in the figure below. The weave maneuver takes place in the vertical plane. Target also has $1g$ acceleration along X_{ref} and Y_{ref} directions to escape from the missile. Missile is seen to achieve required latax commands to pursue the target. The corresponding miss emerged to be 2.582 meters and the total flight took 16.67 seconds.

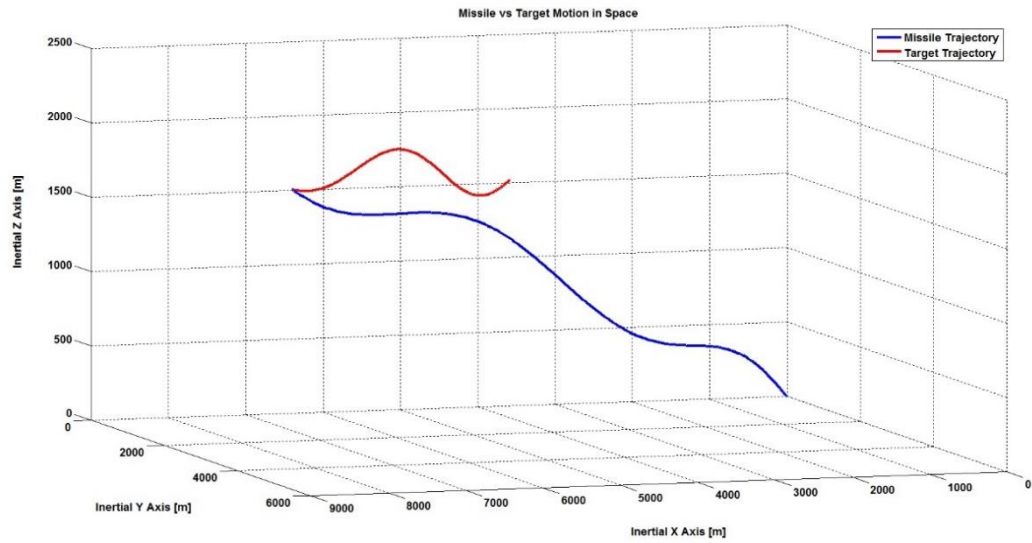


Figure 7.8: $3.5g$ Weaving Maneuver of the Target in Vertical Plane

In the guidance scenario illustrated below, the lock-on range of the seeker is set to be 3 km whereas the initial missile-target range is about 6 km. Target makes $5g$ and $3g$ step maneuvers in horizontal and vertical planes, respectively. Missile is directed towards the target at launch and accelerates to $23g$ along the initial line-of-sight until the relative range drops below 3 km. The acceleration along the initial X_{LOS} is provided by supplying ramp thrust input to the missile. At the moment the missile-target range reduces down to 3 km, the target gets into the field of vision of the seeker and guided flight gets started. Fortunately, the missile hits the target although it required quite huge acceleration values in each direction as can be

observed from the Figure 7.10. For such a challenging engagement scenario, calculated final miss value turned out to be 0.1823 meters. The simulation was completed in 11.92 seconds. The seeker was able to lock on the target 5.43 seconds after it has been launched. Seeker data was not available for the first 5.43 seconds, therefore required latax values could not be computed, which can be seen from the Figure 7.11.

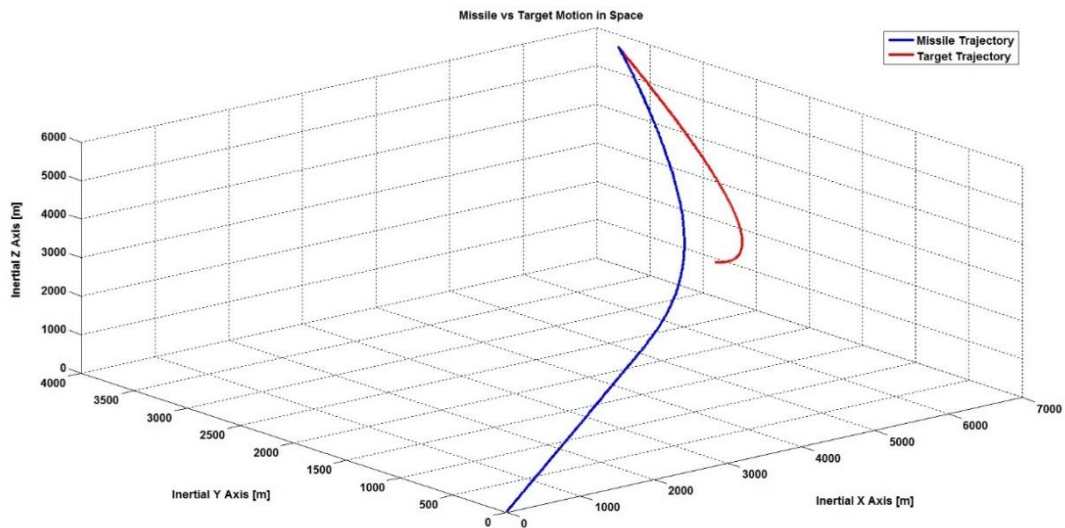


Figure 7.9: Guidance Scenario with ‘Mid-Course Guidance’ Condition

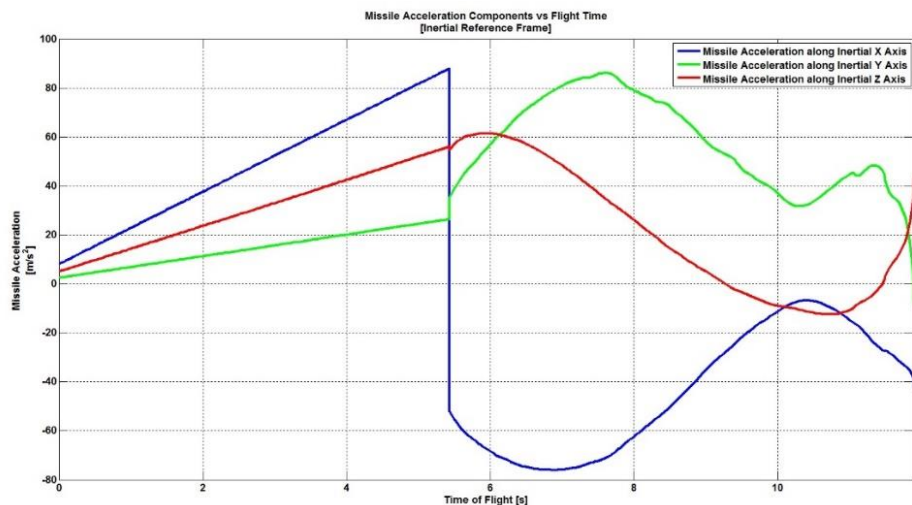


Figure 7.10: Missile Acceleration Components along Inertial Axes

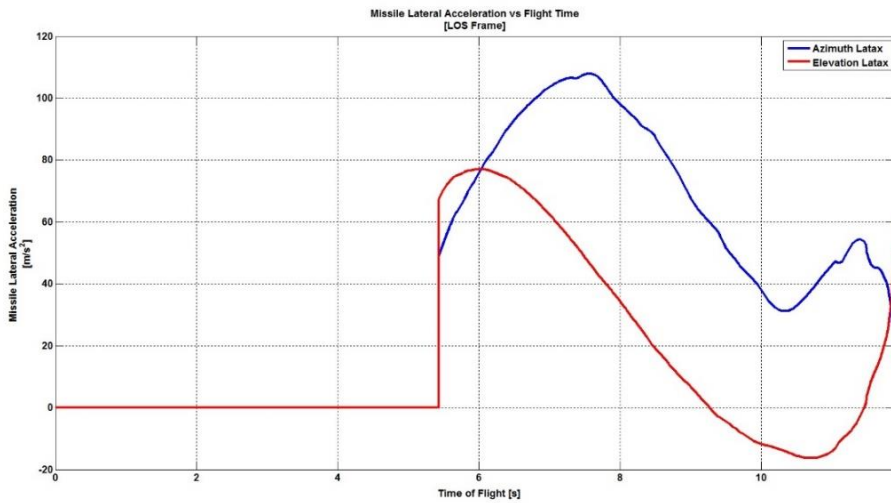


Figure 7.11: Missile Latax Components along LOS Axes

A head-on engagement is simulated in the figure below. Such engagements pose a great deal of difficulty for the pursuer as mentioned before in Chapter 3 due to high closure rates experienced. For this scenario, 5.953 meters of miss distance occurred, and the closest approach was achieved by the pursuer at $t_f = 7.015$ seconds.

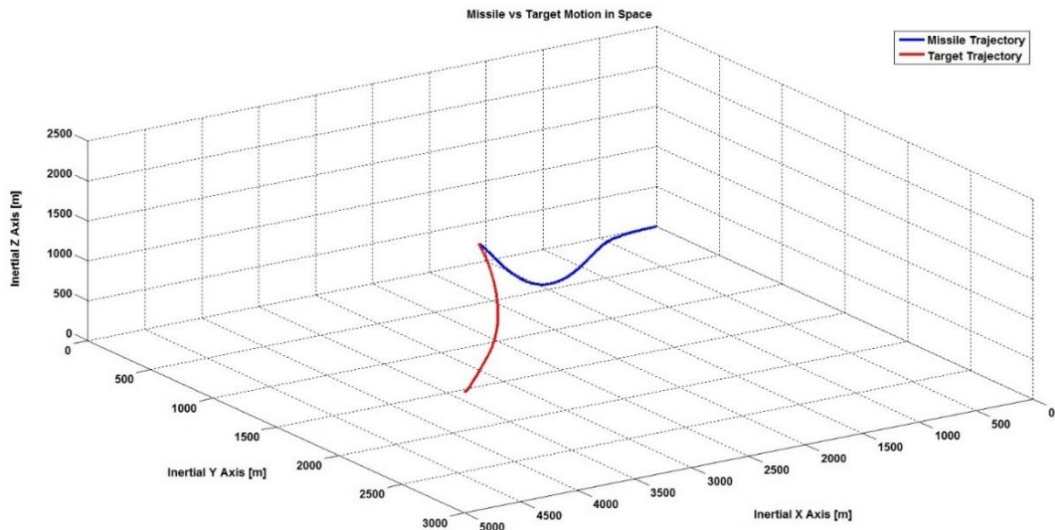


Figure 7.12: Head-On Engagement

An air-to-air engagement is simulated in Figure 7.13. Here, the missile is launched 500 m over the evader that is handling piecewise step maneuver to get rid of the missile. The miss distance was computed to be 1.887 meters and it took 17.05 seconds for the missile to collide the target.

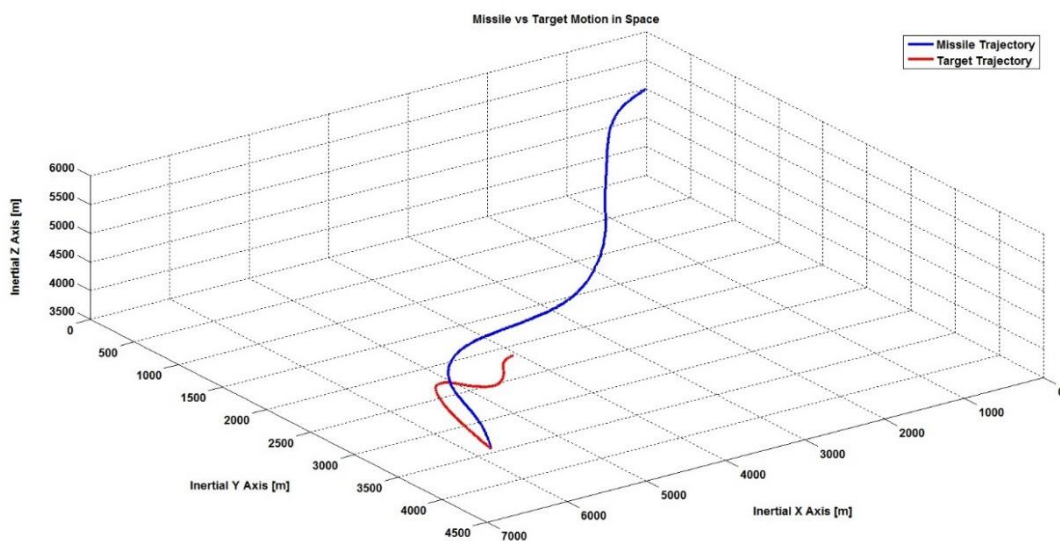


Figure 7.13: Air-to-Air Engagement

In Figure 7.14, an air-to-air tail-chase engagement scenario is shown. Here, target do not start maneuvering but continue flying horizontally with constant speed for 5 seconds. After 5 seconds, when the missile is diving to intercept the evader, the target starts making a $6g$ turn and a $3g$ rising maneuver at the same time to escape from the missile. For this case, calculated miss was 0.06236 meters and the total flight was completed in 10.58 seconds.

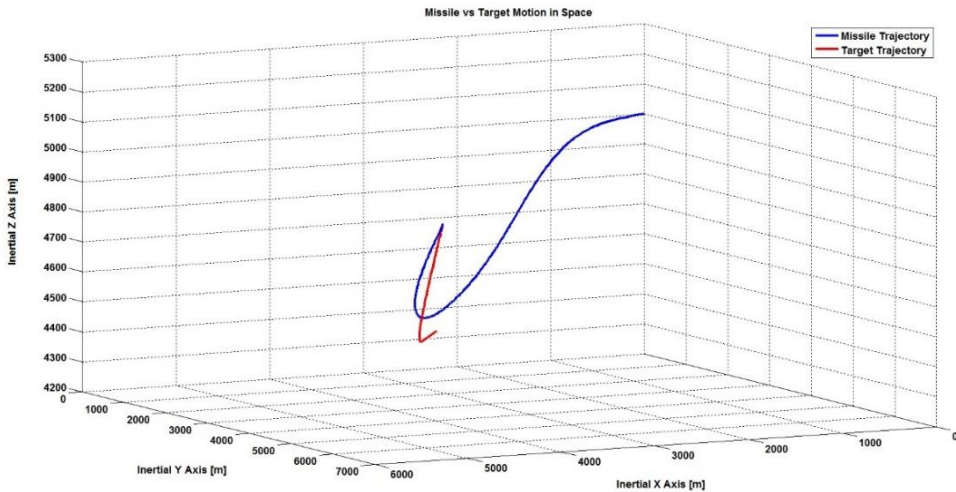


Figure 7.14: Delayed Target Maneuver

Figure 7.15 illustrates another challenging air-to-air pursuit scenario. For this case, the target maneuver is modeled exactly based on the maneuver types indicated in the Section 5.2.1. Therefore, target is performing weaving, step and piecewise step maneuver along X_{ref} , Y_{ref} and Z_{ref} in order to evade from the chasing missile. The scenario ended up in 17.67 seconds resulting in a final miss distance of 2.862 meters.

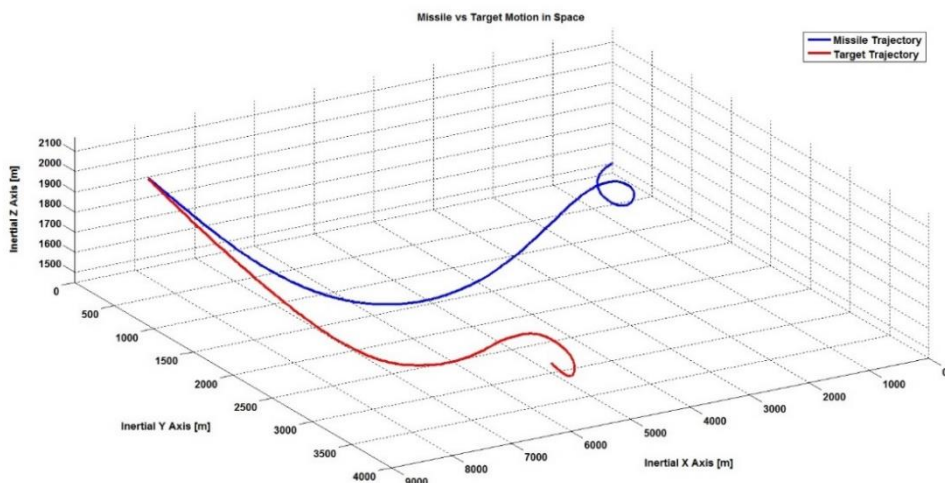


Figure 7.15: Target Making Combined Maneuver Types

In the figure below, target is making a fast circular motion with a radius of 1500m at 5000m altitude while the missile is fired from ground. The pursuer is initially placed at the center of the projected circular path of the evader. In such a pursuit scenario, the pursuer requires pretty high lateral acceleration values to track the evader. The commanded lateral acceleration value in azimuth exceeds the acceleration capability of the missile which is limited at $35g$ for this study. The lateral acceleration demand of missile in azimuth plane is plotted in Figure 7.17. The simulation ended in 5.5 seconds resulting in a miss distance of 19.88m which can be regarded as a miss rather than a successful hit.

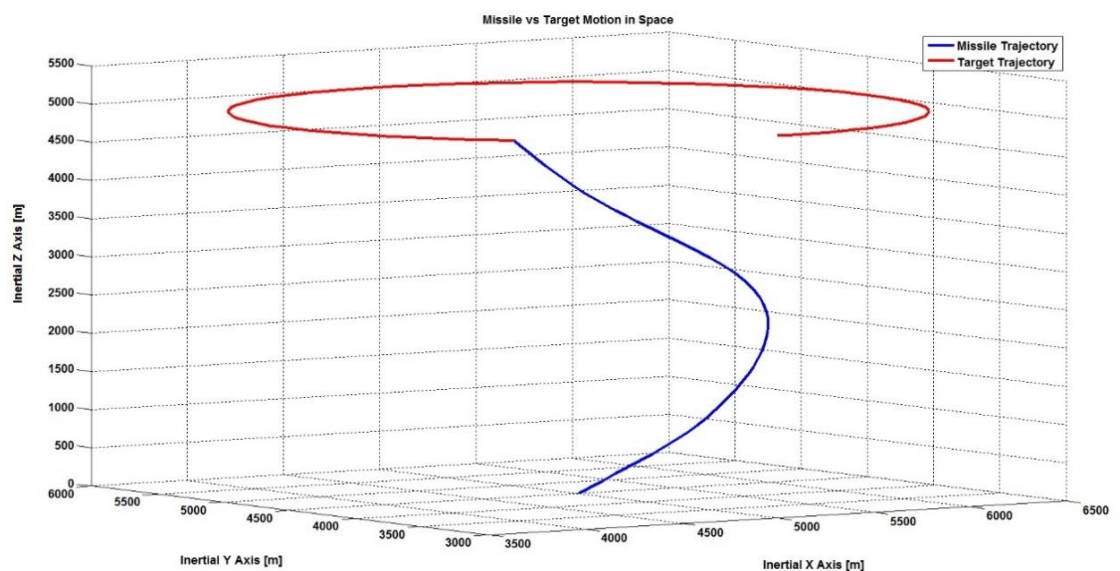


Figure 7.16: Target Making Fast Circular Motion

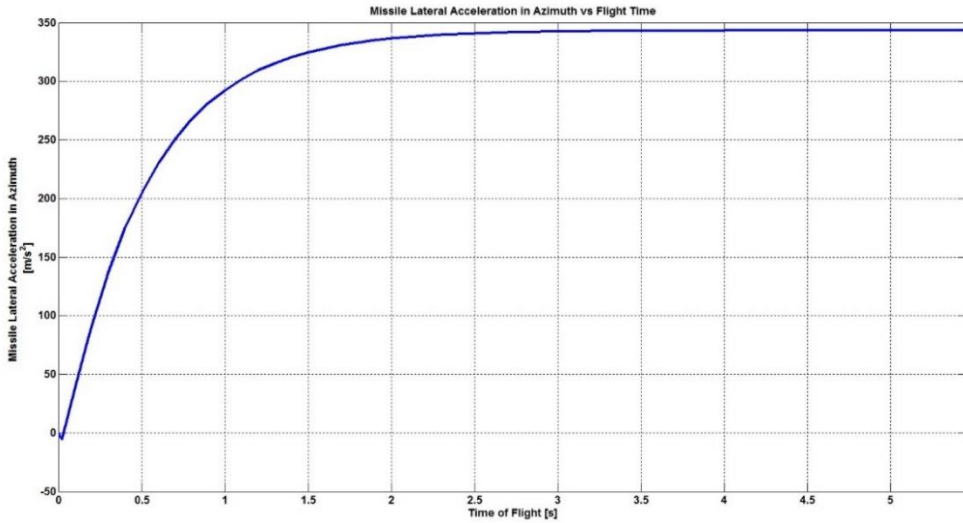


Figure 7.17: Lateral Acceleration Demand of Missile in Azimuth

In Figure 7.18, target is modeled to make distinctive maneuver types along each direction and switch the corresponding maneuver types 5s after the air-to-air engagement begins in order to deceive the target estimator. For this purpose, the evader changes its maneuver type from $7g$ step maneuver to $5g$ weave maneuver with a weaving frequency of 0.7 rad/s along X_{ref} . Similarly, along Y_{ref} , the maneuver type is switched from $5g$ weaving with 0.7 rad/s frequency to piecewise step maneuver with $[4.5g, -1.5g, -5g, 7.5g, 4.5g]$ maneuver amplitudes changing every 3 seconds. This piecewise step maneuver is also what the target handles along Z_{ref} for the first 5 seconds and then, it is altered to $7g$ step maneuver for the rest of the engagement. The whole simulation lasted for 14.34 seconds and the final miss distance was calculated to be 2.83 meters.

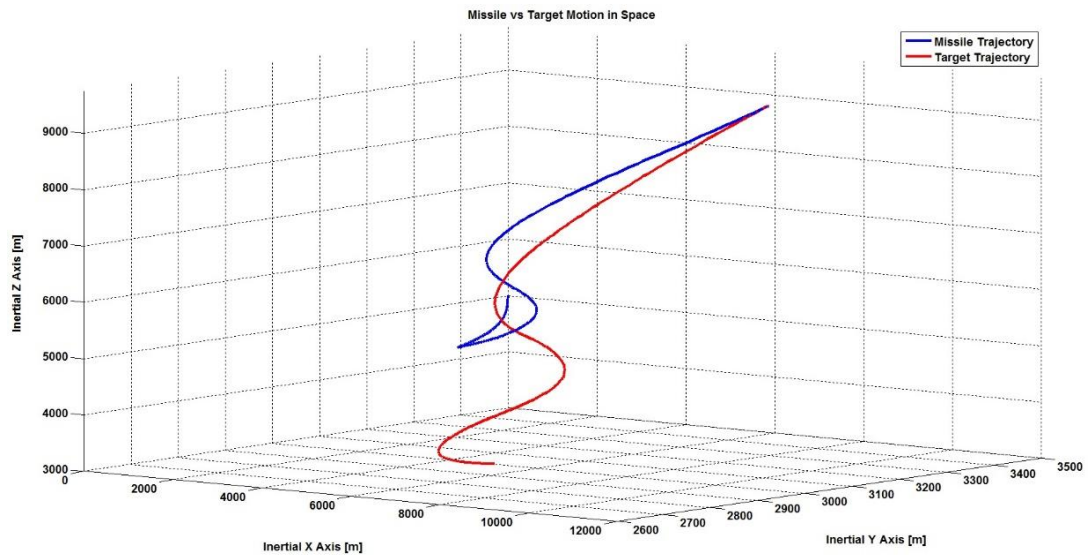


Figure 7.18: Target Switching in between Maneuver Types

7.2 Monte Carlo Simulations and Miss Distance Analysis

A homing guidance system has been developed so far in order to track a maneuverable target in the presence of distinctive noise types. Modeling stages of each subsystem and related simulation results have been presented in detail.

The effectiveness of the modeled guidance system in challenging engagement scenarios has been proven by the end-game simulation results. However, these simulation results were obtained as a consequence of single simulation run. Therefore, it can be concluded that, due to the randomness of the noise sources and target maneuver, it is possible to obtain different results each time the simulation is run. Although random noise sources and target maneuvers are the main contributors of the miss distance, they sometimes may work in the favor of guidance system performance improvement as well. In order to ensure the reliability of the acquired results, multiple simulation trials should be conducted and the results need to be evaluated based on a statistical approach. This process can be considered as collecting experimental data in computer environment.

For this purpose, the well-known *Monte Carlo* simulations will be carried out to reveal the likelihood of guidance system performance indicators including average miss distance, maximum miss distance, minimum miss distance, hit ratio and average engagement times.

Miss distance distributions are also included in the form of histogram where X axis represents the miss distance values in meters and Y axis represents the frequencies of obtained miss distance values.

Since it would be extremely expensive and time consuming to test the performance of the designed guidance system against numerous guidance scenarios by launching hundreds of real missiles targeted at real evaders, *Monte Carlo* simulations serve as a decent and practical way of assessing the performance of the developed homing guidance systems [25]. *Monte Carlo* simulations are repeated randomly for 100 times. Target maneuver and engagement types, noise and error models, seeker and target estimator models as well as guidance algorithms are stated clearly to help reader in visualizing the corresponding guidance scenario.

Unless otherwise stated, only one parameter is varied to compare and contrast the effect of this specific factor on overall guidance performance and all other factors are identical.

7.2.1 Comparison of Target Maneuver Models

Baseline for Target Maneuver Model Comparisons

Engagement Type	Target Estimator Model
Tail-Chase Pursuit	Third Order Fading Memory Filter
Surface-to-Air Engagement	
Noise Model	Guidance Algorithm
Random Gaussian Noise for Range-to-Go	APNG Law ($N' = 3$)
Sinusoidal Noise for LOS Angles	Body Attitude Control
Radome Error for LOS Rates	Novel Extra Latax Algorithm

Seeker Model

Gimbaled Seeker Model
Blind Flight Condition Applicable

Variable Parameters for Cases 1 through 9

Case 1

Target Maneuver

X: $1g$ Step Maneuver
Y: $3g$ Step Maneuver
Z: $2g$ Step Maneuver

Case 2

Target Maneuver

X: $1g$ Step Maneuver
Y: $3g$ 0.8 rad/s Weaving Maneuver
Z: $2g$ Step Maneuver

Case 3

Target Maneuver

X: $1g$ Step Maneuver

Y: $[1 \ 5 \ 3 \ 2 \ 4]g$ 3s Piecewise Step Maneuver

Z: $2g$ Step Maneuver

Case 4

Target Maneuver

X: $1g$ Step Maneuver

Y: $3g$ Step Maneuver

Z: 0 to $5g$ Ramp Maneuver

Case 5

Target Maneuver

X: $1g$ 0.7 rad/s Weaving Maneuver

Y: $[1 \ 5 \ 3 \ 2 \ 4]g$ 2.5s Piecewise Step Maneuver

Z: $2g$ Step Maneuver

Case 6

Target Maneuver

X: $\pm 1g$ Random Step Maneuver

Y: $\pm 3g$ Random Step Maneuver

Z: $\pm 2g$ Random Step Maneuver

Noise Model

Noise-free

Case 7

Target Maneuver

X: $\pm 1g$ Random Step Maneuver

Y: $\pm 3g$ Random Step Maneuver

Z: $\pm 2g$ Random Step Maneuver

Case 8

Target Maneuver

X: $1g$ Step Maneuver

Y: $3g$ 0.8 rad/s 5s Delayed Weaving Maneuver

Z: $2g$ Step Maneuver

Case 9

Target Maneuver

Target Maneuver Switch after 5s

X: $1g$ 0.7 rad/s Weaving Maneuver to $[2.5 \ -1.5 \ -2.5 \ 1.5 \ 2.5]g$ 2.5s Piecewise Step Maneuver

Y: $3g$ Step Maneuver to $3g$ 0.7 rad/s Weaving Maneuver

Z: $[5 \ -3 \ -5 \ 3 \ 5]g$ 2.5s Piecewise Step Maneuver to $2g$ Step Maneuver

Table 7-1: Guidance Performance Index for Target Maneuver Comparisons

Guidance Performance Index	Average Miss [m]	Minimum Miss [m]	Maximum Miss [m]	Hit Ratio %	Average Flight Time [s]
Case 1	1.22	0.07	3.85	97	14.59
Case 2	2.08	0.25	4.59	88	9.83
Case 3	1.62	0.53	4.47	92	14.2
Case 4	1.02	0.06	3.66	99	13.72
Case 5	2.16	0.41	4.57	80	12.52
Case 6	8.29	0.09	666	89	15.3
Case 7	21.25	0.11	1038.6	82	15.57
Case 8	2.5	1.6	3.83	83	12.51
Case 9	2.56	1.19	7.21	73	10.11

Case 1

Target Maneuver

X: $1g$ Step Maneuver

Y: $3g$ Step Maneuver

Z: $2g$ Step Maneuver

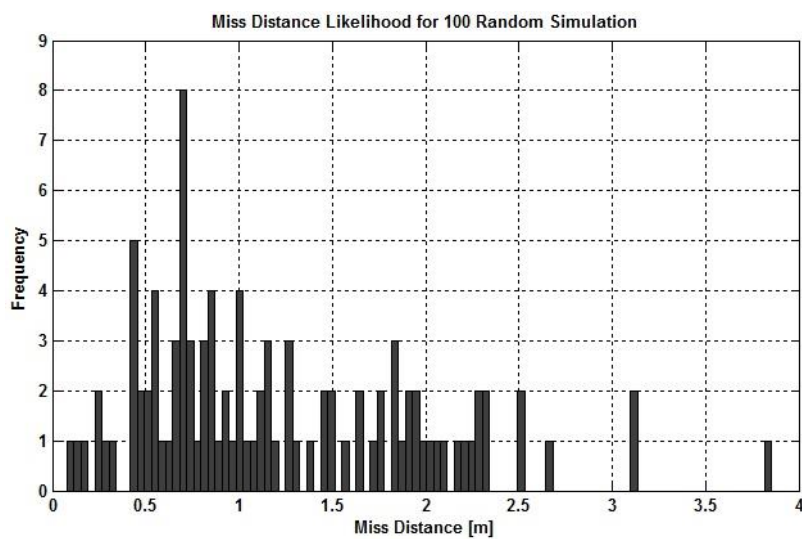


Figure 7.19: Miss Distance Histogram for Case 1

Average Miss Distance: 1.22 m

Minimum Miss Distance: 0.07 m

Maximum Miss Distance: 3.85 m

Hit Ratio: 97 %

Average Flight Time: 14.59 s

Case 2

Target Maneuver

X: $1g$ Step Maneuver

Y: $3g$ 0.8 rad/s Weaving Maneuver

Z: $2g$ Step Maneuver

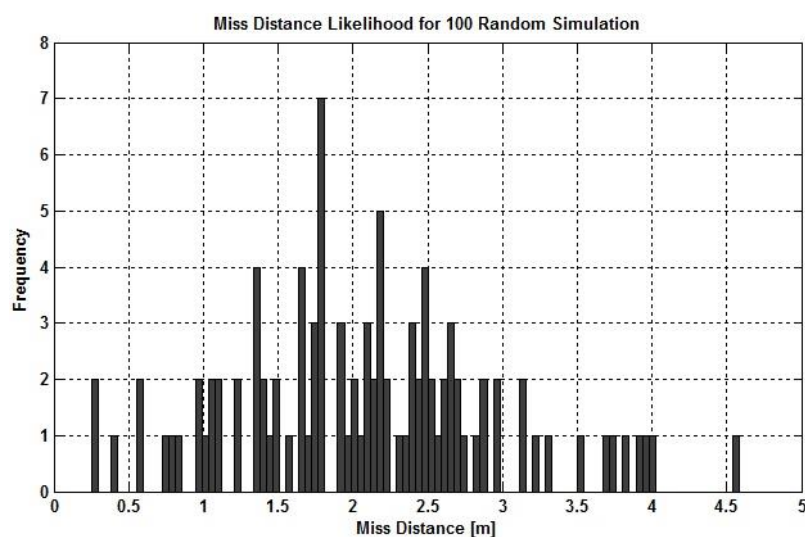


Figure 7.20: Miss Distance Histogram for Case 2

Average Miss Distance: 2.08 m

Minimum Miss Distance: 0.25 m

Maximum Miss Distance: 4.59 m

Hit Ratio: 88 %

Average Flight Time: 9.83 s

Case 3

Target Maneuver

X: $1g$ Step Maneuver

Y: $[1 \ 5 \ 3 \ 2 \ 4]g$ 3s Piecewise Step Maneuver

Z: $2g$ Step Maneuver

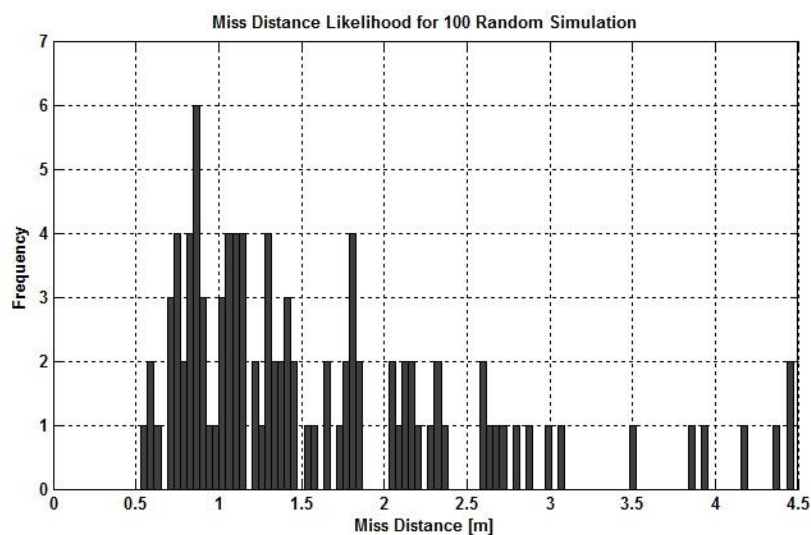


Figure 7.21: Miss Distance Histogram for Case 3

Average Miss Distance: 1.62 m

Minimum Miss Distance: 0.53 m

Maximum Miss Distance: 4.47 m

Hit Ratio: 92 %

Average Flight Time: 14.2 s

Case 4

Target Maneuver

X: $1g$ Step Maneuver

Y: $3g$ Step Maneuver

Z: 0 to $5g$ Ramp Maneuver

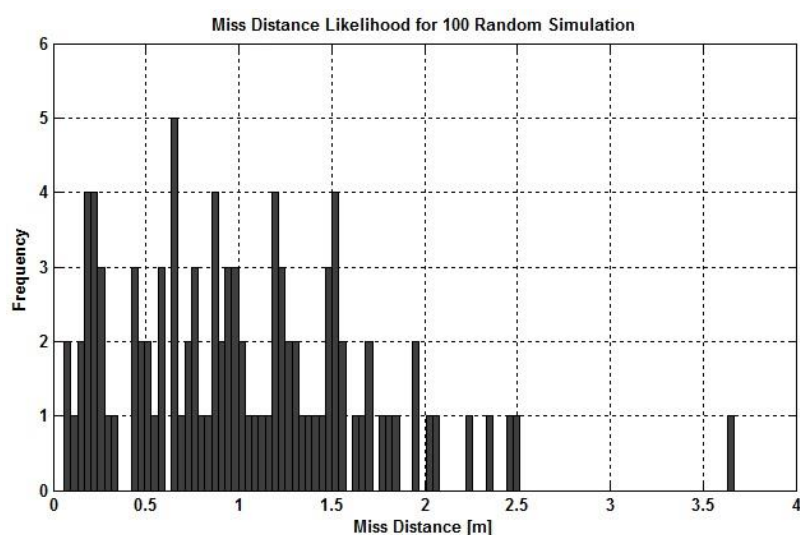


Figure 7.22: Miss Distance Histogram for Case 4

Average Miss Distance: 1.02 m

Minimum Miss Distance: 0.06 m

Maximum Miss Distance: 3.66 m

Hit Ratio: 99 %

Average Flight Time: 13.72 s

Case 5

Target Maneuver

X: $1g$ 0.7 rad/s Weaving Maneuver

Y: $[1\ 5\ 3\ 2\ 4]g$ 2.5s Piecewise Step Maneuver

Z: $2g$ Step Maneuver

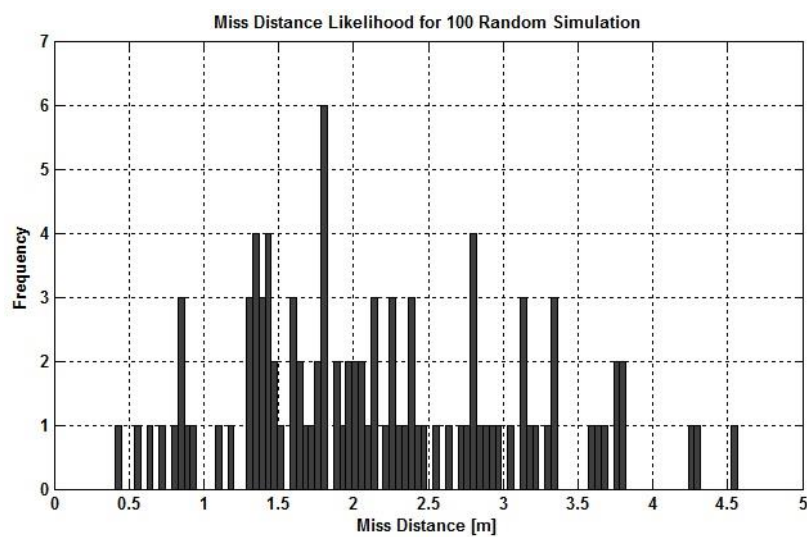


Figure 7.23: Miss Distance Histogram for Case 5

Average Miss Distance: 2.16 m

Minimum Miss Distance: 0.41 m

Maximum Miss Distance: 4.57 m

Hit Ratio: 80 %

Average Flight Time: 12.52 s

Case 6

Target Maneuver

X: $\pm 1g$ Random Step Maneuver

Y: $\pm 3g$ Random Step Maneuver

Z: $\pm 2g$ Random Step Maneuver

Noise Model

Noise-free

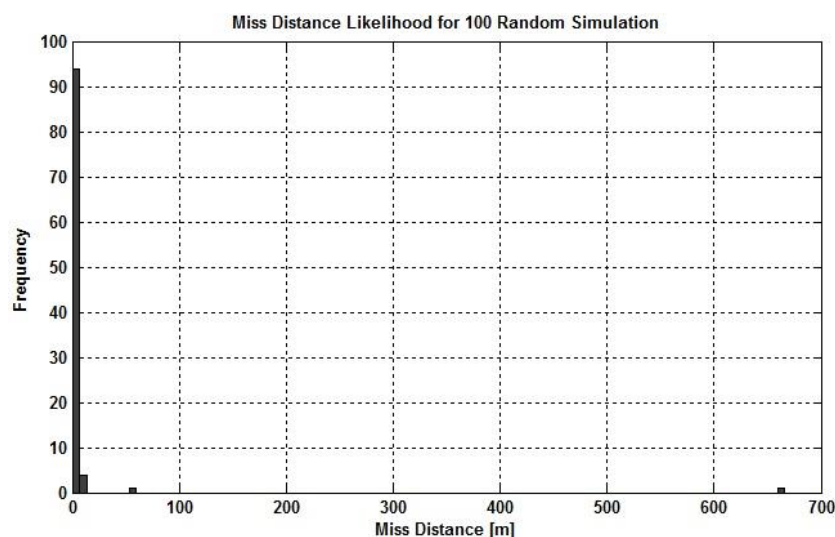


Figure 7.24: Miss Distance Histogram for Case 6

Average Miss Distance: 8.29 m

Minimum Miss Distance: 0.09 m

Maximum Miss Distance: 666 m

Hit Ratio: 89 %

Average Flight Time: 15.3 s

Case 7

Target Maneuver

X: $\pm 1g$ Random Step Maneuver

Y: $\pm 3g$ Random Step Maneuver

Z: $\pm 2g$ Random Step Maneuver

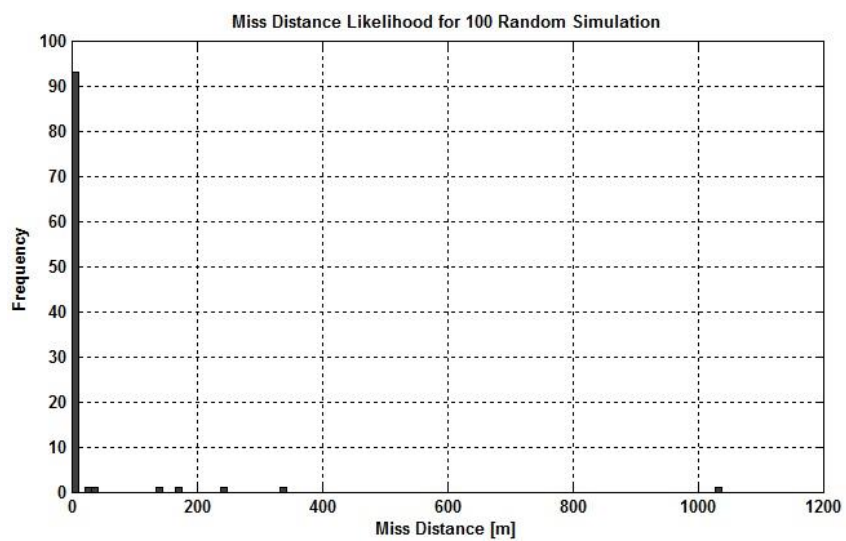


Figure 7.25: Miss Distance Histogram for Case 7

Average Miss Distance: 21.25 m

Minimum Miss Distance: 0.11 m

Maximum Miss Distance: 1038.6 m

Hit Ratio: 82 %

Average Flight Time: 15.57 s

Case 8

Target Maneuver

X: $1g$ Step Maneuver

Y: $3g$ 0.8 rad/s 5s Delayed Weaving Maneuver

Z: $2g$ Step Maneuver

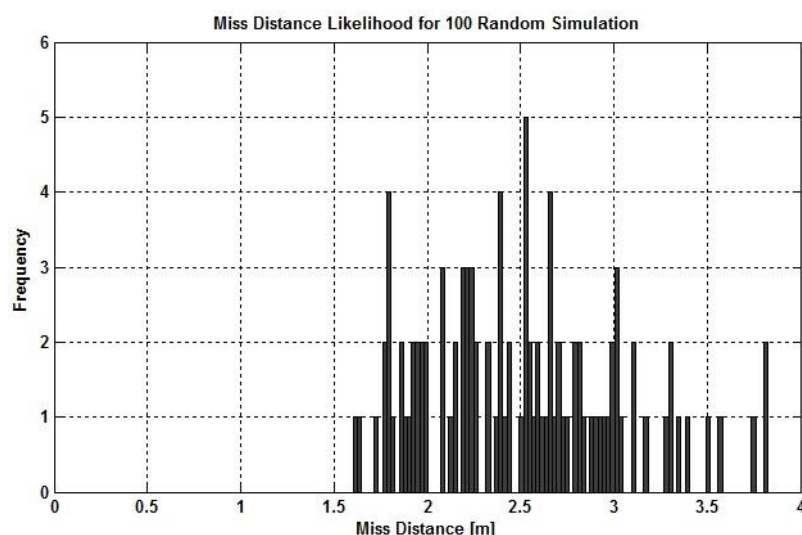


Figure 7.26: Miss Distance Histogram for Case 8

Average Miss Distance: 2.5 m

Minimum Miss Distance: 1.6 m

Maximum Miss Distance: 3.83 m

Hit Ratio: 83 %

Average Flight Time: 12.51 s

Case 9

Target Maneuver

Target Maneuver Switch after 5s

X: $1g$ 0.7 rad/s Weaving Maneuver to $[2.5 \ -1.5 \ -2.5 \ 1.5 \ 2.5]g$ 2.5s Piecewise Step Maneuver

Y: $3g$ SM to $3g$ 0.7 rad/s Weaving Maneuver

Z: $[5 \ -3 \ -5 \ 3 \ 5]g$ 2.5s Piecewise Step Maneuver to $2g$ Step Maneuver

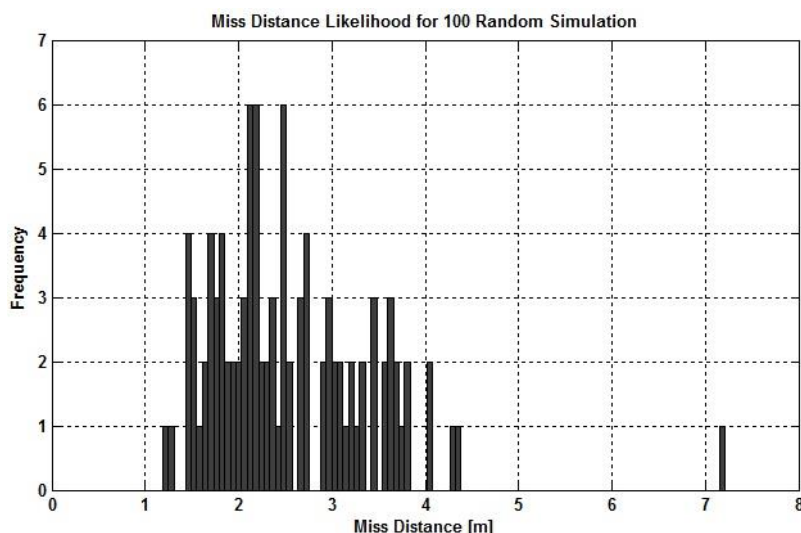


Figure 7.27: Miss Distance Histogram for Case 9

Average Miss Distance: 2.56 m

Minimum Miss Distance: 1.19 m

Maximum Miss Distance: 7.21 m

Hit Ratio: 73 %

Average Flight Time: 10.11 s

Monte Carlo simulations related to first four target maneuver cases show that piecewise step and weaving maneuver types are more effective in evading from a pursuer than step and ramp maneuvers if tail-chase pursuit scenario is assumed.

Weaving maneuver gives the lowest hit ratio while the engagement lasts for a shorter time compared to the other three fundamental maneuver types. Low hit ratio is mainly due to the fact that the weaving frequency is unknown to the target estimator being implemented resulting in target state estimations lagging the actual values. Engagements are completed in a shorter amount of time for this kind of maneuver since the evader cannot gain high velocity values in the particular direction along which the weaving motion takes place.

Piecewise step maneuver is another effective maneuver type that gives less time to the target estimator to make reasonable predictions related to the states of the target, especially acceleration components. Hence, there is a higher possibility of missing a target handling this type of maneuver instead of step and ramp maneuvers for a tail-chase pursuit.

In pursuit scenarios where the target makes step maneuvers along each direction, the engagement times come out to be longer due to high velocity values attained in each direction resulting from accelerating steadily.

Simulations also show that ramp maneuver is not quite effective in tail-chase scenarios whereas it can be a decent way of escaping from a missile in head-on engagements as will be discussed in the next subsection.

Case 5 illustrates a combined maneuver type which influences the hit ratio in a negative manner as each maneuver type contributes separately to the final miss distance value.

In Case 6, target makes random step maneuvers in a noise-free environment. With the addition of random noise effects in Case 7, lower hit ratio together with longer flight time is achieved. For such cases, very high miss distance values are likely to occur due to combined effect of random noise sources and maneuver types.

Case 8 demonstrates a target handling a 5s delayed weaving maneuver which results in lower hit ratios compared to initially started weaving maneuver case since less time is available to predict the weaving frequency and amplitude of target acceleration.

In Case 9, target is modeled to switch its maneuver types along each direction 5s after the engagement begins. These challenging maneuver types together with random noise and radome error effects cause the lowest hit ratio among the discussed target maneuver cases as expected.

7.2.2 Comparison of Engagement Scenarios

Baseline for Engagement Scenario Comparisons

Noise Model

Random Gaussian Noise for Range-to-Go

Sinusoidal Noise for LOS Angles

Radome Error for LOS Rates

Target Estimator Model

Third Order Fading Memory Filter

Seeker Model

Gimbaled Seeker Model

Blind Flight Condition Applicable

Guidance Algorithm

APNG Law ($N' = 3$)

Body Attitude Control

Novel Extra Latax Algorithm

Variable Parameters for Cases 10 through 13

Case 10

Target Maneuver

X: $3g$ Step Maneuver

Y: $[3.5 \ -2.5 \ -5 \ 1.5 \ 4.5]g$ 3s Piecewise Step Maneuver

Z: $1.5g$ Step Maneuver

Engagement Type

Tail-Chase Pursuit

Air-to-Air Engagement

Case 11

Target Maneuver

X: $3g$ Step Maneuver

Y: $[3.5 \ -2.5 \ -5 \ 1.5 \ 4.5]g$ 3s Piecewise Step Maneuver

Z: $1.5g$ Step Maneuver

Engagement Type

Tail-Chase Pursuit

Surface-to-Air Engagement

Case 12

Target Maneuver

X: $-1g$ Step Maneuver

Y: $-3g$ Step Maneuver

Z: 1 to $5g$ Ramp Maneuver

Engagement Type

Head-On Pursuit

Air-to-Air Engagement

Case 13

Target Maneuver

X: $-1g$ Step Maneuver

Y: $-3g$ Step Maneuver

Z: 1 to $5g$ Ramp Maneuver

Engagement Type

Head-On Pursuit

Surface-to-Air Engagement

Table 7-2: Guidance Performance Index for Engagement Scenario Comparisons

Guidance Performance Index	Average Miss [m]	Minimum Miss [m]	Maximum Miss [m]	Hit Ratio %	Average Flight Time [s]
Case 10	1.63	0.13	15.55	91	15.86
Case 11	1.96	0.03	21.67	85	16.08
Case 12	9.05	2.01	141.29	86	7.47
Case 13	15.58	0.13	205.64	82	7.61

Case 10

Target Maneuver

X: $3g$ Step Maneuver

Y: $[3.5 \ -2.5 \ -5 \ 1.5 \ 4.5]g$ 3s Piecewise Step Maneuver

Z: $1.5g$ Step Maneuver

Engagement Type

Tail-Chase Pursuit

Air-to-Air Engagement

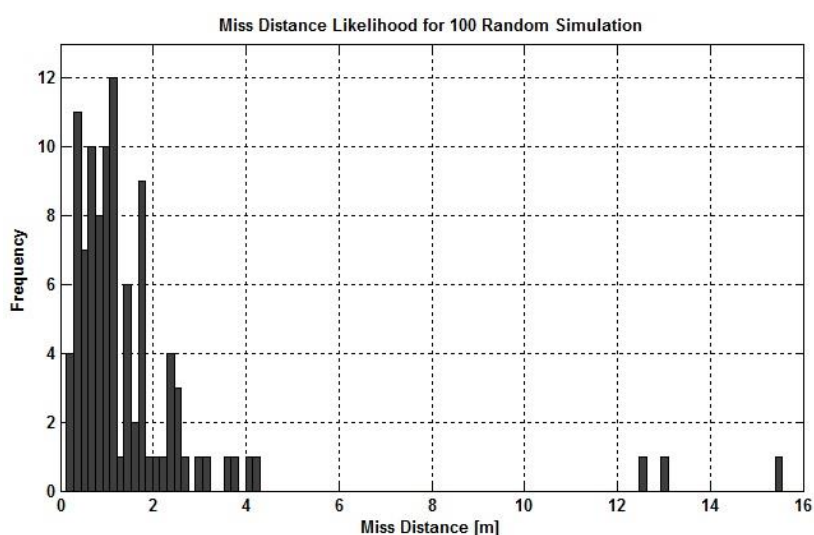


Figure 7.28: Miss Distance Histogram for Case 10

Average Miss Distance: 1.63 m

Minimum Miss Distance: 0.13 m

Maximum Miss Distance: 15.55 m

Hit Ratio: 91 %

Average Flight Time: 15.86 s

Case 11

Target Maneuver

X: $3g$ Step Maneuver

Y: $[3.5 \ -2.5 \ -5 \ 1.5 \ 4.5]g$ 3s Piecewise Step Maneuver

Z: $1.5g$ Step Maneuver

Engagement Type

Tail-Chase Pursuit

Surface-to-Air Engagement

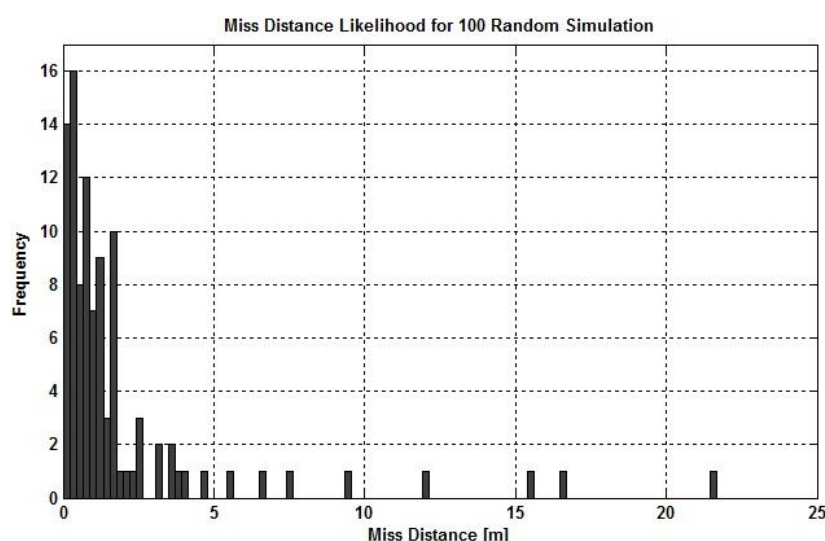


Figure 7.29: Miss Distance Histogram for Case 11

Average Miss Distance: 1.96 m

Minimum Miss Distance: 0.03 m

Maximum Miss Distance: 21.67 m

Hit Ratio: 85 %

Average Flight Time: 16.08 s

Case 12

Target Maneuver

X: $-1g$ Step Maneuver

Y: $-3g$ Step Maneuver

Z: 1 to $5g$ Ramp Maneuver

Engagement Type

Head-On Pursuit

Air-to-Air Engagement

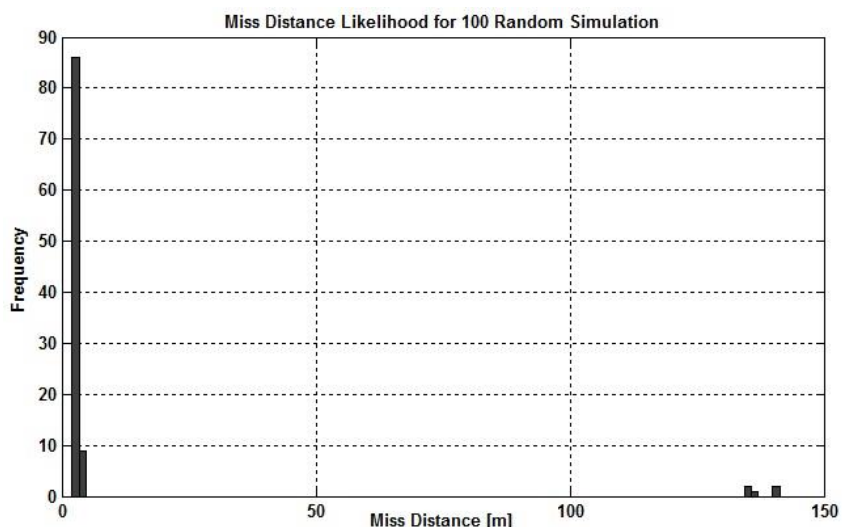


Figure 7.30: Miss Distance Histogram for Case 12

Average Miss Distance: 9.05 m

Minimum Miss Distance: 2.01 m

Maximum Miss Distance: 141.29 m

Hit Ratio: 86 %

Average Flight Time: 7.47 s

Case 13

Target Maneuver

X: $-1g$ Step Maneuver

Y: $-3g$ Step Maneuver

Z: 1 to $5g$ Ramp Maneuver

Engagement Type

Head-On Pursuit

Surface-to-Air Engagement

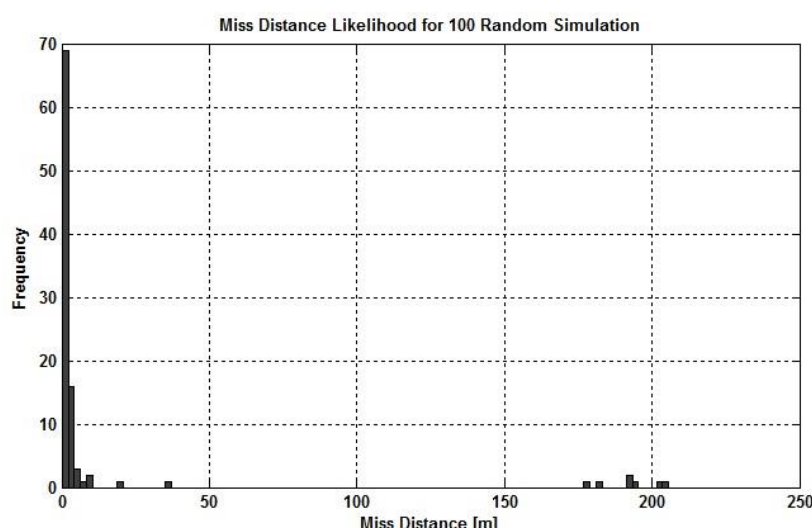


Figure 7.31: Miss Distance Histogram for Case 13

Average Miss Distance: 15.58 m

Minimum Miss Distance: 0.13 m

Maximum Miss Distance: 205.64 m

Hit Ratio: 82 %

Average Flight Time: 7.61 s

As indicated by the *Monte Carlo* simulation results for engagement scenarios, air-to-air engagements are likely to bring about lower average miss distances, lower engagement times and higher hit ratios compared to the surface-to-air engagements for both tail-chase and head-on pursuit cases. These are actually expected results because the missile requires huge lateral acceleration in elevation plane and sufficient time to gain altitude when it is launched from the ground. However, for air-to-air engagements, the ZEM value for the motion taking place in the elevation plane will be less and accordingly, the missile will require less lateral acceleration component in the elevation plane. Due to this fact, the final miss distance values for air-to-air engagements are likely to be smaller.

In addition, head-on engagements are likely to lead to lower hit ratios and higher average miss distances when compared to the tail-chase engagements. The main reason for that is the high closure rate which decreases the total engagement time and gives less time to the target estimator to accomplish its task appropriately. Therefore, missile cannot respond to sudden evasive maneuvers of the evader quickly and effectively. Moreover, there is a risk of reaching the ultimate limits of the lateral acceleration capability of the missile and saturating the autopilot controllers for head-on engagements.

It can also be concluded that, as mentioned before, ramp maneuver of the target is a powerful way of getting away from the pursuer in the case of head-on engagements due to high approach rates. For such cases, the high maneuver capability of the missile and a responsive attitude of the guidance system can aid in decreasing the miss distance values and increasing the chance of hitting the target.

7.2.3 Comparison of Noise and Error Models

Baseline for Noise and Error Model Comparisons

Target Maneuver

X: $1g$ Step Maneuver
Y: $2g$ Step Maneuver
Z: $3g$ Step Maneuver

Seeker Model

Gimbaled Seeker Model
Blind Flight Condition Applicable

Engagement Type

Tail-Chase Pursuit
Air-to-Air Engagement

Target Estimator Model

Third Order Fading Memory Filter

Guidance Algorithm

APNG Law ($N' = 3$)
Body Attitude Control
Novel Extra Latax Algorithm

Variable Parameters for Cases 14 through 22

Case 14

Noise Model

Random Gaussian Noise for Range-to-Go

Case 15

Noise Model

Random Gaussian Noise for Range-to-Go
Sinusoidal Noise for LOS Angles

Case 16

Noise Model

Random Gaussian Noise for Range-to-Go
Sinusoidal Noise for LOS Angles
Radome Error for LOS Rates

Case 17

Noise Model

Random Gaussian Noise for Range-to-Go

Sinusoidal Noise for LOS Angles

Radome Error for LOS Rates

Bias Error

Case 18

Noise Model

Glint Noise

Random Gaussian Noise for Range-to-Go

Sinusoidal Noise for LOS Angles

Radome Error for LOS Rates

Bias Error

Case 19

Noise Model

Receiver Angle Tracking Noise

Random Gaussian Noise for Range-to-Go

Sinusoidal Noise for LOS Angles

Radome Error for LOS Rates

Bias Error

Case 20

Noise Model

Glint Noise

Receiver Angle Tracking Noise

Random Gaussian Noise for Range-to-Go

Sinusoidal Noise for LOS Angles

Radome Error for LOS Rates

Bias Error

Case 21

Noise Model

Glint Noise

Receiver Angle Tracking Noise

Random Gaussian Noise for Range-to-Go

Sinusoidal Noise for LOS Angles

Radome Error for LOS Rates

Bias Error

Heading Error (15° in Azimuth and Elevation)

Case 22

Target Maneuver

X: $\pm 1g$ Random Step Maneuver

Y: $\pm 3g$ Random Step Maneuver

Z: $\pm 2g$ Random Step Maneuver

Noise Model

Glint Noise

Receiver Angle Tracking Noise

Random Gaussian Noise for Range-to-Go

Sinusoidal Noise for LOS Angles

Radome Error for LOS Rates

Bias Error

Heading Error (15° in Azimuth and Elevation)

Table 7-3: Guidance Performance Index for Noise and Error Comparisons

Guidance Performance Index	Average Miss [m]	Minimum Miss [m]	Maximum Miss [m]	Hit Ratio %	Average Flight Time [s]
Case 14	1.89	1.19	2.95	100	16.87
Case 15	1.8	1.02	2.94	100	16.98
Case 16	1.87	0.86	3.19	99	17
Case 17	1.91	0.99	3.69	97	17.15
Case 18	2.29	0.15	27.83	86	17.82
Case 19	1.98	1.01	3.95	93	17.34
Case 20	2.39	0.36	7.63	76	17.83
Case 21	2.83	0.38	23.64	70	17.89
Case 22	349.06	0.03	1821.8	64	16.37

Case 14

Noise Model

Random Gaussian Noise for Range-to-Go

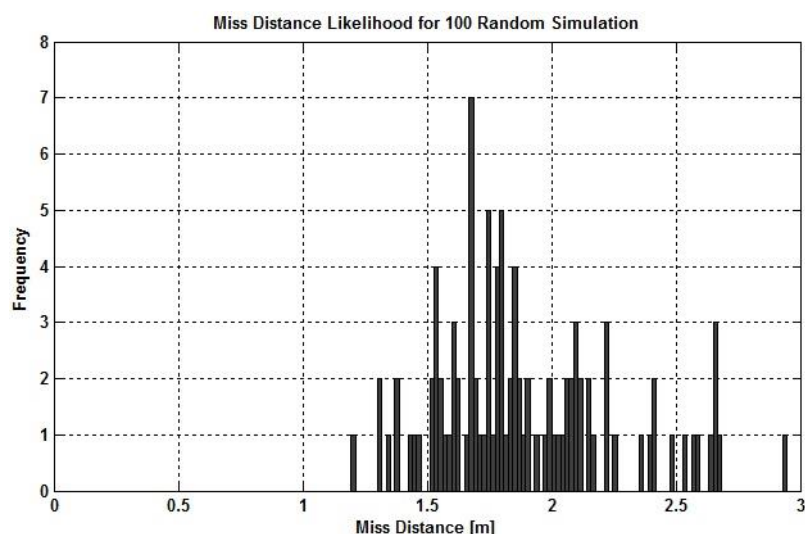


Figure 7.32: Miss Distance Histogram for Case 14

Average Miss Distance: 1.89 m

Minimum Miss Distance: 1.19 m

Maximum Miss Distance: 2.95 m

Hit Ratio: 100 %

Average Flight Time: 16.87 s

Case 15

Noise Model

Random Gaussian Noise for Range-to-Go

Sinusoidal Noise for LOS Angles

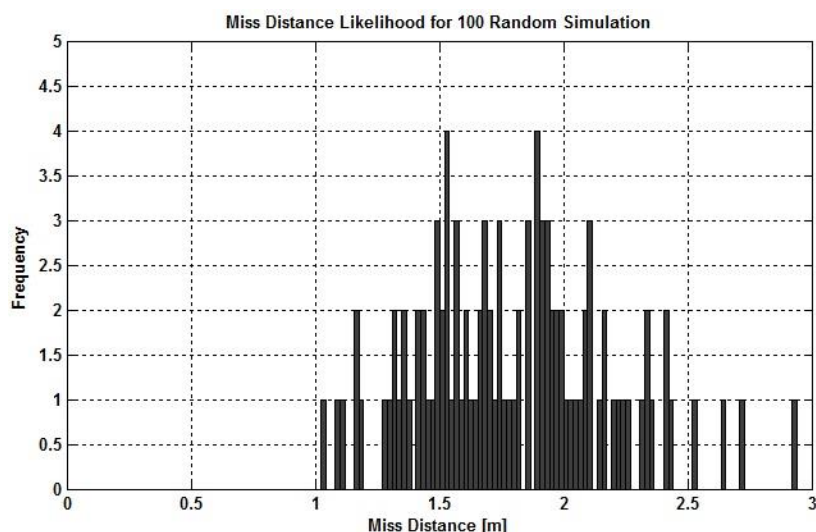


Figure 7.33: Miss Distance Histogram for Case 15

Average Miss Distance: 1.8 m

Minimum Miss Distance: 1.02 m

Maximum Miss Distance: 2.94 m

Hit Ratio: 100 %

Average Flight Time: 16.98 s

Case 16

Noise Model

Random Gaussian Noise for Range-to-Go

Sinusoidal Noise for LOS Angles

Radome Error for LOS Rates

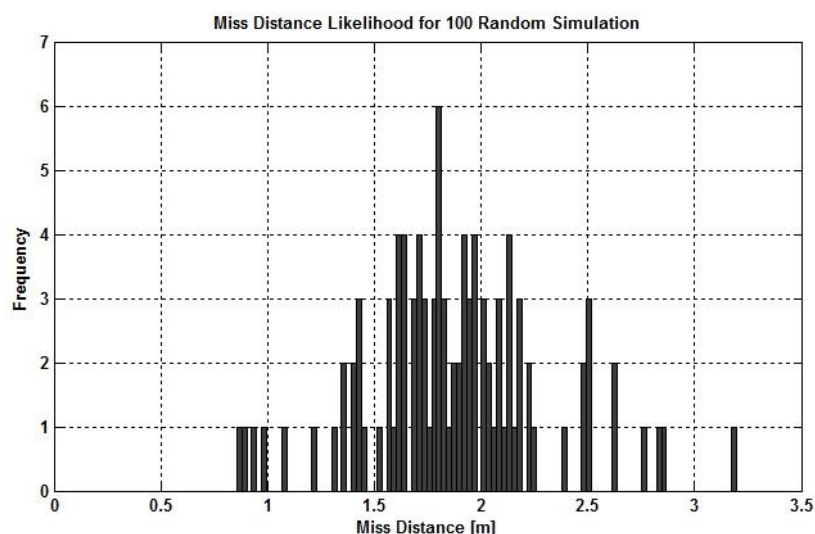


Figure 7.34: Miss Distance Histogram for Case 16

Average Miss Distance: 1.87 m

Minimum Miss Distance: 0.86 m

Maximum Miss Distance: 3.19 m

Hit Ratio: 99 %

Average Flight Time: 17 s

Case 17

Noise Model

Random Gaussian Noise for Range-to-Go

Sinusoidal Noise for LOS Angles

Radome Error for LOS Rates

Bias Error

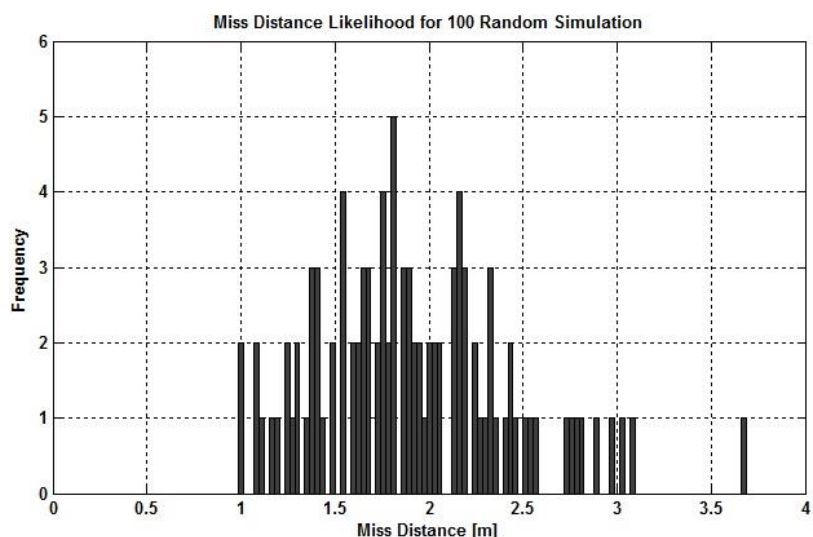


Figure 7.35: Miss Distance Histogram for Case 17

Average Miss Distance: 1.91 m

Minimum Miss Distance: 0.99 m

Maximum Miss Distance: 3.69 m

Hit Ratio: 97 %

Average Flight Time: 17.15 s

Case 18

Noise Model

Glint Noise

Random Gaussian Noise for Range-to-Go

Sinusoidal Noise for LOS Angles

Radome Error for LOS Rates

Bias Error

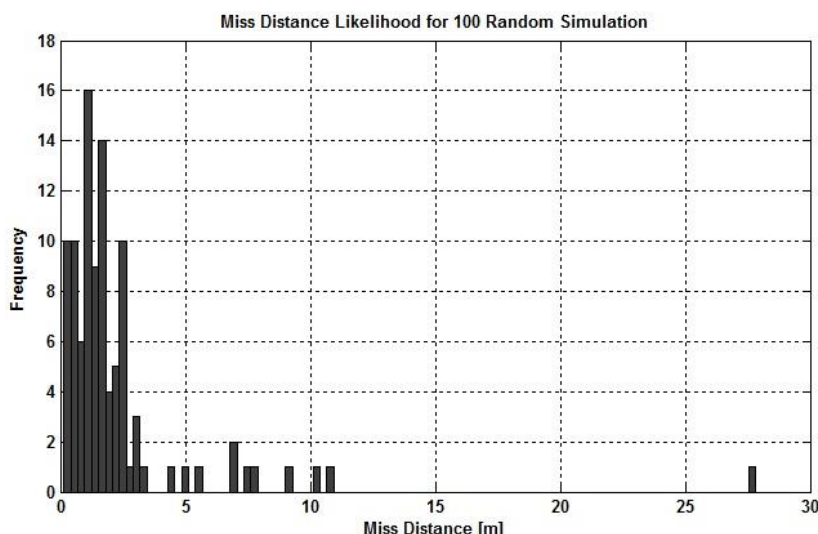


Figure 7.36: Miss Distance Histogram for Case 18

Average Miss Distance: 2.29 m

Minimum Miss Distance: 0.15 m

Maximum Miss Distance: 27.83 m

Hit Ratio: 86 %

Average Flight Time: 17.82 s

Case 19

Noise Model

Receiver Angle Tracking Noise

Random Gaussian Noise for Range-to-Go

Sinusoidal Noise for LOS Angles

Radome Error for LOS Rates

Bias Error

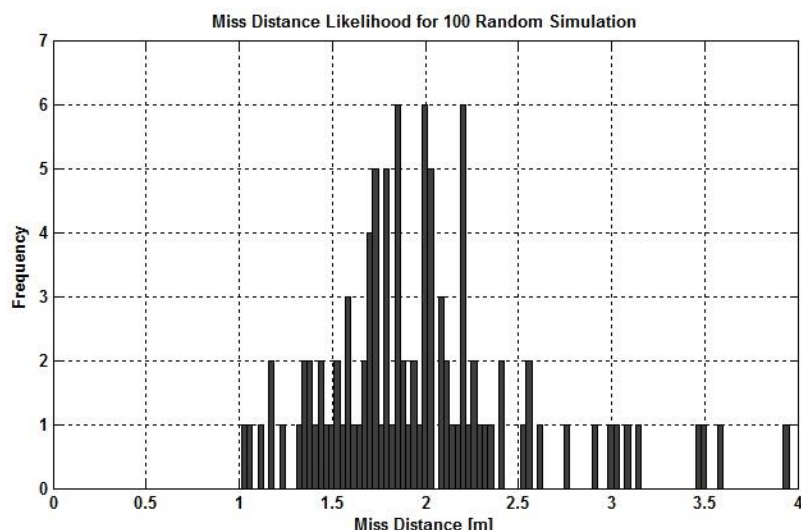


Figure 7.37: Miss Distance Histogram for Case 19

Average Miss Distance: 1.98 m

Minimum Miss Distance: 1.01 m

Maximum Miss Distance: 3.95 m

Hit Ratio: 93 %

Average Flight Time: 17.34 s

Case 20

Noise Model

Glint Noise

Receiver Angle Tracking Noise

Random Gaussian Noise for Range-to-Go

Sinusoidal Noise for LOS Angles

Radome Error for LOS Rates

Bias Error

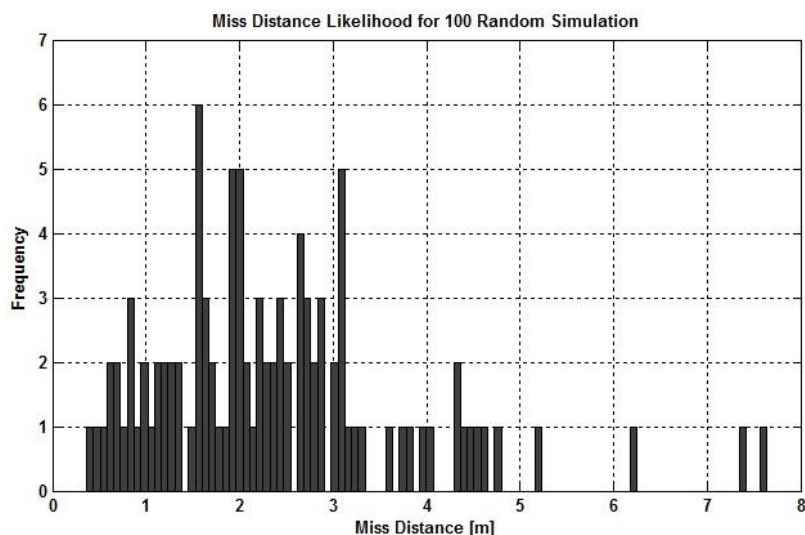


Figure 7.38: Miss Distance Histogram for Case 20

Average Miss Distance: 2.39 m

Minimum Miss Distance: 0.36 m

Maximum Miss Distance: 7.63 m

Hit Ratio: 76 %

Average Flight Time: 17.83 s

Case 21

Noise Model

Glint Noise

Receiver Angle Tracking Noise

Random Gaussian Noise for Range-to-Go

Sinusoidal Noise for LOS Angles

Radome Error for LOS Rates

Bias Error

Heading Error (15° in Azimuth and Elevation)

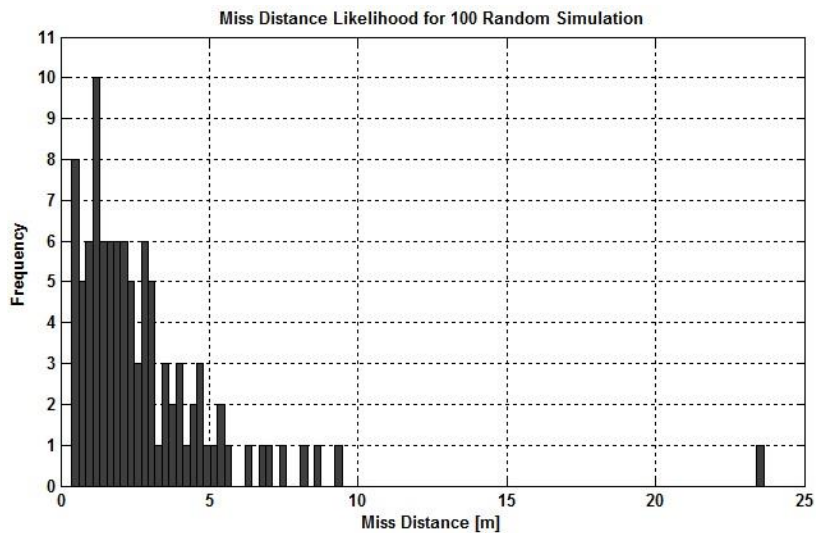


Figure 7.39: Miss Distance Histogram for Case 21

Average Miss Distance: 2.83 m

Minimum Miss Distance: 0.38 m

Maximum Miss Distance: 23.64 m

Hit Ratio: 70 %

Average Flight Time: 17.89 s

Case 22

Target Maneuver

X: $\pm 1g$ Random Step Maneuver

Y: $\pm 3g$ Random Step Maneuver

Z: $\pm 2g$ Random Step Maneuver

Noise Model

Glint Noise

Receiver Angle Tracking Noise

Random Gaussian Noise for Range-to-Go

Sinusoidal Noise for LOS Angles

Radome Error for LOS Rates

Bias Error

Heading Error (15° in Azimuth and Elevation)

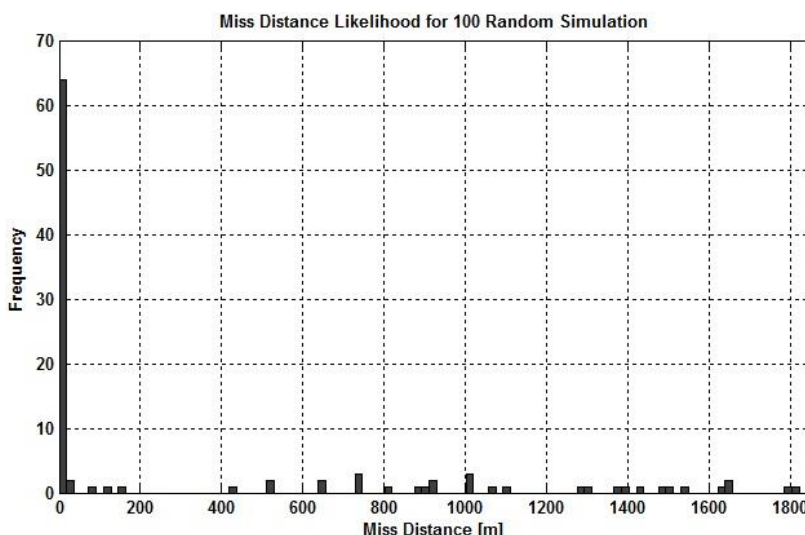


Figure 7.40: Miss Distance Histogram for Case 22

Average Miss Distance: 349.06 m

Minimum Miss Distance: 0.03 m

Maximum Miss Distance: 1821.8 m

Hit Ratio: 64 %

Average Flight Time: 16.37 s

According to *Monte Carlo* simulations, glint noise is observed to have the biggest effect in deteriorating the performance of the homing guidance system. Received angle tracking noise, heading and radome errors turn out to be other significant miss distance contributors.

It has been told previously that the noise may sometimes have positive effects on the system performance as well. Here, the sinusoidal noise affecting the quality of the LOS angle measurements can be seen to reduce the average miss distance value a little bit, which supports the assertion.

It can be noticed that all noise and error sources have an influence on total engagement times in an increasing manner.

The last simulation demonstrate a case wherein all noise and error sources discussed in this study are active and the target is making a random step maneuver as in Case 6. Here, very small miss distances can be observed depending on the random distribution of the noises. Distinctive noise types may also cancel out the effect of each other for some instances. On the other hand, significant miss values can also be experienced due to the same randomness.

7.2.4 Comparison of Seeker Models

Baseline for Seeker Model Comparisons

Target Maneuver	Noise Model
X: $1g$ Step Maneuver	Random Gaussian Noise for Range-to-Go
Y: $3g$ 1 rad/s Weaving Maneuver	Random Gaussian Noise for LOS Angles
Z: $2g$ Step Maneuver	
	Target Estimator Model
Engagement Type	Third Order Fading Memory Filter
Tail-Chase Engagement	
Surface-to-Air Engagement	Guidance Algorithm
	APNG Law ($N' = 3$)

Variable Parameters for Cases 23 through 26

Case 23

Seeker Model

Strapdown Seeker Model ($\beta = 0.3$)

Case 24

Seeker Model

Strapdown Seeker Model ($\beta = 0.7$)

Case 25

Seeker Model

Gimbaled Seeker Model ($\tau_s = 0.1$)

Case 26

Seeker Model

Gimbaled Seeker Model ($\tau_s = 0.05$)

Table 7-4: Guidance Performance Index for Seeker Model Comparisons

Guidance Performance Index	Average Miss [m]	Minimum Miss [m]	Maximum Miss [m]	Hit Ratio %	Average Flight Time [s]
Case 23	2.61	0.45	9.75	70	15.76
Case 24	1.64	0.25	9.89	90	15.85
Case 25	2.48	1.28	8.53	75	18.79
Case 26	2.12	0.83	3.38	93	18.47

Case 23

Seeker Model

Strapdown Seeker Model ($\beta = 0.3$)

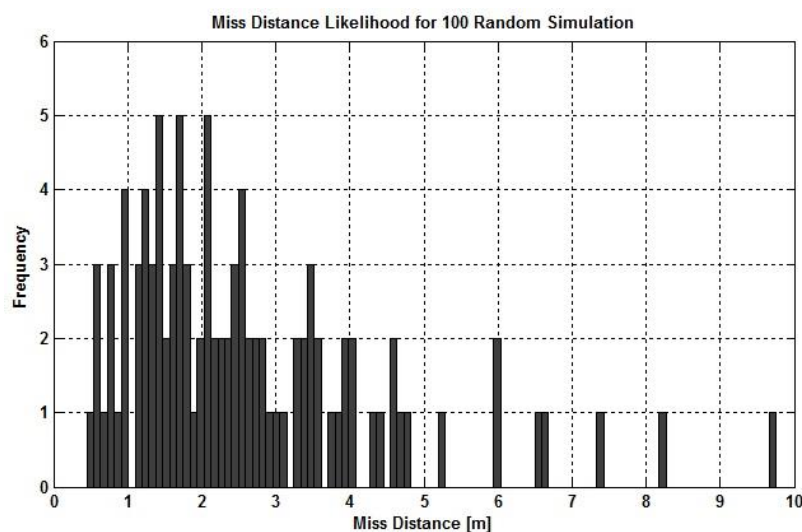


Figure 7.41: Miss Distance Histogram for Case 23

Average Miss Distance: 2.61 m

Minimum Miss Distance: 0.45 m

Maximum Miss Distance: 9.75 m

Hit Ratio: 70 %

Average Flight Time: 15.76 s

Case 24

Seeker Model

Strapdown Seeker Model ($\beta = 0.7$)

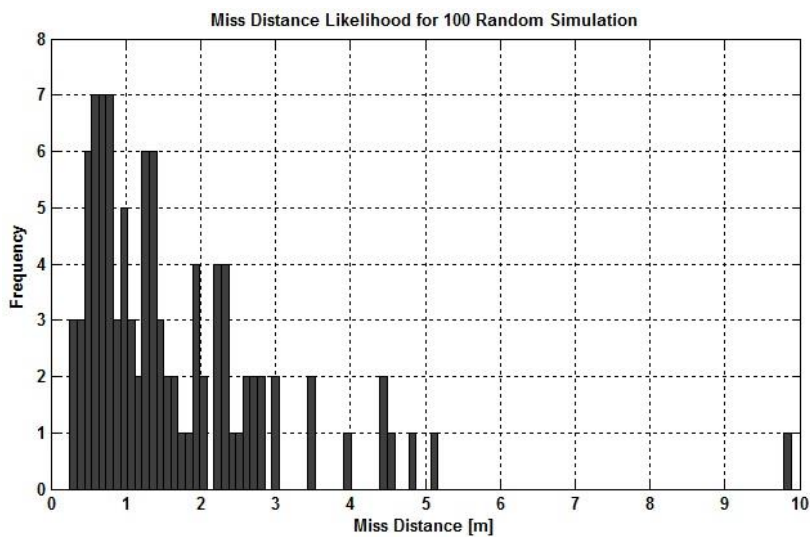


Figure 7.42: Miss Distance Histogram for Case 24

Average Miss Distance: 1.64 m

Minimum Miss Distance: 0.25 m

Maximum Miss Distance: 9.89 m

Hit Ratio: 90 %

Average Flight Time: 15.85 s

Case 25

Seeker Model

Gimbaled Seeker Model ($\tau_s = 0.1$)

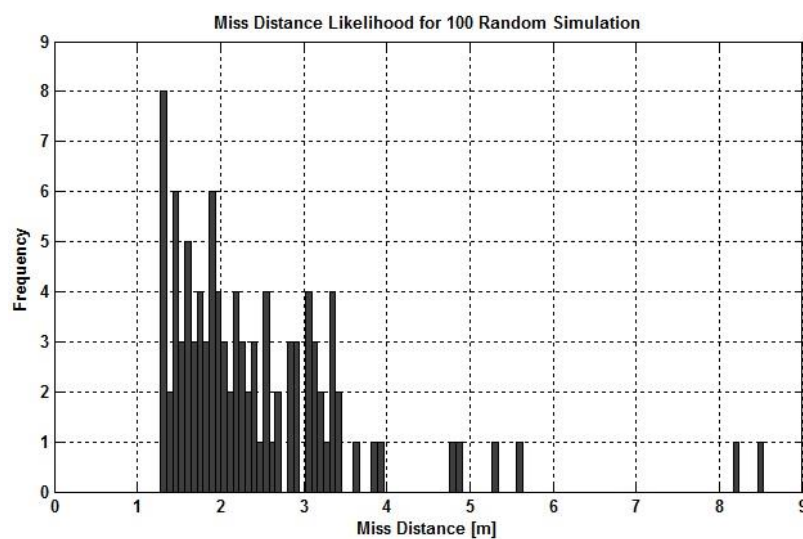


Figure 7.43: Miss Distance Histogram for Case 25

Average Miss Distance: 2.48 m

Minimum Miss Distance: 1.28 m

Maximum Miss Distance: 8.53 m

Hit Ratio: 75 %

Average Flight Time: 18.79 s

Case 26

Seeker Model

Gimbaled Seeker Model ($\tau_s = 0.05$)

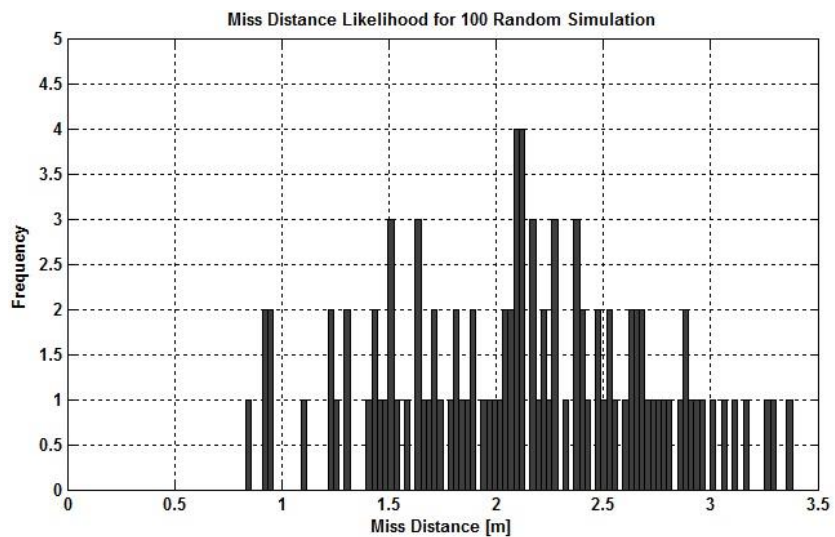


Figure 7.44: Miss Distance Histogram for Case 26

Average Miss Distance: 2.12 m

Minimum Miss Distance: 0.83 m

Maximum Miss Distance: 3.38 m

Hit Ratio: 93 %

Average Flight Time: 18.47 s

As gimbaled and strapdown seeker models are compared for the same target maneuver types and engagement scenarios, the superiority of the gimbaled seeker model in terms of hit ratio and average miss distance values can be noticed from the *Monte Carlo* simulation results. On the other hand, gimbaled target sensor model is seen to require more time to acquire and track the target until the interception compared to the strapdown seeker model, which may be associated with the tracking and stabilization loop structure of the gimbaled seeker model requiring higher computing capability to derive the LOS rates. Here, all simulations are carried out based on no blind flight condition exists and the missile stays focused on the target throughout the engagement.

It has been mentioned that by increasing the memory length of the strapdown seeker model, the LOS rate filter remembers more about the previous measurements and smoother estimates can be obtained for the LOS angles corrupted by noise and their rates. However, increasing the memory length beyond a certain value can make the filter react slower and higher miss ratios can be experienced due to a sluggish LOS rate filter. Likewise, a responsive filter do not guarantee a good guidance performance as the noise transmission becomes higher if a more agile missile is desired in a noisy environment.

First two cases show how the average miss value and hit ratio improve as the second order fading memory filter is tuned appropriately although it takes longer time for the missile to collide with the intended target.

Last two cases illustrate the effect of gimbaled seeker time constant on the overall guidance performance. As the time constant is lowered a more responsive seeker model is obtained resulting in lower miss distance values, increased hit ratios and decreased engagement times as expected.

7.2.5 Comparison of Target Estimator Models

Baseline for Target Estimator Model Comparisons

Target Maneuver

X: $\pm 1g$ 5s Random Piecewise Step Maneuver
Y: $\pm 2g$ 0.5 rad/s Random Weaving Maneuver
Z: $3g$ Step Maneuver

Seeker Model

Gimbaled Seeker Model
Blind Flight Condition Applicable

Engagement Type

Tail-Chase Pursuit
Surface-to-Air Engagement

Guidance Algorithm

APNG Law ($N' = 3$)
Body Attitude Control
Novel Extra Latax Algorithm

Noise Model

Random Gaussian Noise for Range-to-Go
Sinusoidal Noise for LOS Angles
Radome Error for LOS Rates
Constant Angular Bias Error

Variable Parameters for Cases 27 and 28

Case 27

Target Estimator Model

Third Order Fading Memory Filter ($\beta = 0.8$)

Case 28

Target Estimator Model

Third Order Fading Memory Filter ($\beta = 0.9$)

Table 7-5: Guidance Performance Index for Target Estimator Comparisons

Guidance Performance Index	Average Miss [m]	Minimum Miss [m]	Maximum Miss [m]	Hit Ratio %	Average Flight Time [s]
Case 27	2.5	0.31	6.63	65	15.95
Case 28	1.45	0.01	4.98	89	16.62

Case 27

Target Estimator Model

Third Order Fading Memory Filter ($\beta = 0.8$)

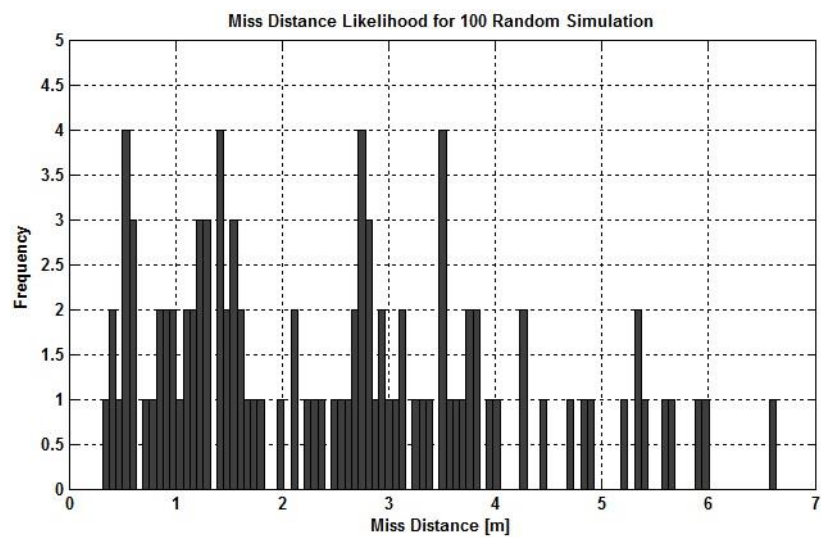


Figure 7.45: Miss Distance Histogram for Case 27

Average Miss Distance: 2.5 m

Minimum Miss Distance: 0.31 m

Maximum Miss Distance: 6.63 m

Hit Ratio: 65 %

Average Flight Time: 15.95 s

Case 28

Target Estimator Model

Third Order Fading Memory Filter ($\beta = 0.9$)

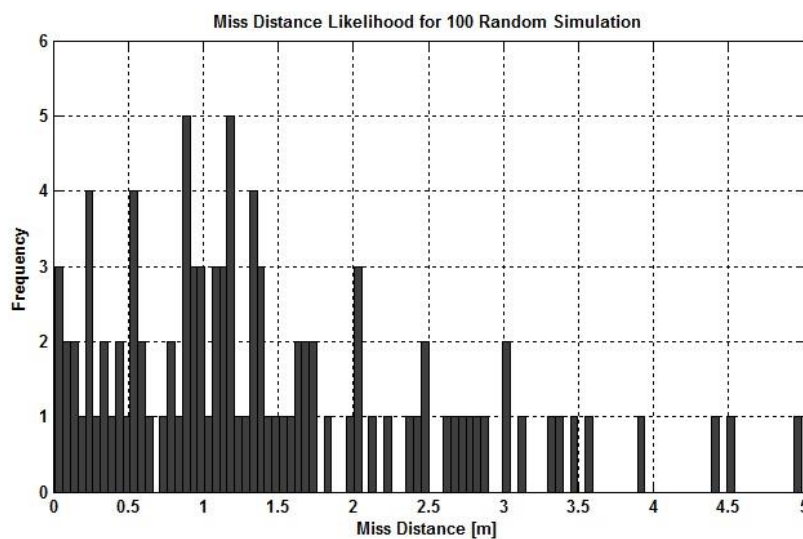


Figure 7.46: Miss Distance Histogram for Case 28

Average Miss Distance: 1.45 m

Minimum Miss Distance: 0.01 m

Maximum Miss Distance: 4.98 m

Hit Ratio: 89 %

Average Flight Time: 16.62 s

As mentioned before, third order fading memory filtering technique is implemented in this study to predict the target states, including the acceleration components of the target, simultaneously during the engagement. The memory length of this constant gain recursive filtering method can also be varied to examine the effects of responsiveness of the filter and transmission of noise on the overall guidance performance. It has been stated that the filter uses noisy position measurements of the target to derive the corresponding velocity and acceleration states of the target. Hence, the noise transmission should be kept low to estimate the target acceleration accurately if the target estimator is expected to be exposed to high amount of noise during range measurements.

These two cases present how the average miss distance and hit ratio can be improved in a noisy environment by an appropriate tuning of the filter at the expense of higher flight times.

7.2.6 Comparison of Guidance Law Algorithms

Baseline for Guidance Law Algorithm Comparisons

Engagement Type	Seeker Model
Tail-Chase Pursuit	Gimbaled Seeker Model
Surface-to-Air Engagement	Blind Flight Condition Applicable

Target Estimator Model

Third Order Fading Memory Filter

Variable Parameters for Cases 29 through 38

Case 29

Target Maneuver

X: $\pm 1g$ 5s Random Piecewise Step Maneuver

Y: $\pm 3g$ 0.5 rad/s Random Weaving Maneuver

Z: 0 to $5g$ Ramp Maneuver

Noise Model

Random Gaussian Noise for Range-to-Go

Sinusoidal Noise for LOS Angles

Radome Error for LOS Rates

Guidance Algorithm

APNG Law ($N' = 3$)

Body Attitude Control

Novel Extra Latax Algorithm

Latax Limit $\pm 35g$

Case 30

Target Maneuver

X: $\pm 1g$ 5s Random Piecewise Step Maneuver

Y: $\pm 3g$ 0.5 rad/s Random Weaving Maneuver

Z: 0 to $5g$ Ramp Maneuver

Noise Model

Random Gaussian Noise for Range-to-Go

Sinusoidal Noise for LOS Angles

Radome Error for LOS Rates

Guidance Algorithm

APNG Law ($N' = 5$)

Body Attitude Control

Novel Extra Latax Algorithm

Latax Limit $\pm 35g$

Case 31

Target Maneuver

X: $\pm 1g$ 5s Random Piecewise Step Maneuver

Y: $\pm 3g$ 0.5 rad/s Random Weaving Maneuver

Z: 0 to $5g$ Ramp Maneuver

Noise Model

Random Gaussian Noise for Range-to-Go

Sinusoidal Noise for LOS Angles

Radome Error for LOS Rates

Guidance Algorithm

PNG Law ($N' = 3$)

Body Attitude Control

Novel Extra Latax Algorithm

Latax Limit $\pm 35g$

Case 32

Target Maneuver

X: $\pm 1g$ 5s Random Piecewise Step Maneuver

Y: $\pm 3g$ 0.5 rad/s Random Weaving Maneuver

Z: 0 to $5g$ Ramp Maneuver

Noise Model

Random Gaussian Noise for Range-to-Go

Sinusoidal Noise for LOS Angles

Radome Error for LOS Rates

Guidance Algorithm

APNG Law ($N' = 3$)

Body Attitude Control

Novel Extra Latax Algorithm

Latax Limit $\pm 10g$

Case 33

Target Maneuver

X: $3g$ Step Maneuver

Y: $4g$ 0.75 rad/s Weaving Maneuver

Z: 0 to $5g$ Ramp Maneuver

Noise Model (Low Level Noise)

Random Gaussian Noise for Range-to-Go

Sinusoidal Noise for LOS Angles

Radome Error for LOS Rates

Heading Error (25° in Azimuth)

Guidance Algorithm

APNG Law ($N' = 3$)

Body Attitude Control

Latax Limit $\pm 35g$

Yaw Gimbal Saturation

Case 34

Target Maneuver

X: $3g$ Step Maneuver

Y: $4g$ 0.75 rad/s Weaving Maneuver

Z: 0 to $5g$ Ramp Maneuver

Noise Model (Low Level Noise)

Random Gaussian Noise for Range-to-Go

Sinusoidal Noise for LOS Angles

Radome Error for LOS Rates

Heading Error (25° in Azimuth)

Guidance Algorithm

APNG Law ($N' = 3$)

Body Attitude Control

Novel Extra Latax Algorithm

Latax Limit $\pm 35g$

Yaw Gimbal Saturation

Case 35

Target Maneuver

X: 0 to $3g$ Ramp Maneuver

Y: $1.5g$ 0.75 rad/s Weaving Maneuver

Z: $5g$ Step Maneuver

Noise Model (High Level Noise)

Random Gaussian Noise for Range-to-Go

Sinusoidal Noise for LOS Angles

Radome Error for LOS Rates

Heading Error (25° in Elevation)

Guidance Algorithm

APNG Law ($N' = 3$)

Body Attitude Control

Latax Limit $\pm 35g$

Pitch Gimbal Saturation

Case 36

Target Maneuver

X: 0 to $3g$ Ramp Maneuver

Y: $1.5g$ 0.75 rad/s Weaving Maneuver

Z: $5g$ Step Maneuver

Noise Model (High Level Noise)

Random Gaussian Noise for Range-to-Go

Sinusoidal Noise for LOS Angles

Guidance Algorithm

APNG Law ($N' = 3$)

Body Attitude Control

Novel Extra Latax Algorithm

Latax Limit $\pm 35g$

Pitch Gimbal Saturation

Radome Error for LOS Rates
Heading Error (25° in Elevation)

Case 37

Target Maneuver

X: $0g$
Y: $5g$ 0.5 rad/s Weaving Maneuver
Z: $5g$ Step Maneuver

Noise Model (Medium Level Noise)

Random Gaussian Noise for Range-to-Go
Sinusoidal Noise for LOS Angles
Radome Error for LOS Rates
Heading Error (25° in Azimuth and Elevation)

Guidance Algorithm

APNG Law ($N' = 3$)
Body Attitude Control
Latax Limit $\pm 35g$
Yaw & Pitch Gimbal Saturation

Case 38

Target Maneuver

X: $0g$
Y: $5g$ 0.5 rad/s Weaving Maneuver
Z: $5g$ Step Maneuver

Noise Model (Medium Level Noise)

Random Gaussian Noise for Range-to-Go
Sinusoidal Noise for LOS Angles
Radome Error for LOS Rates
Heading Error (25° in Azimuth and Elevation)

Guidance Algorithm

APNG Law ($N' = 3$)
Body Attitude Control
Novel Extra Latax Algorithm
Latax Limit $\pm 35g$
Yaw & Pitch Gimbal Saturation

Table 7-6: Guidance Performance Index for Guidance Algorithm Comparisons

Guidance Performance Index	Average Miss [m]	Minimum Miss [m]	Maximum Miss [m]	Hit Ratio %	Average Flight Time [s]
Case 29	1.41	0.1	6.28	91	14.76
Case 30	1.97	0.07	16.92	83	14.42
Case 31	95.29	0.55	568.34	18	16.9
Case 32	2.43	0.23	11.25	77	15.44
Case 33	1.87	0.07	5.25	87	11.68
Case 34	1.3	0.07	4.25	96	11.57
Case 35	9.18	0.01	202.44	85	13.16
Case 36	3.43	0.03	124.8	96	12.55
Case 37	2.57	0.4	3.93	75	14.23
Case 38	1.5	0.35	3.18	99	13.8

Case 29

Target Maneuver

X: $\pm 1g$ 5s Random Piecewise Step Maneuver

Y: $\pm 3g$ 0.5 rad/s Random Weaving Maneuver

Z: 0 to $5g$ Ramp Maneuver

Noise Model

Random Gaussian Noise for Range-to-Go

Sinusoidal Noise for LOS Angles

Radome Error for LOS Rates

Guidance Algorithm

APNG Law ($N' = 3$)

Body Attitude Control

Novel Extra Latax Algorithm

Latax Limit $\pm 35g$

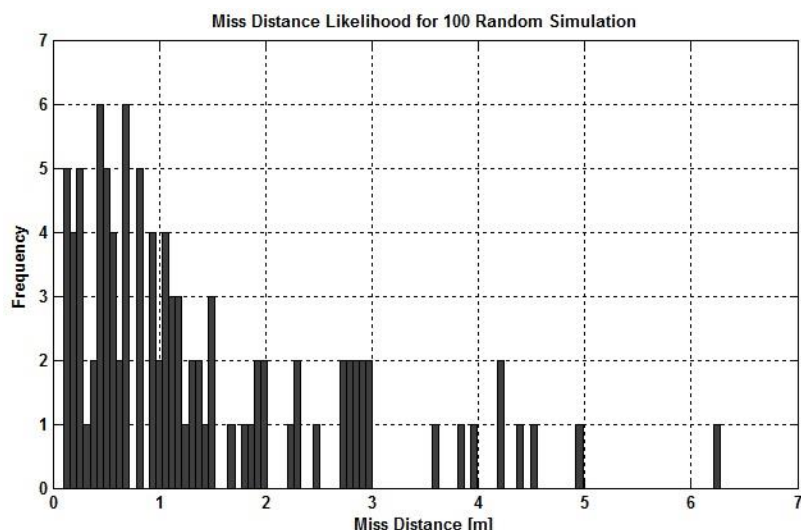


Figure 7.47: Miss Distance Histogram for Case 29

Average Miss Distance: 1.41 m

Minimum Miss Distance: 0.1 m

Maximum Miss Distance: 6.28 m

Hit Ratio: 91 %

Average Flight Time: 14.76 s

Case 30

Target Maneuver

X: $\pm 1g$ 5s Random Piecewise Step Maneuver

Y: $\pm 3g$ 0.5 rad/s Random Weaving Maneuver

Z: 0 to $5g$ Ramp Maneuver

Noise Model

Random Gaussian Noise for Range-to-Go

Sinusoidal Noise for LOS Angles

Radome Error for LOS Rates

Guidance Algorithm

APNG Law ($N' = 5$)

Body Attitude Control

Novel Extra Latax Algorithm

Latax Limit $\pm 35g$

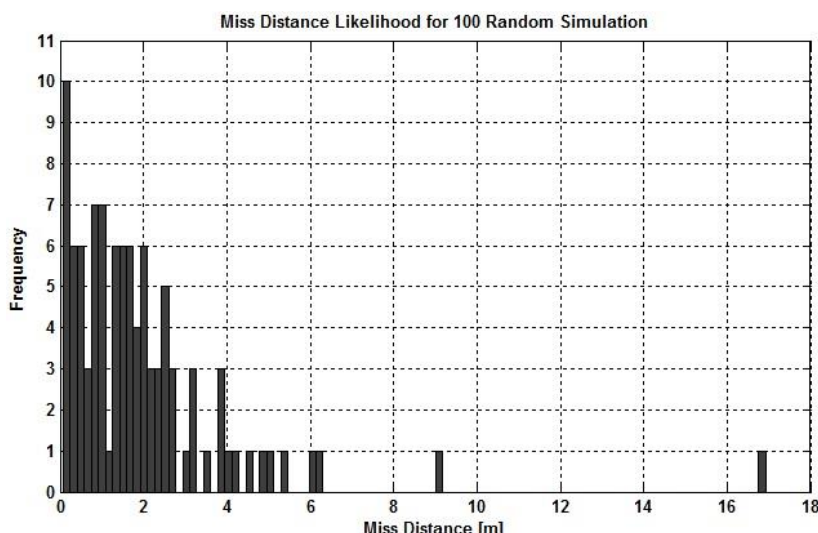


Figure 7.48: Miss Distance Histogram for Case 30

Average Miss Distance: 1.97 m

Minimum Miss Distance: 0.07 m

Maximum Miss Distance: 16.92 m

Hit Ratio: 83 %

Average Flight Time: 14.42 s

Case 31

Target Maneuver

X: $\pm 1g$ 5s Random Piecewise Step Maneuver

Y: $\pm 3g$ 0.5 rad/s Random Weaving Maneuver

Z: 0 to $5g$ Ramp Maneuver

Noise Model

Random Gaussian Noise for Range-to-Go

Sinusoidal Noise for LOS Angles

Radome Error for LOS Rates

Guidance Algorithm

PNG Law ($N' = 3$)

Body Attitude Control

Novel Extra Latax Algorithm

Latax Limit $\pm 35g$

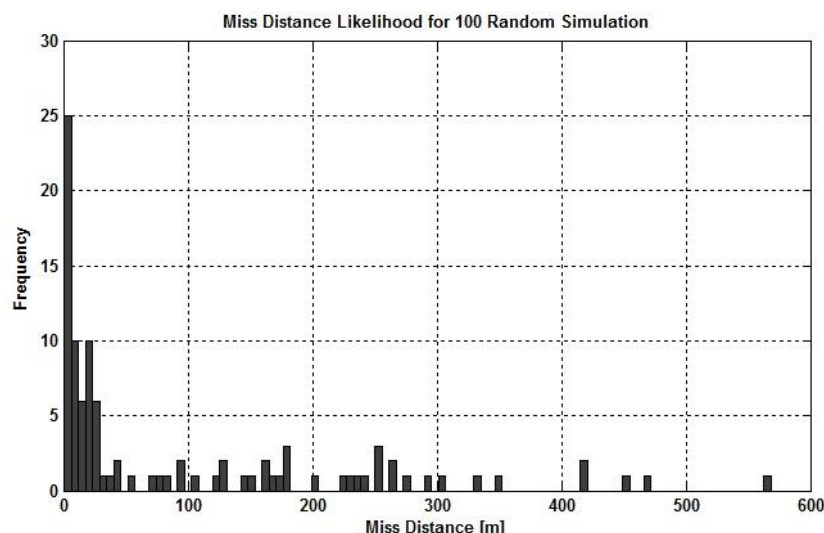


Figure 7.49: Miss Distance Histogram for Case 31

Average Miss Distance: 95.29 m

Minimum Miss Distance: 0.55 m

Maximum Miss Distance: 568.34 m

Hit Ratio: 18 %

Average Flight Time: 16.9 s

Case 32

Target Maneuver

X: $\pm 1g$ 5s Random Piecewise Step Maneuver

Y: $\pm 3g$ 0.5 rad/s Random Weaving Maneuver

Z: 0 to $5g$ Ramp Maneuver

Noise Model

Random Gaussian Noise for Range-to-Go

Sinusoidal Noise for LOS Angles

Radome Error for LOS Rates

Guidance Algorithm

APNG Law ($N' = 3$)

Body Attitude Control

Novel Extra Latax Algorithm

Latax Limit $\pm 10g$

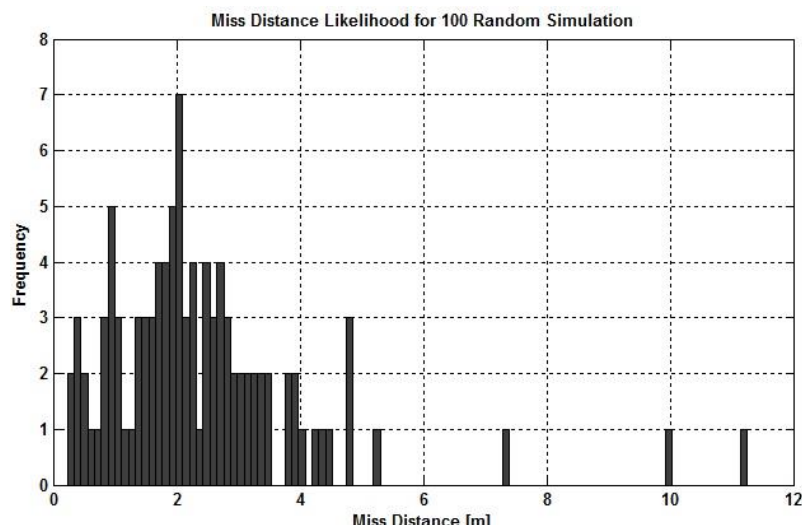


Figure 7.50: Miss Distance Histogram for Case 32

Average Miss Distance: 2.43 m

Minimum Miss Distance: 0.23 m

Maximum Miss Distance: 11.25 m

Hit Ratio: 77 %

Average Flight Time: 15.44 s

Case 33

Target Maneuver

X: 3g Step Maneuver

Y: 4g 0.75 rad/s Weaving Maneuver

Z: 0 to 5g Ramp Maneuver

Noise Model (Low Level Noise)

Random Gaussian Noise for Range-to-Go

Sinusoidal Noise for LOS Angles

Radome Error for LOS Rates

Heading Error (25° in Azimuth)

Guidance Algorithm

APNG Law ($N' = 3$)

Body Attitude Control

Latax Limit $\pm 35g$

Yaw Gimbal Saturation

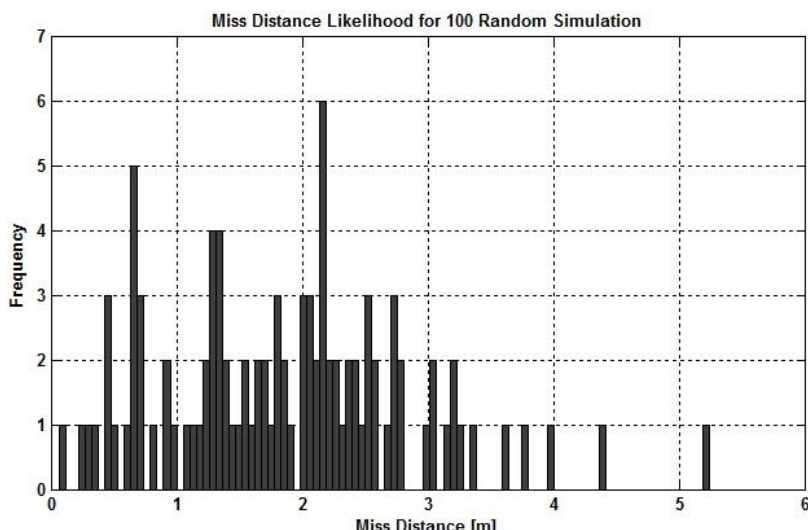


Figure 7.51: Miss Distance Histogram for Case 33

Average Miss Distance: 1.87 m

Minimum Miss Distance: 0.07 m

Maximum Miss Distance: 5.25 m

Hit Ratio: 87 %

Average Flight Time: 11.68 s

Case 34

Target Maneuver

X: $3g$ Step Maneuver

Y: $4g$ 0.75 rad/s Weaving Maneuver

Z: 0 to $5g$ Ramp Maneuver

Noise Model (Low Level Noise)

Random Gaussian Noise for Range-to-Go

Sinusoidal Noise for LOS Angles

Radome Error for LOS Rates

Heading Error (25° in Azimuth)

Guidance Algorithm

APNG Law ($N' = 3$)

Body Attitude Control

Novel Extra Latax Algorithm

Latax Limit $\pm 35g$

Yaw Gimbal Saturation

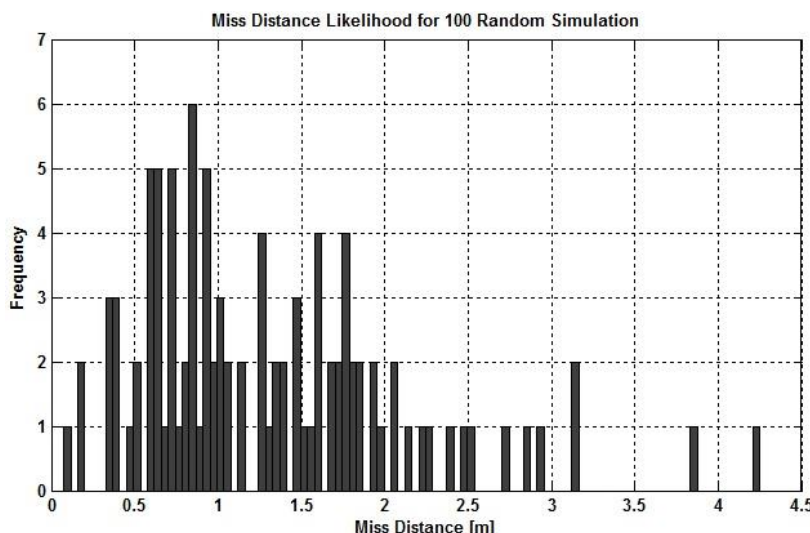


Figure 7.52: Miss Distance Histogram for Case 34

Average Miss Distance: 1.3 m

Minimum Miss Distance: 0.07 m

Maximum Miss Distance: 4.25 m

Hit Ratio: 96 %

Average Flight Time: 11.57 s

Case 35

Target Maneuver

X: 0 to $3g$ Ramp Maneuver

Y: $1.5g$ 0.75 rad/s Weaving Maneuver

Z: $5g$ Step Maneuver

Noise Model (High Level Noise)

Random Gaussian Noise for Range-to-Go

Sinusoidal Noise for LOS Angles

Radome Error for LOS Rates

Heading Error (25° in Elevation)

Guidance Algorithm

APNG Law ($N' = 3$)

Body Attitude Control

Latax Limit $\pm 35g$

Pitch Gimbal Saturation

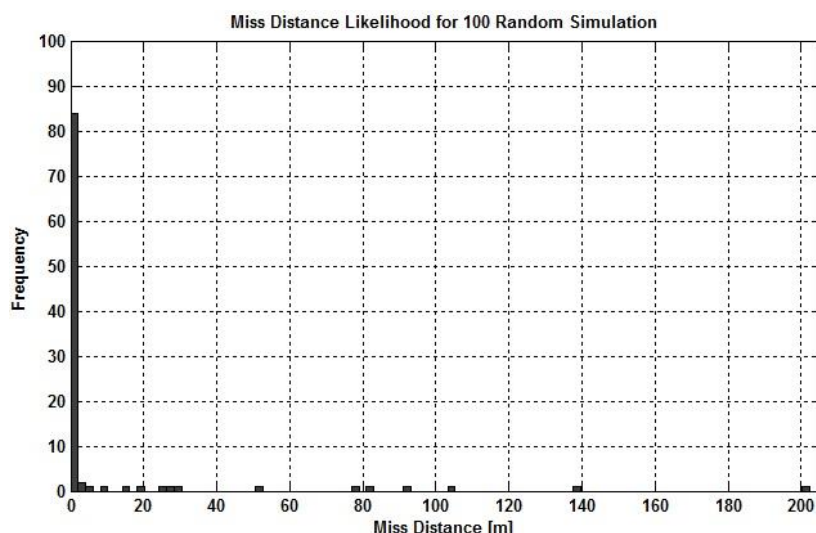


Figure 7.53: Miss Distance Histogram for Case 35

Average Miss Distance: 9.18 m

Minimum Miss Distance: 0.01 m

Maximum Miss Distance: 202.44 m

Hit Ratio: 85 %

Average Flight Time: 13.16 s

Case 36

Target Maneuver

X: 0 to $3g$ Ramp Maneuver

Y: $1.5g$ 0.75 rad/s Weaving Maneuver

Z: $5g$ Step Maneuver

Noise Model (High Level Noise)

Random Gaussian Noise for Range-to-Go

Sinusoidal Noise for LOS Angles

Radome Error for LOS Rates

Heading Error (25° in Elevation)

Guidance Algorithm

APNG Law ($N' = 3$)

Body Attitude Control

Novel Extra Latax Algorithm

Latax Limit $\pm 35g$

Pitch Gimbal Saturation

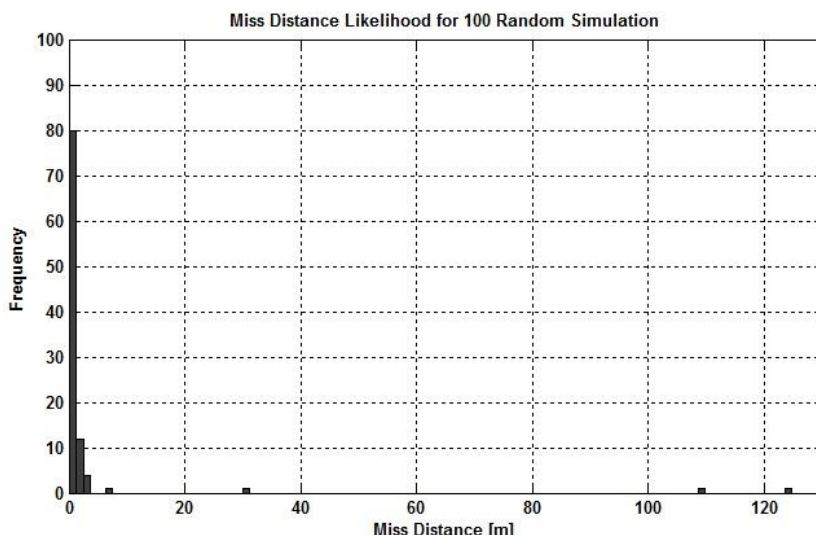


Figure 7.54: Miss Distance Histogram for Case 36

Average Miss Distance: 3.43 m

Minimum Miss Distance: 0.03 m

Maximum Miss Distance: 124.8 m

Hit Ratio: 96 %

Average Flight Time: 12.55 s

Case 37

Target Maneuver

X: $0g$

Y: $5g$ 0.5 rad/s Weaving Maneuver

Z: $5g$ Step Maneuver

Noise Model (Medium Level Noise)

Random Gaussian Noise for Range-to-Go

Sinusoidal Noise for LOS Angles

Radome Error for LOS Rates

Heading Error (25° in Azimuth and Elevation)

Guidance Algorithm

APNG Law ($N' = 3$)

Body Attitude Control

Latax Limit $\pm 35g$

Yaw & Pitch Gimbal Saturation

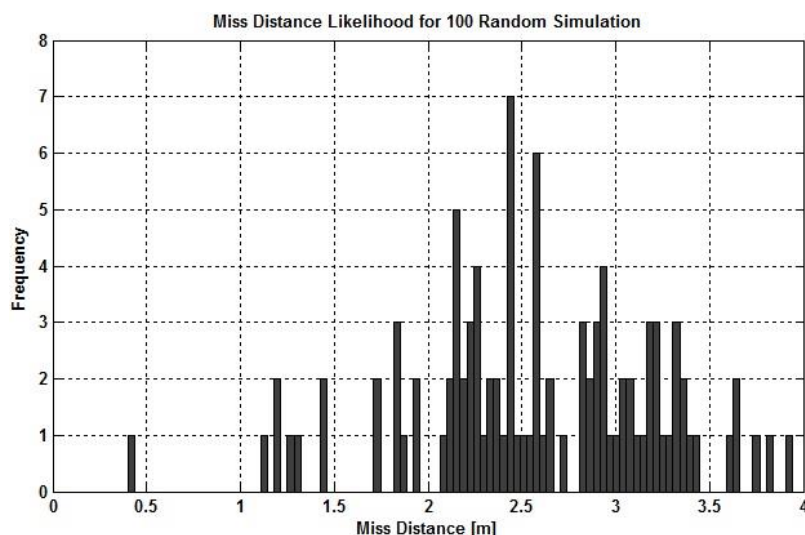


Figure 7.55: Miss Distance Histogram for Case 37

Average Miss Distance: 2.57 m

Minimum Miss Distance: 0.4 m

Maximum Miss Distance: 3.93 m

Hit Ratio: 75 %

Average Flight Time: 14.23 s

Case 38

Target Maneuver

X: $0g$

Y: $5g$ 0.5 rad/s Weaving Maneuver

Z: $5g$ Step Maneuver

Noise Model (Medium Level Noise)

Random Gaussian Noise for Range-to-Go

Sinusoidal Noise for LOS Angles

Radome Error for LOS Rates

Heading Error (25° in Azimuth and Elevation)

Guidance Algorithm

APNG Law ($N' = 3$)

Body Attitude Control

Novel Extra Latax Algorithm

Latax Limit $\pm 35g$

Yaw & Pitch Gimbal Saturation

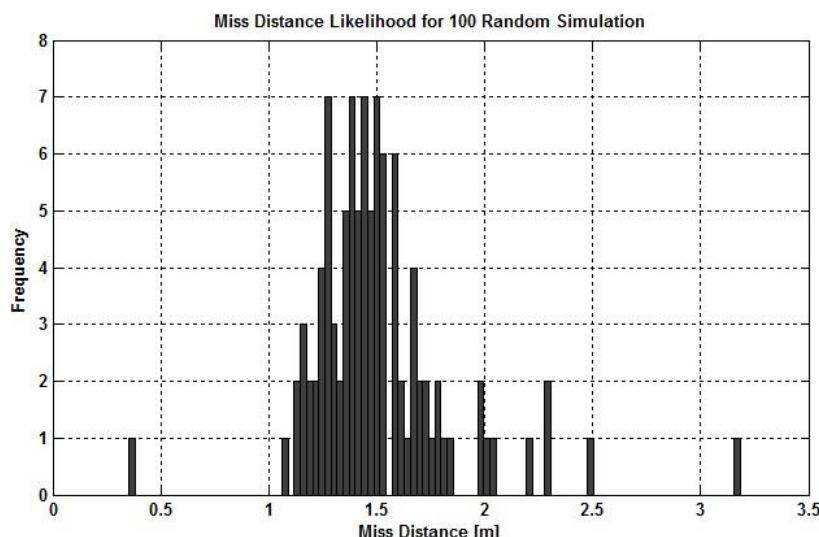


Figure 7.56: Miss Distance Histogram for Case 38

Average Miss Distance: 1.5 m

Minimum Miss Distance: 0.35 m

Maximum Miss Distance: 3.18 m

Hit Ratio: 99 %

Average Flight Time: 13.8 s

Monte Carlo simulations show that the increased agility of the pursuer may not result in better guidance performance since noise involved in LOS rate, closing velocity and target's acceleration estimates is also amplified during the calculation of the required lateral acceleration components.

It is also presented that APNG Law performs so much better than the PNG Law against maneuverable targets. As discussed in Chapter 6, APNG Law includes an additional term which accounts for the acceleration estimates of the target and this may be very helpful in tracking a target successfully up to interception.

Cases 29 and 32 can be compared with respect to the allowable limits of the lateral acceleration components. As can be seen from the simulation results, restriction of the lateral acceleration capability of the missile can have a noticeable increase in the average miss distance value and the total flight time whereas the hit ratio for the proposed guidance scenario decreases remarkably.

Later, the effectiveness of the proposed algorithm on improving the guidance performance in case of gimbal saturation is scrutinized. It is proved by the *Monte Carlo* simulations that a significant decrease in the average miss distance values and total flight times as well as a remarkable improvement in the hit ratios can be achieved by the incorporation of the novel guidance algorithm in blind flight conditions.

CHAPTER 8

CONCLUSION

8.1 Evaluation of Modeling and Simulation Studies

In this study, a homing loop for guided missiles is modeled via Matlab-Simulink software. The guidance problem is formulated as a closed-loop feedback control system and the role of each subcomponent in this homing loop is explained.

The targets of interest were the maneuvering ones and challenging maneuver types together with different engagement geometries are examined. Target motions are modeled to reflect realistic maneuver types that can be encountered in real guidance scenarios.

Later, missile-target kinematics is investigated and the use of line-of-sight concept in missile guidance applications is scrutinized. Gimbaled and strapdown seeker models are designed in order to derive the LOS rates in azimuth and elevation directions. Tracking and stabilization loops of the gimbaled seeker are formed to keep track of the acquired target and stabilize the motion of the gimbal against significant body motion. For strapdown systems, 2nd order fading memory filtering method is applied to filter the noisy LOS angle measurements and derive the LOS rates to be fed into the guidance system. Then, distinct random noise and error types that lead to corruption in the measured data are presented in depth. Each of these noise and error sources has different characteristics and the degree of their effects on miss distances is closely related to these characteristics.

The application of 1st order fading memory filters are exemplified for filtering noisy LOS rate information. Afterwards, 3rd order digital fading memory filtering algorithms are applied to serve as a target state estimator for the guidance

problem in hand. By making use of the noisy target position data, velocity and acceleration of the target are aimed to be predicted in inertial reference frame for challenging target maneuver types. Estimated acceleration components are then sent to the guidance section to be used by the selected guidance law. The reader is also informed about the use of one of the most sophisticated estimation methods, namely *Kalman* filtering.

Since the intended targets were highly maneuverable ones, a modified version of the well-known PN guidance law, named as Augmented Proportional Navigation Guidance Law is mechanized to calculate the required lateral acceleration components in LOS frame. A new technique is proposed to take role in “Blind Flight” conditions, which can be considered as a contribution to the missile guidance literature. Autopilot and missile maneuver models are also mentioned for the sake of completeness.

Finally, numerous end-game plots of pursuer and evader for challenging guidance scenarios are illustrated to show the effectiveness of the overall homing loop. In order to compare the effect of different target maneuver types, seeker models, noise sources and guidance algorithms on overall guidance performance in terms of average miss distances, hit ratios and average engagement times, multiple simulation trials, called as *Monte Carlo* simulations, are performed randomly. By doing so, it was possible to assess the performance of the overall guidance system based on a statistical approach.

8.2 Summary of Outcomes

Here, the results of *Monte Carlo* simulations are summed up to present the outcomes of the study in a compact form and the main contributors to the miss distance are listed as well.

Weaving and piecewise step maneuvers emerge to be the most effective target maneuver models that can be used to deceive and get rid of the pursuer for

tail-chase engagements. High average miss distance values and low hit ratios are experienced against such maneuver types according to the *Monte Carlo* simulation results. Furthermore, for head-on engagements, ramp maneuver can be counted as an effective way of escaping from a pursuer.

According to simulation studies, head-on engagements are likely to lead to more miss distance and lower hit ratio due to high closure rates encountered in such engagement scenarios.

Among random noise and error sources, glint noise is proved to be the most dangerous noise type from the pursuer's point of view. This result was expected since the glint noise is known to become very dominant at the last phases of the engagement by corrupting the measured LOS angles. LOS rate derivations and target acceleration estimations are directly influenced by the existence of glint noise resulting in increased miss distances. Receiver angle tracking noise in addition to heading and radome-boresight errors can be counted as the primary sources of miss as well.

The effects of time constant and the memory length of the LOS rate filter are examined for gimbaled and strapdown seeker models, respectively. It is shown that guidance performance can be improved in terms of average miss distance, hit ratio and engagement times by proper selection of these two dominant factors.

It is also discussed that the performance of the target estimator can be improved by tuning the filter parameters, especially the memory length of the third order fading memory filter.

The supportive role of the novel algorithm is verified statistically by the randomly repeated multiple *Monte Carlo* simulations as the inclusion of the new method in "Blind Flight" scenarios led to improved hit ratios and smaller miss distances as well as reduced flight time. The superiority of APNG Law over the PNG Law against highly maneuverable targets is proven once again with the obtained *Monte Carlo* simulation results. Besides, the effect of the lateral

acceleration limits and the effective navigation constant on the overall guidance performance is questioned.

8.3 Recommendations for Further Work

This study involves a few areas on which further work is possible for the avid guidance and control engineer.

First of all, an advanced *Kalman* filtering algorithm can be applied to estimate the states of the target quicker and more accurately. This can also offer an opportunity to compare constant gain and variable gain target estimator models in terms of the overall guidance performance.

Another area in which further research can be conducted is the guidance laws being implemented. Advanced modern guidance laws that rely on optimal control theory can be integrated to the guidance system. By doing so, the advantages and disadvantages of modern guidance laws in terms of robustness, sensitivity to random noise sources, ease of implementation, required lateral acceleration values and computing capabilities can be observed and compared with the classical guidance laws.

Lastly, aerodynamic stability derivatives can be tabulated via Missile Datcom software to derive the corresponding transfer functions related to the airframe dynamics of the missile. Hence, a detailed autopilot model can be developed that accounts for aerodynamic effects thoroughly.

REFERENCES

- [1] Palumbo, N.F., "Homing Missile Guidance and Control", Johns Hopkins APL Technical Digest, vol. 29, no. 1, pp. 2-8, 2010.
- [2] Zarchan, P., "Tactical and Strategic Missile Guidance", 4th ed., Progress in Astronautics and Aeronautics, vol. 199, 2002.
- [3] Royal Air Force Museum Cosford Guidebook, 1976.
- [4] Retrieved March 18, 2014, from <http://www.luftarchiv.de>
- [5] Fitzsimons, B., "The Encyclopedia of 20th Century Weapons and Warfare", Phoebus Publishing Company, vol. 24, pp. 2602-2603, 1978.
- [6] Retrieved March 23, 2014, from <http://www.astronautix.com>
- [7] San Diego Air and Space Museum Archive
- [8] Christopher, J., "The Race for Hitler's X-Planes", History Press, pp. 126-145, 2013.
- [9] Retrieved March 25, 2014, from <http://www.ww2-landmarkscout.com>
- [10] Retrieved March 29, 2014, from <http://en.valka.cz>
- [11] Retrieved March 29, 2014, from <http://www.luft46.com>
- [12] Siouris, G.M., "Missile Guidance and Control Systems", Springer, 2003.
- [13] Palumbo, N.F.; Blauwkamp, A.B.; Lloyd, J.M., "Modern Homing Missile Guidance Theory and Techniques", Johns Hopkins APL Technical Digest, vol. 29, no. 1, pp. 42-59, 2010.
- [14] Walter, R.D., "Modern Missile Analysis Course by Applied Technology Institute (ATI)", 2004.
- [15] Vergez, P.L.; McClendon, J.R., "Optimal Control and Estimation for Strapdown Seeker Guidance of Tactical Missiles", J. Guidance, vol. 5, no. 3, pp. 225-226, May-June 1982.
- [16] Ryoo, C-K.; Kim, Y-H.; Tahk, M-J.; Choi, K., "A Missile Guidance Law Based on Sontag's Formula to Intercept Maneuvering Targets", International Journal of Control, Automation and Systems, vol. 5, no. 4, pp. 397-409, August 2007.

- [17] Palumbo, N.F.; Blauwkamp, A.B.; Lloyd, J.M., "Basic Principles of Homing Guidance", Johns Hopkins APL Technical Digest, vol. 29, no. 1, pp. 25-41, 2010.
- [18] Retrieved April 16, 2014, from <http://www.air-and-space.com>
- [19] Shneydor, N.A., "Missile Guidance and Pursuit: Kinematics, Dynamics and Control", Horwood Publishing, 1998.
- [20] Weston, A.C., "Dual-Seeker Measurement Processing for Tactical Missile Guidance", Air Force Institute of Technology, p. 4, December 1982.
- [21] Carroll, T., "Seeker/Sensor Technology Assessment Presentation", UAH, AIAA, January 2004.
- [22] Retrieved April 30, 2014, from <http://tempest.das.ucdavid.edu>
- [23] Kumar, N.S.; Kashyap, S.K, "Target Tracking in Non-Gaussian Environment", National Conference on Range Technology, 2006.
- [24] Ananthasayanam, M.R.; Sarkar, A.K.; Vohra, P.; Bhattacharya, A.; Srivastava, R., "Estimation of LOS Rates and Angles using EKF from Noisy Seeker Measurements", International Conference on Signal Processing & Communications, 2004.
- [25] Yanushevsky, R., "Modern Missile Guidance", CRC Press, 2008.
- [26] Fossier, M.W., "The Development of Radar Homing Missiles", J. Guidance, vol. 7, pp. 641-651, Nov-Dec 1984.
- [27] Nesline, F.W; Zarchan, P., "A New Look at Classical vs Modern Homing Missile Guidance", J. Guidance, vol. 4, no. 1, pp.78-85, 1981.

APPENDIX A

COORDINATE TRANSFORMATIONS

A.1 Coordinate Transformation from Inertial Reference Frame to Line of Sight Frame

Inertial reference frame coordinate axes are transformed into the line of sight frame coordinate axes after two successive axis rotations as illustrated in Figure A.1.

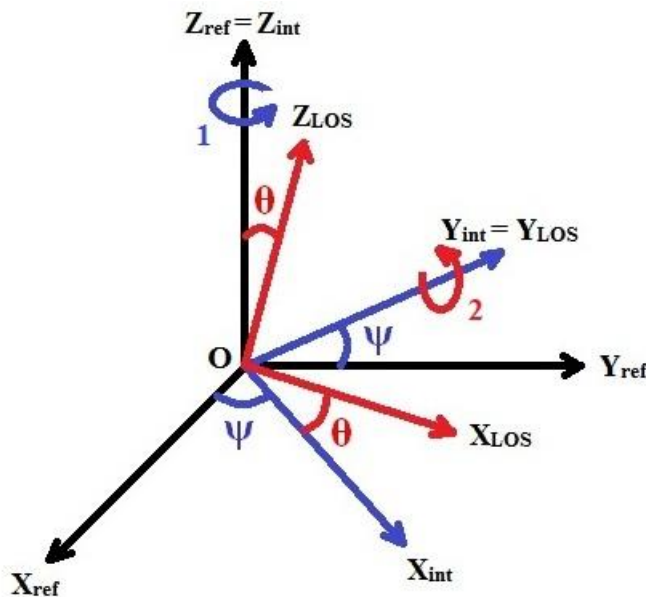


Figure A.1: Coordinate Transformation from Inertial Reference Frame to Line of Sight Frame

If the inertial reference frame is rotated about Z_{ref} in the CCW direction by an angle of ψ , an intermediate frame is obtained that enables the transition to the LOS frame. The rotation matrix associated with this rotation is given in equation (A.1).

$$\hat{R}_Z(\psi) = \begin{bmatrix} \cos(\psi) & \sin(\psi) & 0 \\ -\sin(\psi) & \cos(\psi) & 0 \\ 0 & 0 & 1 \end{bmatrix} \quad (\text{A.1})$$

Later, the intermediate frame is rotated about the rotated axis Y_{int} in the CW direction by an angle of θ in order to obtain the line of sight frame. The rotation matrix related to this rotation is given in equation (A.2). The rotation angle is taken to be negative in this case due to sign convention. Rotation angles in CW directions are taken to be negative and vice versa according to the sign convention being adapted.

$$\hat{R}_Y(-\theta) = \begin{bmatrix} \cos(-\theta) & 0 & -\sin(-\theta) \\ 0 & 1 & 0 \\ \sin(-\theta) & 0 & \cos(-\theta) \end{bmatrix} \quad (\text{A.2})$$

These two rotation sequences can be combined in matrix form as given in equation (A.3) in order to get the overall transformation matrix $\hat{T}_{IRF-LOS}$.

$$\hat{T}_{IRF-LOS} = \hat{R}_Y(-\theta) \hat{R}_Z(\psi) \quad (\text{A.3})$$

The transformation matrix denoted by $\hat{T}_{IRF-LOS}$ is given in equation (A.4).

$$\hat{T}_{IRF-LOS} = \begin{bmatrix} \cos \theta \cos \psi & \cos \theta \sin \psi & \sin \theta \\ -\sin \psi & \cos \psi & 0 \\ -\sin \theta \cos \psi & -\sin \theta \sin \psi & \cos \theta \end{bmatrix} \quad (\text{A.4})$$

Equation (A.5) expresses the coordinate transformation from inertial reference frame to line of sight frame in matrix form.

$$\begin{bmatrix} X_{LOS} \\ Y_{LOS} \\ Z_{LOS} \end{bmatrix} = \begin{bmatrix} \cos \theta \cos \psi & \cos \theta \sin \psi & \sin \theta \\ -\sin \psi & \cos \psi & 0 \\ -\sin \theta \cos \psi & -\sin \theta \sin \psi & \cos \theta \end{bmatrix} \begin{bmatrix} X_{ref} \\ Y_{ref} \\ Z_{ref} \end{bmatrix} \quad (\text{A.5})$$

A.2 Coordinate Transformation from Line of Sight Frame to Inertial Reference Frame

Line of sight frame coordinate axes are transformed into the inertial reference frame coordinate axes after two successive axis rotations as illustrated in Figure A.2. These rotations are actually the reversed versions of the ones discussed in Appendix A.1.

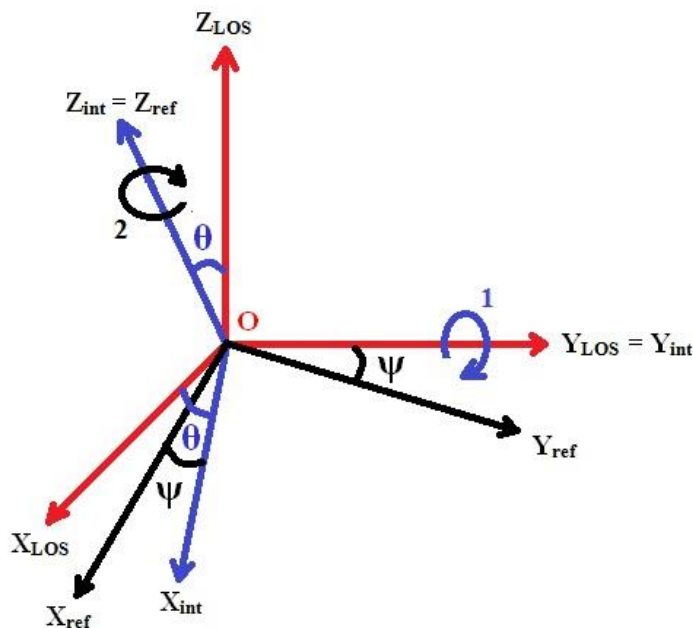


Figure A.2: Coordinate Transformation from Line of Sight Frame to Inertial Reference Frame

At this stage, it should be noted that there holds a relationship between the orthogonal transformation matrices $\hat{T}_{LOS-IRF}$ and $\hat{T}_{IRF-LOS}$. Due to orthogonality, the transpose of the $\hat{T}_{IRF-LOS}$ is equal to its inverse. Hence, the relationship given in equation (A.6) holds true.

$$\hat{T}_{LOS-IRF} = [\hat{T}_{IRF-LOS}]^T \quad (\text{A.6})$$

The corresponding transformation matrix denoted by $\hat{T}_{LOS-IRF}$ is given in equation (A.7).

$$\hat{T}_{LOS-IRF} = \begin{bmatrix} \cos \psi \cos \theta & -\sin \psi & -\cos \psi \sin \theta \\ \sin \psi \cos \theta & \cos \psi & -\sin \psi \sin \theta \\ \sin \theta & 0 & \cos \theta \end{bmatrix} \quad (A.7)$$

Finally, equation (A.8) expresses the coordinate transformation from line of sight frame to inertial reference frame in matrix form.

$$\begin{bmatrix} X_{ref} \\ Y_{ref} \\ Z_{ref} \end{bmatrix} = \begin{bmatrix} \cos \psi \cos \theta & -\sin \psi & -\cos \psi \sin \theta \\ \sin \psi \cos \theta & \cos \psi & -\sin \psi \sin \theta \\ \sin \theta & 0 & \cos \theta \end{bmatrix} \begin{bmatrix} X_{LOS} \\ Y_{LOS} \\ Z_{LOS} \end{bmatrix} \quad (A.8)$$